



Measurement of substructure-dependent jet suppression in Pb+Pb collisions at 5.02 TeV with the ATLAS detector

The ATLAS Collaboration

The ATLAS detector at the Large Hadron Collider has been used to measure jet substructure modification and suppression in Pb+Pb collisions at a nucleon–nucleon center-of-mass energy $\sqrt{s_{NN}} = 5.02$ TeV in comparison with pp collisions at $\sqrt{s} = 5.02$ TeV. The Pb+Pb data, collected in 2018, have an integrated luminosity of 1.72 nb^{-1} , while the pp data, collected in 2017, have an integrated luminosity of 260 pb^{-1} . Jets used in this analysis are clustered using the anti- k_r algorithm with a radius parameter $R = 0.4$. The jet constituents, defined by both tracking and calorimeter information, are used to determine the angular scale r_g of the first hard splitting inside the jet by reclustering them using the Cambridge–Aachen algorithm and employing the soft-drop grooming technique. The nuclear modification factor, R_{AA} , used to characterize jet suppression in Pb+Pb collisions, is presented differentially in r_g , jet transverse momentum, and in intervals of collision centrality. The R_{AA} value is observed to depend significantly on jet r_g . Jets produced with the largest measured r_g are found to be twice as suppressed as those with the smallest r_g in central Pb+Pb collisions. The R_{AA} values do not exhibit a strong variation with jet p_T in any of the r_g intervals. The r_g and p_T dependence of jet R_{AA} is qualitatively consistent with a picture of jet quenching arising from coherence and provides the most direct evidence in support of this approach.

1 Introduction

In ultrarelativistic heavy-ion collisions a hot and dense state of matter known as a quark-gluon plasma (QGP) is produced. The temperatures attained in the fireball are such that quarks and gluons are no longer confined within their parent hadrons [1, 2]. Producing a QGP in the laboratory provides unique opportunities to study quantum chromodynamics (QCD). Experimental results from the Relativistic Heavy Ion Collider (RHIC) and the Large Hadron Collider (LHC) comparing proton–proton (pp) and heavy-ion collisions have led to the conclusion that the QGP expands hydrodynamically. The remarkably small viscosity needed to describe the data suggests that this matter exhibits strong-coupling behavior at large distance scales [3]. In contrast, at short distance scales the interactions among quarks and gluons are expected to become weaker because QCD exhibits asymptotic freedom. It is not fully understood how such hydrodynamic behavior arises from the interactions among elementary quarks and gluons [4]. To address this challenge, the dynamics of the QGP must be characterized over a range of length scales.

Jets are highly collimated sprays of particles resulting from the point-like, hard scattering of quarks and gluons, collectively referred to as partons. Jets are produced at the earliest stages of a high-energy heavy-ion collision and become attenuated while passing through the plasma, a phenomenon known as jet quenching [5, 6]. The energy loss suffered by a jet and the modification of its radiation pattern provide information about the plasma’s microscopic structure. Scattered partons in the vacuum, studied using pp collisions, experience a cascade of radiative processes and thus the modification of the jet evolution process in the QGP is inherently a multiscale problem.

Techniques that enable the identification of the hardest splitting in the parton shower of a jet, and more generally the substructure of the jet and its overall radiation pattern, have been developed [7, 8]. In theoretical calculations the soft-drop grooming procedure [9], a generalization of the modified mass-drop tagger [8], shows less sensitivity to the effects of initial-state radiation, multiparton interactions, and nonperturbative contributions to substructure observables. Since these effects typically contribute large uncertainties, their mitigation allows more rigorous comparisons with experimental data [10, 11]. The potential of such techniques to characterize jet substructure in heavy-ion collisions has also been recognized [12–14], and a first series of measurements have been performed indicating a mild modification of jet-substructure variables in Pb+Pb collisions relative to pp results [15–19]. However these initial studies have not yet elucidated the relationship between the observed modifications and the energy loss of the jet.

Measurements of jet quenching in heavy-ion collisions performed at RHIC and the LHC [20, 21] typically fall into one of two categories: quantifying the total energy loss or studying the modification of the jet’s radiation pattern. The rate of jets produced in central heavy-ion collisions at a given jet transverse momentum, p_T^{jet} , is observed to be approximately a factor of two lower than in pp collisions [22–26]. Additionally, back-to-back dijet and photon/Z–jet pairs are observed to have poorer p_T balance in Pb+Pb collisions than in pp collisions [27–30]. These measurements provide information about the total jet energy loss and its parametric dependence on the in-medium path length and flavor of the initiating parton. They also constrain how energy loss may fluctuate on a jet-by-jet basis. Another class of measurements which studies the fragmentation properties of quenched jets, typically through the particle-momentum distributions within jets [31–35], is less sensitive to the energy loss but can directly assess how the radiation pattern is modified. This class includes the current heavy-ion jet-substructure measurements [15–18, 36] because the distributions of substructure quantities are normalized per jet. Currently missing from the experimental program are analyses that correlate a jet’s energy loss with its radiation pattern.

A common theoretical framework for describing jet quenching is the coherence picture in which interference effects, crucial for determining the structure of the vacuum parton shower [37], become disrupted by the medium, resulting in energy loss in the form of additional radiation [38]. Recent studies have also shown the emergence of a critical angle in the first hard splitting of a jet, above which the jet loses energy incoherently, i.e. as multiple color entities [39–43]. This approach leads to the expectation that a wide jet with two prongs, each of which may act as a separate emitter of radiation, will lose more energy than a narrow jet which acts as a single source of radiation. More generally, jets with different substructure are expected to experience different amounts of energy loss according to the degree to which the medium resolves the jet and induces decoherence of its radiation pattern [12].

This paper describes a measurement of jet suppression, a measure of the energy loss, as a function of the observed substructure of the jet. The measurements are based on 1.72 nb^{-1} of Pb+Pb collision data collected in 2018 and 260 pb^{-1} of pp collision data collected in 2017, both at $\sqrt{s_{\text{NN}}} = 5.02 \text{ TeV}$. The jets are reconstructed from energy deposits in the ATLAS calorimeters with the anti- k_t algorithm with a radius parameter of $R = 0.4$ [44] and by applying a subtraction procedure that removes the underlying event contribution to the jet kinematics on an event-by-event basis [22]. The soft-drop grooming procedure is applied with parameters $\beta = 0$ and $z_{\text{cut}} = 0.2$ to jet constituents formed from charged-particle tracks and calorimeter energy deposits. The substructure is quantified through r_g , the angle subtended by the subjects chosen using the soft-drop procedure to tag the first hard splitting of a jet. Jets which fail the soft-drop requirement are considered as single-prong jets and assigned $r_g = 0$. The per-event jet yields as a function of p_T^{jet} and r_g are measured in four centrality intervals, which characterize the overlap of the colliding nuclei in Pb+Pb collisions. The analogous differential cross-sections are measured in pp collisions, and the suppression is quantified through the nuclear modification factor, R_{AA} . The cross-sections, yields, and R_{AA} are reported for jets with $p_T^{\text{jet}} > 158 \text{ GeV}$ and $0 \leq r_g < 0.4$. The measured cross-sections and yields are unfolded to a particle-level phase space.

2 ATLAS detector

The ATLAS detector [45] at the LHC is a multipurpose particle detector with a forward–backward symmetric cylindrical geometry and a near- 4π coverage in solid angle.¹ It consists of an inner tracking detector surrounded by a thin superconducting solenoid, electromagnetic and hadron calorimeters, and a muon spectrometer. The inner-detector system is immersed in a 2 T axial magnetic field and provides charged-particle tracking within $|\eta| < 2.5$. The high-granularity silicon pixel detector covers the vertex region and typically provides four measurements per track, with the first hit typically being in the insertable B-layer installed before Run 2 [46, 47]. It is followed by the silicon microstrip tracker (SCT) which usually provides eight measurements per track. These silicon detectors are complemented by the transition radiation tracker, a drift-tube-based detector, which surrounds the SCT and has coverage up to $|\eta| = 2.0$.

The calorimeter system covers the pseudorapidity range $|\eta| < 4.9$. Within the region $|\eta| < 3.2$, electromagnetic calorimetry is provided by barrel and endcap high-granularity lead/liquid-argon (LAr)

¹ ATLAS uses a right-handed coordinate system with its origin at the nominal interaction point (IP) in the centre of the detector and the z -axis along the beam pipe. The x -axis points from the IP to the centre of the LHC ring, and the y -axis points upwards. Cylindrical coordinates (r, ϕ) are used in the transverse plane, ϕ being the azimuthal angle around the z -axis. The pseudorapidity is defined in terms of the polar angle θ as $\eta = -\ln \tan(\theta/2)$. The rapidity is defined as $y = 0.5 \ln[(E + p_z)/(E - p_z)]$ where E and p_z are the energy and z -component of the momentum along the beam direction, respectively. Angular distance is measured in units of $\Delta R \equiv \sqrt{(\Delta\eta)^2 + (\Delta\phi)^2}$.

calorimeters, with an additional thin LAr presampler covering $|\eta| < 1.8$ to correct for energy loss in material upstream of the calorimeters. Hadronic calorimetry is provided by the steel/scintillator-tile calorimeter, segmented into three barrel structures within $|\eta| < 1.7$, and two copper/LAr hadronic endcap calorimeters. The solid angle coverage is completed with copper/LAr and tungsten/LAr calorimeter modules (FCal), covering the forward regions of $3.1 < |\eta| < 4.9$. The zero-degree calorimeters (ZDC) consist of layers of alternating quartz rods and tungsten plates and are located symmetrically at $z = \pm 140$ m and cover $|\eta| \geq 8.3$. In Pb+Pb collisions, the ZDCs primarily measure ‘spectator’ neutrons: neutrons that do not interact hadronically when the incident nuclei collide.

Events of interest are selected for recording and offline analysis by the first-level (L1) trigger system implemented in custom hardware, followed by selections made by algorithms implemented in software in the high-level trigger [48].

An extensive software suite [49] is used in data simulation, in reconstruction and analysis of real and simulated events, in detector operations, and in the trigger and data acquisition systems of the experiment. The events used in this analysis were selected by a jet trigger [48]. The L1 trigger identified jet candidates by applying a sliding-window algorithm and selecting events passing a p_T threshold of 30 GeV. These events were then passed to the high-level jet trigger, which uses a jet reconstruction and background subtraction procedure similar to that used in the offline analysis and requires a minimum p_T^{jet} of 100 GeV for anti- k_r $R = 0.4$ jets. The jet trigger was fully efficient for the p_T^{jet} range considered in this measurement.

3 Data samples and event selection

The data used in this analysis are taken from the 2018 Pb+Pb and 2017 pp runs, both at $\sqrt{s_{\text{NN}}} = 5.02$ TeV. The average number of collisions per bunch-crossing (pileup) was 0.003 in the Pb+Pb data and ranges from 1.4 to 4.4 in the pp data depending on the data-taking run. Events from both the Pb+Pb and pp collisions were collected using the jet triggers with the same p_T threshold as described above. The events are required to have been collected during stable beam conditions, and to satisfy detector and data-quality requirements [50]. Both the pp and Pb+Pb events are required to have at least one reconstructed primary vertex, and the Pb+Pb events are also required to satisfy nominal offline minimum-bias Pb+Pb collision criteria, identical to those used in Ref. [51]. This additional requirement, based on a combination of the total transverse energy E_T measured in the FCal, denoted by ΣE_T^{FCal} , and the total energy deposited in the ZDC identifies and rejects 0.2% of the selected events as pile-up events.

The degree of geometric overlap of the colliding Pb nuclei is characterized by ‘event centrality’, and each collision event is assigned to a centrality interval. The procedure used to experimentally define centrality intervals in this paper follows that used in other measurements of Pb+Pb collisions performed by the ATLAS Collaboration [28]. The distribution of the total transverse energy deposited in the FCal is divided into successive quantiles of the total inelastic cross-section for Pb+Pb collisions, with the highest ΣE_T^{FCal} events corresponding, on average, to the events with the largest geometric overlap between the colliding nuclei. The centrality intervals used are: 0–10% (highest ΣE_T^{FCal}), 10–30%, 30–50%, and 50–80%. A Glauber model analysis of the ΣE_T^{FCal} distribution is used to evaluate the mean nuclear thickness function, $\langle T_{\text{AA}} \rangle$, for different centrality intervals [52, 53]. The $\langle T_{\text{AA}} \rangle$ values and uncertainties, which are discussed in Ref. [54], are listed in Table 1 for each centrality selection considered in this measurement.

The Monte Carlo (MC) simulations used in this analysis are multijet events modeled with the PYTHIA 8 [55] MC generator with leading-order matrix elements for dijet production which were matched to the parton

Table 1: The $\langle T_{AA} \rangle$ values and uncertainties for the centrality selections used in this measurement.

Centrality selection	$\langle T_{AA} \rangle \pm \delta \langle T_{AA} \rangle [1/mb]$	$\delta \langle T_{AA} \rangle / \langle T_{AA} \rangle [\%]$
0–10%	23.21 ± 0.06	0.26
10–30%	11.57 ± 0.12	1.04
30–50%	3.92 ± 0.11	2.73
50–80%	0.73 ± 0.04	5.67

shower. The A14 set of tuned parameters [56] and the NNPDF23_{LO} parton distribution functions [57] were used. The events generated by PYTHIA 8 were passed through a GEANT4-based simulation [58, 59] of the ATLAS detector and its response. By reproducing the detector conditions in the data-taking run, this allows the simulations to account for underlying-event (UE) effects in the jet reconstruction. For Pb+Pb collisions, the simulated dijet events were overlaid with minimum-bias Pb+Pb data, and this ‘overlay’ sample was reweighted on an event-by-event basis to obtain the same centrality distribution as in the jet-triggered Pb+Pb data sample. The simulated events are digitized and reconstructed in the same way as data events.

4 Analysis procedure

4.1 Jet reconstruction

The jet reconstruction procedures follow those used by the ATLAS Collaboration for previous jet measurements in Pb+Pb collisions [24, 60]. Jets are reconstructed using the anti- k_t algorithm [44] implemented in the FastJet software package [61]. In both pp and Pb+Pb collisions, jets with $R = 0.4$ are formed by clustering calorimeter towers with $\Delta\eta \times \Delta\phi = 0.1 \times \pi/32$ in the pseudorapidity range $|\eta| < 4.9$ over the full azimuthal range. The energies in the towers are obtained by summing the energies of calorimeter cells at the electromagnetic energy scale [62] within the tower boundaries. The UE contribution to each tower is subtracted on an event-by-event basis by estimating the average local energy density, $\rho(\eta, \phi)$. This estimate is obtained by measuring the average energy in calorimeter towers as a function of η and including the azimuthal modulation due to harmonic flow characterized by the second-, third-, and fourth-order flow coefficients [63]. The ϕ -dependent background subtraction is performed only for jet reconstruction in Pb+Pb events, as the event activity is observed to be azimuthally symmetric in minimum-bias pp data [64]. An iterative procedure is applied to prevent the jets from biasing the determination of ρ [60]. Following the UE subtraction, new estimates of ρ are obtained by excluding the contributions coming from towers within jets from the average energy density and flow parameterization. Additionally, the UE is also corrected for η - and ϕ -dependent nonuniformities in the detector response to soft particles by applying correction factors derived in minimum-bias Pb+Pb data. In pp collisions, the same background subtraction procedure is used, but without the nonuniformity correction and no harmonic modulation of the UE.

Following the UE subtraction, η - and p_T -dependent multiplicative calibration factors derived in MC simulations are applied to the jet four-momentum vector to account for the noncompensating hadronic response of the calorimeter [65]. An additional correction based on in situ studies of jets recoiling against photons, Z bosons, and jets in other regions of the calorimeter is applied to account for known differences between data and the MC sample used to derive the calibration [28]. This calibration is followed by a cross-calibration which relates the jet energy scale (JES) of jets reconstructed using the procedure outlined

in this section to the JES in 13 TeV pp collisions [65]. The performance of the jet reconstruction in pp and Pb+Pb collisions has been studied in detail as described in Ref. [24]. The jet transverse momentum, denoted by p_T^{jet} , is defined as the calibrated p_T of $R = 0.4$ jets formed from calorimeter towers. Calibrations are applied to the p_T of the jet and not individually to the constituent calorimeter towers in this procedure. Fully calibrated jets having $p_T^{\text{jet}} > 158$ GeV and $|y| < 2.1$ are used in this measurement. The p_T^{jet} binning was designed to match previous jet measurements by ATLAS [22–24] and have uniformly spaced bins on the logarithmic scale. MC-truth jets are defined in simulated events at particle level by applying the anti- k_t algorithm with $R = 0.4$ to stable particles with a proper lifetime greater than 30 ps in the generator’s event record, but excluding muons and neutrinos, which do not leave significant energy deposits in the calorimeter.

4.2 Jet constituents

The granularity of the ATLAS calorimeter towers, which are used as constituents in the initial jet reconstruction, is too coarse to resolve collimated prongs within a jet that have small opening angles comparable to the expected resolving power of the QGP [41, 42]. In order to improve the angular and energy resolution of the jet constituents, new constituents are defined by combining the superior angular resolution of the tracker with calorimeter information. These objects, referred to as track-calorimeter clusters (TCCs), are built using the energies of topological cell clusters (topo-clusters) [66] and the spatial coordinates of charged-particle tracks [67]. TCCs were used in previous ATLAS studies to improve the resolution of jet-substructure variables used in W/Z -boson tagging [68]. They were also used in combination with particle-flow [69] objects to optimize jet reconstruction in pp collisions [70]. In this measurement, TCCs are reconstructed in a manner similar to that in Ref. [67] but with some adjustments to account for the UE in Pb+Pb collisions as detailed below.

Topo-clusters, used to define the energy scale of the TCCs, are built from calorimeter cells using a noise-suppression algorithm [66] and have been used extensively in jet-substructure measurements in pp collisions [10, 11]. In Pb+Pb collisions, a ϕ -modulated background subtraction, similar to the UE subtraction procedure employed for jet reconstruction (Section 4.1), is applied to the calorimeter cells before using them to build topo-clusters. Charged-particle tracks are reconstructed from hits in the inner detector using standard optimization algorithms for Pb+Pb collisions as detailed in Refs. [71, 72]. Reconstructed tracks used as seeds in the TCC reconstruction are required to have $p_T > 3$ GeV and to also meet several criteria designed to select primary charged particles [31]. Tracks in an event are extrapolated to the calorimeter and are matched to one or more topo-clusters, depending on the topo-cluster size and the track extrapolation uncertainty.

Following the track and topo-cluster matching, the procedure to determine TCC four-momentum vectors is described briefly below and is detailed further in Ref. [67]. For an isolated match between a track from the selected primary vertex and a topo-cluster, the topo-cluster energy and the track direction are used to form a single TCC. In the case of topo-clusters which do not match any tracks, the topo-cluster’s four-momentum vector is directly used to create a TCC. Conversely, instances where tracks are not matched to any topo-clusters, observed to occur in less than 1% of the cases, are treated analogously by creating a TCC using the track’s four-momentum vector. In cases where multiple tracks are matched to one or more topo-clusters, the TCC algorithm is designed to create exactly one TCC object per track originating from the primary vertex. Such multiple matches are handled by using the track’s angular coordinates, while splitting the topo-cluster energy between the corresponding TCC objects to account for energy sharing between the different matches.

The topo-cluster energy sharing procedure for tracks matched to clusters makes use of three general concepts and is detailed in Ref. [67]. First, each cluster matched to the seed track should contribute to the resulting TCC object in proportion to its share of the total p_T of all matched clusters. Second, if a cluster is matched to multiple TCC objects, its contribution to a given TCC should be proportional to the share of the seed track of the total p_T of all tracks matched to the cluster. Third, the proportion of topo-cluster energy assigned to each of those tracks should itself be weighted by that cluster's share of the total energy of all clusters matching the track. The 3 GeV p_T threshold for charged tracks in the TCC reconstruction is optimized to prevent low- p_T UE tracks from sharing the energy of high- p_T topo-clusters.

All TCCs having $p_T > 4$ GeV are used in this measurement. Jets considered in this measurement with $p_T^{\text{jet}} > 158$ GeV and $|y| < 2.1$ have an average of 6–7 associated TCCs above the 4 GeV threshold in pp and Pb+Pb collisions. TCCs built by matching tracks to topo-clusters account for $\approx 77\%$ of the total number of TCCs within a jet in pp collisions. Due to the lower tracking efficiency in Pb+Pb compared to pp collisions, the fraction of TCCs within a jet built by matching tracks to topo-clusters drops to $\approx 59\%$ in central Pb+Pb collisions. The remaining TCCs are mostly cases where topo-clusters are not matched to any tracks.

4.3 Jet Grooming and r_g

Jet grooming algorithms are used to isolate the prongs of a jet that correspond to a hard splitting in the evolution of the parton shower by systematically removing the contributions of soft wide-angle radiation. The soft-drop grooming procedure [9], a generalization of the modified mass-drop tagger [8] is employed in this measurement to distinguish perturbative radiation from soft, mostly nonperturbative, components of the jet [15–17, 36]. The angular distance r_g between the subjets that tag the first hard splitting of a jet is measured in this analysis.

The procedure starts with reclustering the constituents of a jet using the Cambridge–Aachen (C/A) algorithm [73, 74] to form a clustering tree with a purely angle-ordered structure. In this measurement, jets are initially reconstructed from calorimeter towers with the anti- k_t algorithm as described in Section 4.1, and the calorimeter's response is well-defined [60]. Calorimeter-tower jets satisfying the kinematic thresholds listed in Section 4.1 are selected to be reclustered using the TCCs associated with the jet. TCCs having p_T above 4 GeV and within $\Delta R < 0.4$ of a reconstructed jet's axis are utilized in the jet reclustering process of the soft-drop procedure. The 4 GeV p_T threshold for the TCCs, applied only at the detector level, is used to further reduce the influence of the UE on the measurement of r_g . When reclustering MC-truth particle-level jets, all stable charged and neutral particles within the jets are used in the soft-drop reclustering procedure. The C/A algorithm clusters the nearest constituents first, working outwards towards the wider-angle constituents, independent of their p_T . The C/A reclustered jet is then recursively declustered into two 'subjets' and it is determined whether the subjets s_{j_1} and s_{j_2} with transverse momenta $p_T^{s_{j_1}}$ and $p_T^{s_{j_2}}$ satisfy the soft-drop condition:

$$\frac{\min(p_T^{s_{j_1}}, p_T^{s_{j_2}})}{p_T^{s_{j_1}} + p_T^{s_{j_2}}} > z_{\text{cut}} \left(\frac{\Delta R_{12}}{R} \right)^\beta, \quad (1)$$

where z_{cut} and β are algorithm parameters, R is the radius parameter value used to cluster the jets ($R = 0.4$), and $\Delta R_{12} = \sqrt{(\Delta y_{12})^2 + (\Delta \phi_{12})^2}$ is the distance in y - ϕ between the subjets, where y is the rapidity. If the soft-drop condition in Eq. (1) is not satisfied, then the subjet with the smaller p_T is dropped and the

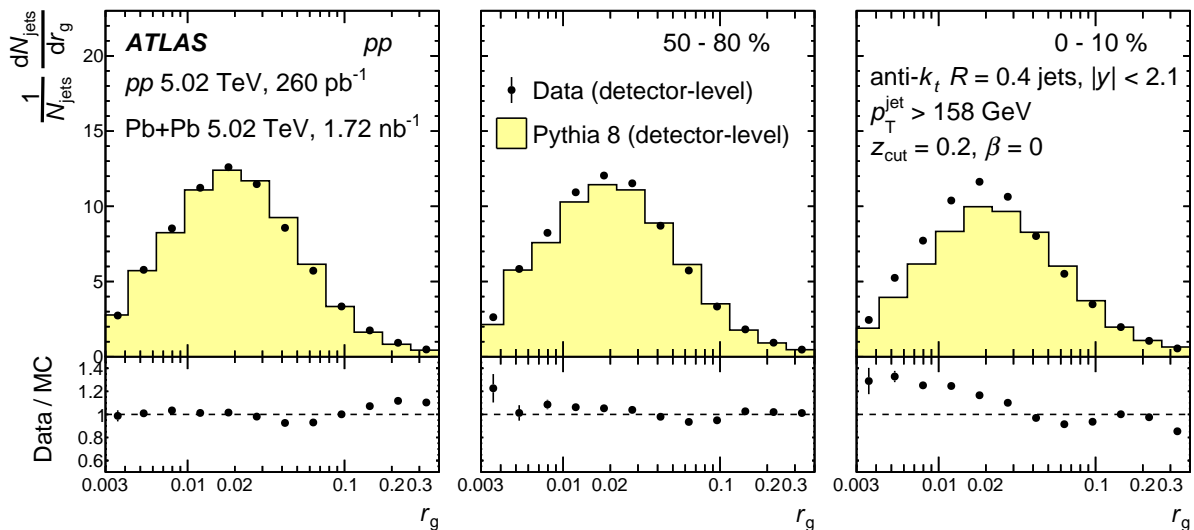


Figure 1: Top: Self-normalized r_g distributions measured using detector-level TCCs from pp data at $\sqrt{s} = 5.02$ TeV (left) and Pb+Pb data at $\sqrt{s_{NN}} = 5.02$ TeV (second and third panels) for different centrality intervals, compared with the detector-level distributions predicted by the PYTHIA 8 generator. The error bars represent statistical uncertainties. Bottom: Data-to-MC ratios of r_g distributions at detector level. The legend applies to all the panels.

procedure is iterated on the remaining subjects. If the soft-drop condition is satisfied at any point, the algorithm terminates and r_g is set to the ΔR_{12} value between the subjects s_{j_1} and s_{j_2} .

If the condition described in Eq. (1) cannot be satisfied, $r_g = 0$ is assigned to the jet to indicate that the soft-drop procedure cannot find two subjects that satisfy Eq. (1). Jets with $r_g = 0$ are primarily those with a single TCC object or MC-truth particle carrying a significant fraction of the jet energy. For all $z_{\text{cut}} > 0$ and $\beta > 0$, the procedure is infrared- and collinear-safe, while it is infrared-safe when $\beta = 0$ [9]. The soft-drop parameter values $z_{\text{cut}} = 0.2$ and $\beta = 0$, corresponding to an angle-independent grooming setting, are used for the results shown. These values are chosen to maximize the efficiency of selecting the two hardest prongs of the jet against the competing effect of jets failing the soft-drop grooming with a high z_{cut} value [75]. At the particle level, less than 4% of the jets fail the soft-drop condition when using $z_{\text{cut}} = 0.2$ and $\beta = 0$, thereby minimizing a possible bias from looking at different populations of jets in pp and Pb+Pb collisions. The r_g value of a jet measured using $z_{\text{cut}} = 0.2$ and $\beta = 0$ is also observed to be insensitive to lowering the 4 GeV threshold for the TCCs.

Distributions of r_g measured using detector-level TCCs from pp and Pb+Pb data are shown in Figure 1, and are compared with the detector-level distributions from the PYTHIA 8 MC events. The detector-level r_g distributions measured using TCCs show good agreement between data and MC events in pp and peripheral Pb+Pb collisions. The r_g distribution differences between data and simulation for central Pb+Pb collisions can plausibly be attributed to effects from jet quenching, not modeled in simulation, and are discussed in detail in Section 6. No systematic uncertainties are shown in Figure 1 because it is only intended to demonstrate the performance of TCCs in measuring r_g .

4.4 Unfolding

The jet yields are unfolded in both jet p_T^{jet} and r_g to the particle level in order to account for nonuniformities in detector performance and bin migration due to the finite resolution in jet energy, TCC energy, and TCC position, including migration in and out of the measurement phase space. The measurement phase space in this analysis corresponds to $p_T^{\text{jet}} > 158$ GeV, $|y| < 2.1$, and $0 < r_g < 0.4$ for the jets.

At the particle level, the soft-drop procedure is applied to MC-truth jets using all stable charged and neutral particles within the jet as constituents. Utilizing the RooUnfold package [76], the yields of groomed jets are unfolded using a two-dimensional iterative Bayesian unfolding algorithm [77] simultaneously in p_T^{jet} and r_g , while the inclusive jet yields are unfolded using a one-dimensional unfolding in p_T^{jet} . The migration matrices are reweighted simultaneously in MC-truth p_T^{jet} and r_g by the ratios of the corresponding distributions in data to those in the reconstructed MC sample, separately for pp collisions and each centrality interval in Pb+Pb collisions. The reweighting factors are smoothed as a function of r_g and p_T^{jet} , and their effect on bin values of the migration matrices is typically less than 25%. The uncertainty from the reweighting procedure is estimated by unfolding with and without the reweighting factors and is detailed in Section 5. The effects of inefficiencies and misidentified jets in the measurement are accounted for in the analysis by applying an efficiency correction and subtraction procedure, respectively, through the unfolding procedure. In the iterative Bayesian unfolding method implemented in RooUnfold, the inefficiencies are handled by applying a multiplicative factor to each MC-truth bin of the migration matrix. The inefficiencies in this measurement arise mainly from jets migrating out of the measurement phase space at the detector level because of energy resolution effects and from jets that fail the soft-drop grooming procedure. MC-truth jets having significantly lower p_T than 158 GeV (the p_T^{jet} threshold) that migrate into the measurement phase space at the detector level are treated as misidentified jets. The rate of such misidentified jets is observed to be negligible in this measurement, and are accounted for by treating them as an additive background. The effect of jets reconstructed entirely from overlapping UE particles in this measurement is insignificant.

The migration matrices used in the unfolding procedure are binned uniformly on a logarithmic scale and have 13 bins along r_g from 0 to 0.4 and 16 bins along p_T^{jet} from 158 GeV to 1 TeV. Additionally, in the MC-truth phase space, p_T^{jet} has one overflow bin and six underflow bins down to 80 GeV for a smooth inefficiency correction, and r_g has one overflow and one underflow bin in the migration matrix. There is no significant migration between centrality intervals in this measurement. A separate migration matrix is generated for each centrality interval in Pb+Pb collisions, using the PYTHIA 8 sample overlaid with minimum-bias Pb+Pb data and for pp collisions, using the PYTHIA 8 sample. The number of iterations in the unfolding procedure is optimized independently for different centrality intervals to balance minimizing any bias from the unfolding against fluctuations in MC samples. The optimal number of iterations ranges from four to six depending on the centrality interval. The remnant unfolding bias evaluated in MC samples is better than 1%.

The differential jet cross-section in pp collisions is defined as:

$$\frac{d^2\sigma_{\text{jet}}}{dp_T^{\text{jet}} dr_g} = \frac{1}{L_{\text{int}}} \frac{N_{\text{jets}}}{\Delta p_T^{\text{jet}} \Delta r_g},$$

where N_{jets} is the unfolded jet yield, Δp_T^{jet} and Δr_g are the widths of the p_T^{jet} and r_g bins, respectively, and L_{int} is the integrated luminosity.

The jet yield per minimum-bias event jet yield in Pb+Pb collisions, referred to as the per-event yield for simplicity, is defined as:

$$\frac{1}{N_{\text{evt}}^{\text{cent}}} \frac{d^2 N_{\text{jet}}^{\text{cent}}}{dp_{\text{T}}^{\text{jet}} dr_{\text{g}}} = \frac{1}{N_{\text{evt}}^{\text{cent}}} \frac{N_{\text{jets}}^{\text{cent}}}{\Delta p_{\text{T}}^{\text{jet}} \Delta r_{\text{g}}},$$

where $N_{\text{jet}}^{\text{cent}}$ is the unfolded jet yield in Pb+Pb collisions within intervals of $p_{\text{T}}^{\text{jet}}$ and r_{g} for a given centrality (denoted by the superscript ‘cent’), and $N_{\text{evt}}^{\text{cent}}$ is the the number of minimum-bias events in the centrality interval.

Modification of the jet yield in Pb+Pb collisions in a given centrality interval relative to the jet yield in pp collisions is quantified using the nuclear modification factor, R_{AA} , defined as:

$$R_{\text{AA}}(p_{\text{T}}^{\text{jet}}, r_{\text{g}}) = \frac{1}{N_{\text{evt}}^{\text{cent}}} \frac{1}{\langle T_{\text{AA}} \rangle} \frac{d^2 N_{\text{jet}}^{\text{cent}}}{dp_{\text{T}}^{\text{jet}} dr_{\text{g}}} \bigg/ \frac{d^2 \sigma_{\text{jet}}}{dp_{\text{T}}^{\text{jet}} dr_{\text{g}}}, \quad (2)$$

where $\langle T_{\text{AA}} \rangle$ is the mean nuclear thickness function, presented in Table 1. At a given $p_{\text{T}}^{\text{jet}}$, r_{g} , and centrality interval, $R_{\text{AA}} < 1$ indicates a suppression of jet production in Pb+Pb collisions relative to that in pp collisions.

5 Systematic uncertainties

Several sources of systematic uncertainty are considered for this analysis. The systematic uncertainties in the jet cross-sections in pp collisions and per-event yields in Pb+Pb collisions arise from the jet energy scale and resolution, the constituent TCC energy scale and resolution, the unfolding procedure, integrated pp luminosity, and $\langle T_{\text{AA}} \rangle$ (Pb+Pb only). The jet- and TCC-related uncertainties are evaluated in the analysis by modifying the migration matrix for each uncertainty contribution. The deviations from the nominal unfolded result for each variation are then combined in quadrature to calculate the total contribution.

The systematic uncertainty in the JES has three parts. The first (labeled ‘JES baseline’ in Figures 2–5) is a centrality-independent component that is determined from in situ studies of the calorimeter response to jets reconstructed with the procedure used in 13 TeV pp collisions [62, 78], with an additional component which accounts for the relative energy-scale difference between the jet reconstruction procedures used in 13 TeV pp collisions and in this measurement [65]. The potential mismodeling of relative abundances of jets initiated by quarks and gluons in the MC events, and of the calorimetric response to quark and gluon jets, are accounted for by the second component (labeled ‘JES flavor’ in Figures 2–5). The third, centrality-dependent component (applicable in Pb+Pb collisions only and labeled ‘JES quenching’ in Figures 2–5) accounts for modifications of the parton shower due to quenching [31, 35] resulting in a different detector response to jets in Pb+Pb collisions that is not modeled by the MC simulation. It is evaluated by the method used for data collected by ATLAS in 2011 and 2015 [65], which compares the jet p_{T} measured in the calorimeter with the sum of the p_{T} of charged particles within the jet, in both the data and MC samples. The selected charged-particle tracks have $p_{\text{T}} > 4$ GeV to exclude particles from the UE. The ratio of the sum of the charged-particle p_{T} to the $p_{\text{T}}^{\text{jet}}$ provides a data-driven estimate of the centrality-dependence of the JES. The centrality-dependent JES component, pertinent only to jets in Pb+Pb collisions, is the dominant source of uncertainty in the jet R_{AA} measurement, contributing to a relative uncertainty of $\approx 8\%$ in central collisions.

The uncertainty due to the jet energy resolution (JER) is evaluated by applying a Gaussian smearing factor to the reconstructed p_T^{jet} in the MC sample. The smearing factor is evaluated using an in situ technique in 13 TeV pp data that involves studies of dijet p_T balance [78, 79]. Further, an uncertainty is included to account for differences between the tower-based jet reconstruction and the jet reconstruction used in 13 TeV pp data analyses, as well as differences between calibration procedures [65]. The jet energy scale and resolution are the dominant sources of uncertainty in measuring the jet cross-sections and R_{AA} in this analysis and contribute a maximum relative uncertainty of about 14% and 9%, respectively.

Although the TCC energies are not utilized in measuring p_T^{jet} , they are used in the measurement of r_g via the soft-drop procedure. The TCC energy response is primarily determined by the topo-cluster energy response. The uncertainties in the topo-cluster energy scale and resolution, measured using 13 TeV pp data [11], are applied directly to pp data. The cluster uncertainties from 13 TeV pp data [11] are scaled conservatively by a factor of two for Pb+Pb data to cover the uncertainty in the topo-cluster energy response in the dense Pb+Pb collision environment. The inefficiency of matching between tracks and topo-clusters is driven by the angular resolution of the topo-clusters, which is used to match these objects in the TCC reconstruction. A random Gaussian smearing of 5-mrad is applied independently in η and ϕ , following previous ATLAS measurements [11, 80], to account for potential mismodeling of topo-cluster positions and is observed to have a negligible effect on the resulting TCCs and the r_g distributions. TCCs are reconstructed using topo-clusters with energies and positions varied according to their uncertainties in MC events and are used to unfold the data. The deviations from the nominal unfolded result, due to individual topo-cluster uncertainty sources, are combined in quadrature.

The effects of topo-cluster splitting and merging were studied in detail, following the method used in previous measurements [11]. The MC generator predictions precisely match each of the splitting and merging scenarios tested in data and thus no systematic uncertainty is assigned to these effects.

The angular coordinates (η , ϕ) of a TCC corresponding to a charged particle are determined by the track seeding the TCC object. Systematic variations of these coordinates are evaluated to account for tracking mismodeling in MC events. These differences are decomposed into two components: one from the uncertainty in the inner-detector material derived from studies in pp collisions [81], and the other from the modeling of pixel cluster merging inside dense environments [71, 82], such as inside the core of high-energy jets and in central Pb+Pb collisions. These track uncertainties are propagated through the TCC reconstruction and are observed to have a negligible effect on the final r_g distributions.

In this measurement the TCC-related uncertainties typically have a more modest effect than jet-related uncertainties as only the angular distance between the subjects (r_g) is measured. They become significant, contributing a relative uncertainty of up to 15%, at large r_g (>0.3) in central Pb+Pb collisions as UE fluctuations in the outer region of the jet lead to poorer performance in identifying the hard subjects.

The differences between the unfolded results with and without the migration-matrix reweighting factors are assigned as systematic uncertainties arising from the unfolding procedure. The unfolding uncertainty is observed to have a smaller effect than other sources, contributing a relative uncertainty of $<5\%$ to the cross-section, yield, and R_{AA} results.

The statistical uncertainties in the unfolding due to the statistical uncertainties associated with the size of the accumulated dataset are evaluated using the pseudo-experiment technique with 500 separate stochastic variations of the input spectrum as described in Ref. [83]. The contributions from statistical fluctuations in the response matrix are similarly evaluated using the same number of stochastic variations. The two contributions to the statistical uncertainty are combined in quadrature and are observed to contribute $<1\%$ to the total systematic uncertainty in the results.

For the 2017 pp data, the LUCID-2 detector [84] was used for the primary luminosity measurement. The uncertainty in the integrated luminosity is estimated to be 1.6% using the methods described in Ref. [85]. For Pb+Pb collisions, the systematic uncertainty in the mean nuclear thickness function, $\langle T_{AA} \rangle$, is estimated by varying the MC Glauber model parameters as detailed in Ref. [63], and is listed in Table 1.

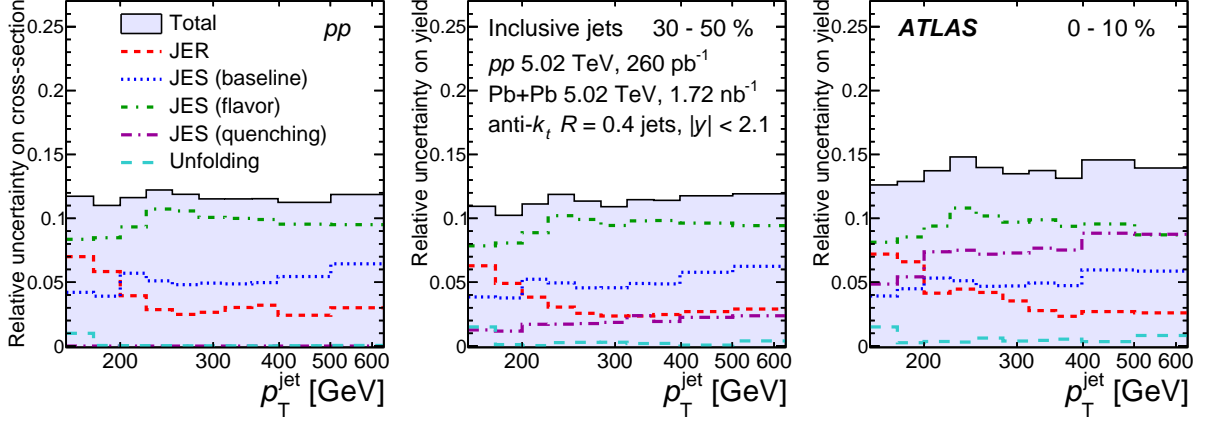


Figure 2: The relative systematic uncertainties in inclusive p_T^{jet} cross-sections in pp collisions at $\sqrt{s} = 5.02$ TeV (left) and in per-event jet yields in Pb+Pb collisions at $\sqrt{s_{\text{NN}}} = 5.02$ TeV for different event centralities (middle and right panels). The legend applies to all of the panels.

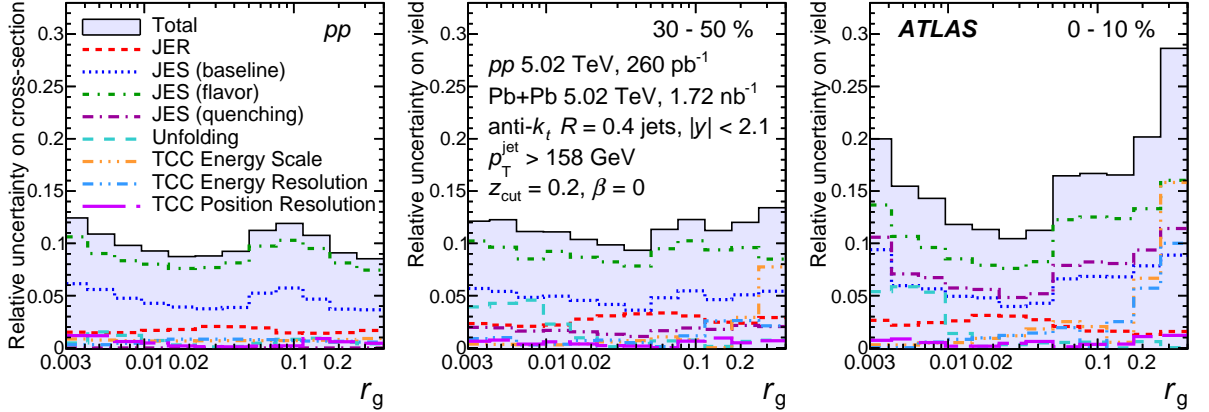


Figure 3: The relative systematic uncertainties in inclusive r_g cross-sections in pp collisions at $\sqrt{s} = 5.02$ TeV (left) and in per-event jet yields in Pb+Pb collisions at $\sqrt{s_{\text{NN}}} = 5.02$ TeV for different event centralities (middle and right panels) shown for soft-drop parameters $z_{\text{cut}} = 0.2$ and $\beta = 0$. The legend applies to all of the panels.

A summary of the relative uncertainties in the unfolded inclusive jet cross-sections, yields, and nuclear modification factor are shown in Figures 2–5. Figures 2 and 3 present a summary of the total and individual relative uncertainties in the jet cross-sections and per-event yields as a function of p_T^{jet} and r_g , respectively. The individual uncertainties are summed in quadrature to obtain the total uncertainty. The jet energy scale is the dominant source of uncertainty in the cross-sections and per-event jet yields except at large r_g in central Pb+Pb collisions, where the TCC energy-scale uncertainties have a comparable effect. A summary of the total and individual relative uncertainties in the R_{AA} is shown in Figures 4 and 5 as a function of p_T^{jet} and r_g , respectively. The uncertainties which are common to pp and Pb+Pb collisions, such as the centrality-independent JES and JER uncertainties, are treated as correlated when determining

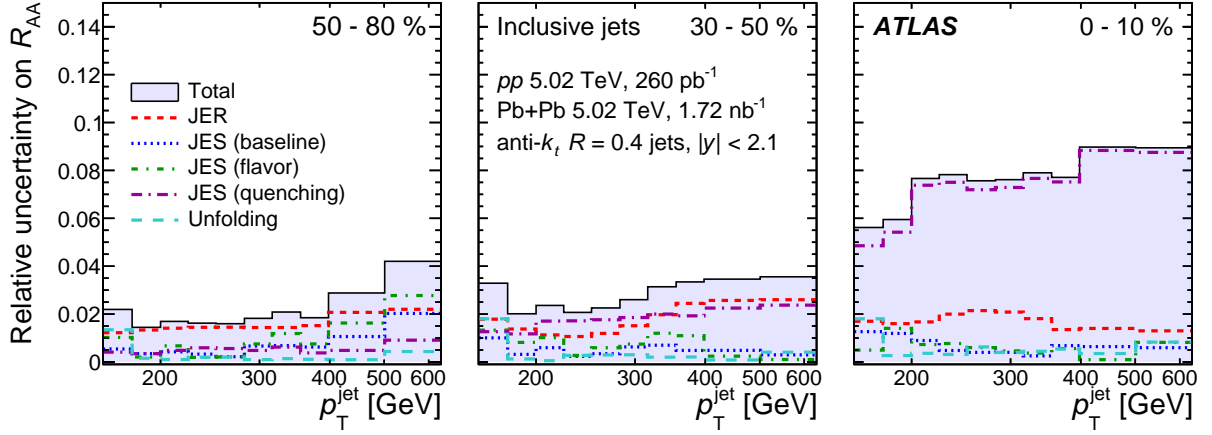


Figure 4: The relative systematic uncertainties in the R_{AA} measurements as a function of p_T^{jet} in different centrality intervals of Pb+Pb collisions at $\sqrt{s_{NN}} = 5.02$ TeV. The legend applies to all of the panels.

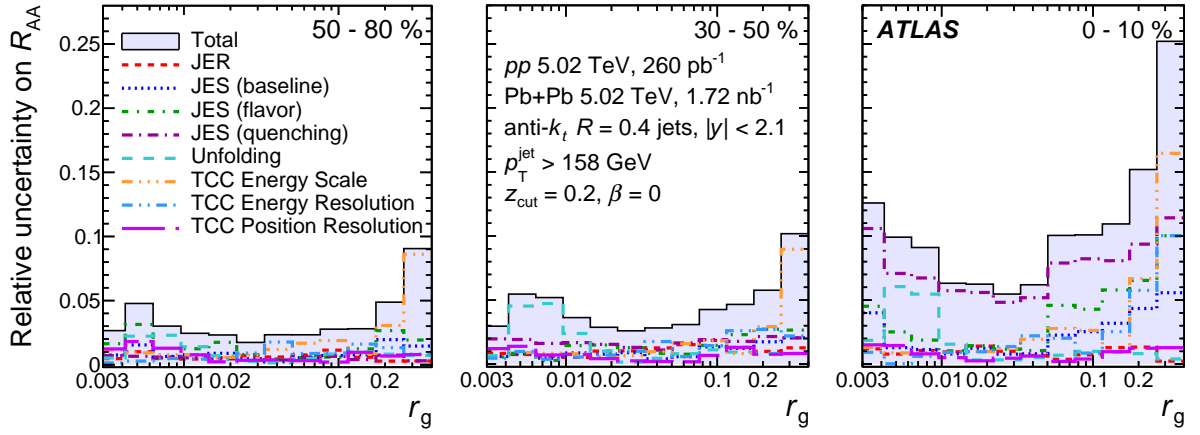


Figure 5: The relative systematic uncertainties in the R_{AA} measurements as a function of r_g in different centrality intervals of Pb+Pb collisions at $\sqrt{s_{NN}} = 5.02$ TeV shown for soft-drop parameters $z_{\text{cut}} = 0.2$ and $\beta = 0$. The legend applies to all of the panels.

the uncertainty in R_{AA} . However, as the centrality-dependent component of the JES uncertainty (only for Pb+Pb collisions) does not cancel out in the cross-section ratios, it becomes the dominant source of uncertainty in the R_{AA} results.

6 Results

The unfolded differential jet cross-sections obtained from pp collision data are shown in Figure 6 as a function of p_T^{jet} and r_g . The differential cross-sections are reported for four intervals in r_g , each scaled up by successive powers of 10. The cross-sections are also reported for jets that fail the soft-drop grooming condition. These are assigned a value of $r_g = 0$ in this analysis and they make up about 3.5% of the inclusive pp jet cross-section, and are also shown in Figure 6.

Figure 7 shows the unfolded inclusive differential cross-section in pp collision data as a function of r_g . The differential cross-sections in r_g are also reported for four bins in p_T^{jet} . The distributions are observed to peak at lower values of r_g with increasing p_T^{jet} . Tighter collimation of jets with increasing p_T^{jet} is expected from the larger boost of the fragmenting parton and an increased quark-initiated jet fraction [67].

The jet differential cross-sections measured in pp data are compared with particle-level predictions from the PYTHIA 8, HERWIG, and SHERPA generators in Figures 6 and 7. The HERWIG predictions are obtained from multijet events generated at next-to-leading order by HERWIG 7.1.3 [86] with the NNPDF3.0 PDF set [87] for the matrix element calculation. The SHERPA predictions are from multijet events generated using SHERPA 2.2.5 [88]. The matrix element calculation was included for the $2 \rightarrow 2$ process at leading order, and the default SHERPA parton shower [89] based on Catani–Seymour dipole factorization was used for the showering with p_T ordering, using the CT14NNLO PDF set [90]. The PYTHIA 8 predictions overestimate the pp data jet cross-sections but describe the shape of the p_T^{jet} and r_g distributions well, both inclusively and differentially in p_T^{jet} and r_g . The HERWIG and SHERPA predictions underestimate the cross-sections but describe the shape of both the inclusive jet differential cross-section as a function of p_T^{jet} and the differential cross-section in different r_g bins. The HERWIG generator predicts a slightly wider r_g distribution than seen in pp data across all p_T^{jet} regions studied here. The SHERPA generator predicts a significantly narrower r_g distribution than seen in pp data at low p_T^{jet} and underestimates the jet cross-sections at high p_T^{jet} . The trend of tighter collimation of jets with increasing p_T^{jet} observed in pp data is reproduced by all three MC generators with varying levels of accuracy.

Figures 8 and 9 show the Pb+Pb per-event yields normalized by $\langle T_{AA} \rangle$ for four centrality intervals as a function of p_T^{jet} and r_g , respectively. The yields are also shown for jets that fail the soft-drop grooming condition (denoted by $r_g = 0$) as a function of p_T^{jet} ; they account for about 4–5.5% of the inclusive Pb+Pb jet yield. The per-event jet yields in Pb+Pb data normalized by $\langle T_{AA} \rangle$ fall below the corresponding pp jet cross-sections for a given r_g or p_T^{jet} interval, indicating jet suppression, and this difference increases for more central events and for increasing r_g . The r_g distributions are also observed to peak at lower values of r_g with increasing p_T^{jet} in both pp collisions and all centrality intervals in Pb+Pb collisions. The p_T^{jet} spectra are observed to have similar slopes in the different r_g regions for both pp and Pb+Pb collisions.

The nuclear modification factor R_{AA} , which quantifies the jet suppression in Pb+Pb collisions relative to pp collisions, is shown as a function of p_T^{jet} in Figure 10 and as a function of r_g in Figure 11 for four centrality intervals. The R_{AA} value for inclusive jets is observed to vary from ≈ 0.95 for jets in the 50–80% centrality interval to ≈ 0.55 for the most central collisions. The R_{AA} values for inclusive jets are also observed to have an upward slope with increasing p_T^{jet} and are consistent with the results measured for jets using 2015 Pb+Pb data with a lower integrated luminosity of 0.49 nb^{-1} [24].

The values of R_{AA} are observed to depend significantly on r_g , with a clear ordering with respect to the splitting angle. Jets that fail the soft-drop grooming procedure or have $r_g < 0.02$ are observed to be the

least suppressed with an R_{AA} value of ≈ 0.75 in central Pb+Pb collisions. In contrast, jets with the widest splitting angle between their hardest subjets are observed to be suppressed with an R_{AA} value of ≈ 0.3 . Notably, the difference in the R_{AA} values is largest between jets having r_g values below or above 0.02, supporting a coherence picture of jet quenching [41, 42]. The R_{AA} values for jets in different r_g regions are observed to have a weaker dependence on p_T^{jet} in comparison with the R_{AA} behavior for the inclusive jets, especially in more central collisions. The increase in R_{AA} for inclusive jets as a function of p_T^{jet} may be explained as arising from tighter jet collimation with increasing p_T^{jet} . Jets with lower r_g values in Pb+Pb collisions are significantly less suppressed than jets with large r_g values and they also constitute a larger fraction of the inclusive jets with increasing p_T^{jet} , resulting in a rising trend for R_{AA} as a function of p_T^{jet} . As a function of r_g , R_{AA} decreases smoothly with increasing r_g (shown on logarithmic scale) in all centrality intervals and is again noted to not significantly depend on p_T^{jet} in the measured kinematic range.

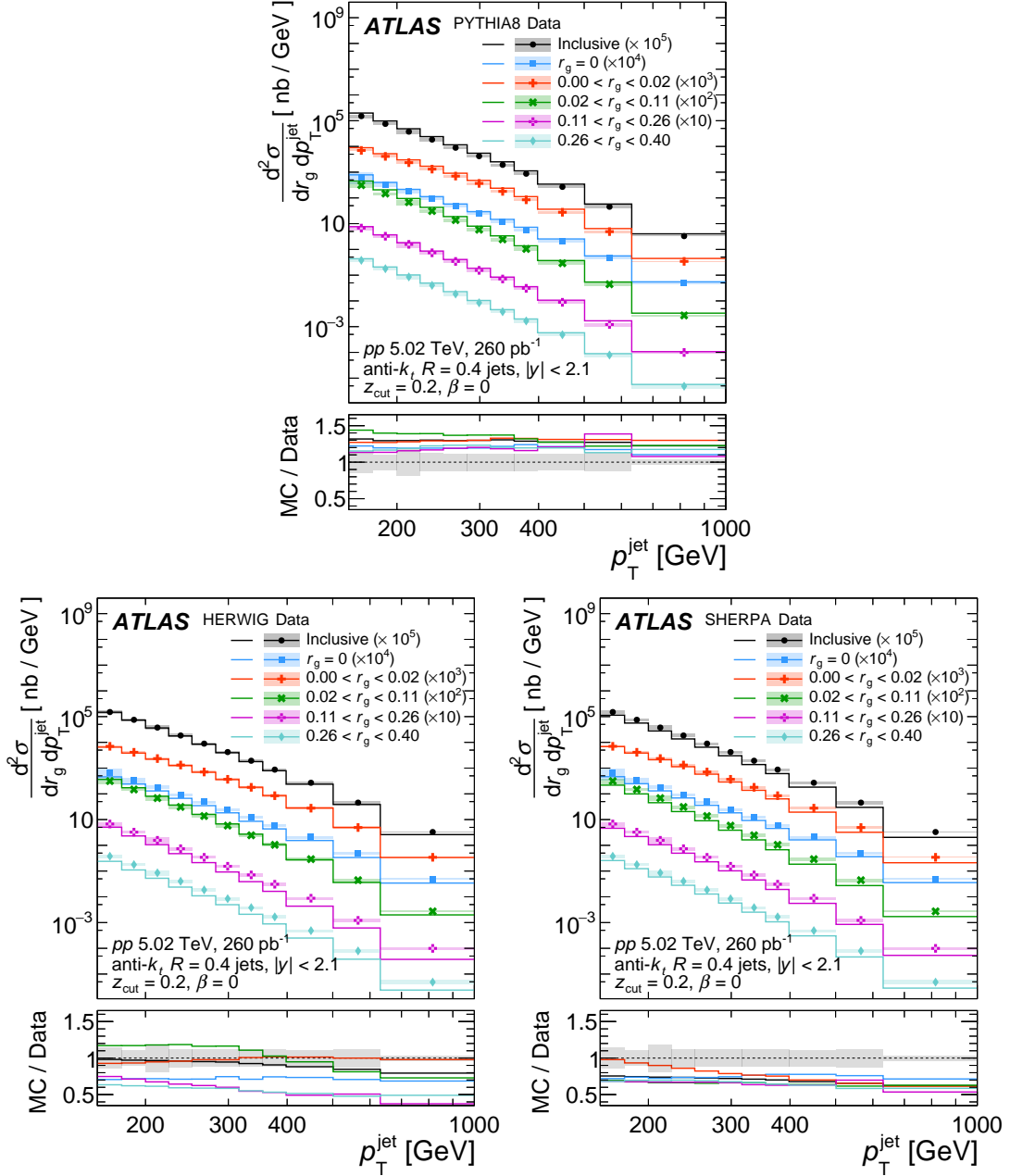


Figure 6: Differential cross-section of jets passing the soft-drop grooming condition in different r_g intervals in pp collisions at $\sqrt{s} = 5.02$ TeV as a function of p_T^{jet} . Distributions for inclusive jets (no grooming) and for those jets that fail the soft-drop requirement ($r_g = 0$) are also shown. For visual clarity, the distributions are scaled by factors specified in the legend. The statistical uncertainties are smaller than the symbols, while shaded bars represent systematic uncertainties. Note that the highest p_T^{jet} bin does not contain the overflow and that the 1.6% luminosity uncertainty is not shown. The pp jet cross-sections are compared with predictions from three MC generators, PYTHIA 8 (top), HERWIG (bottom left) and SHERPA (bottom right). The ratios of jet cross-section predictions from different MC generators to the unfolded data are shown in the lower panels. The statistical uncertainties on the ratios are smaller than the line widths, while shaded bars in the lower panels represent systematic uncertainties in inclusive cross-section ratios.

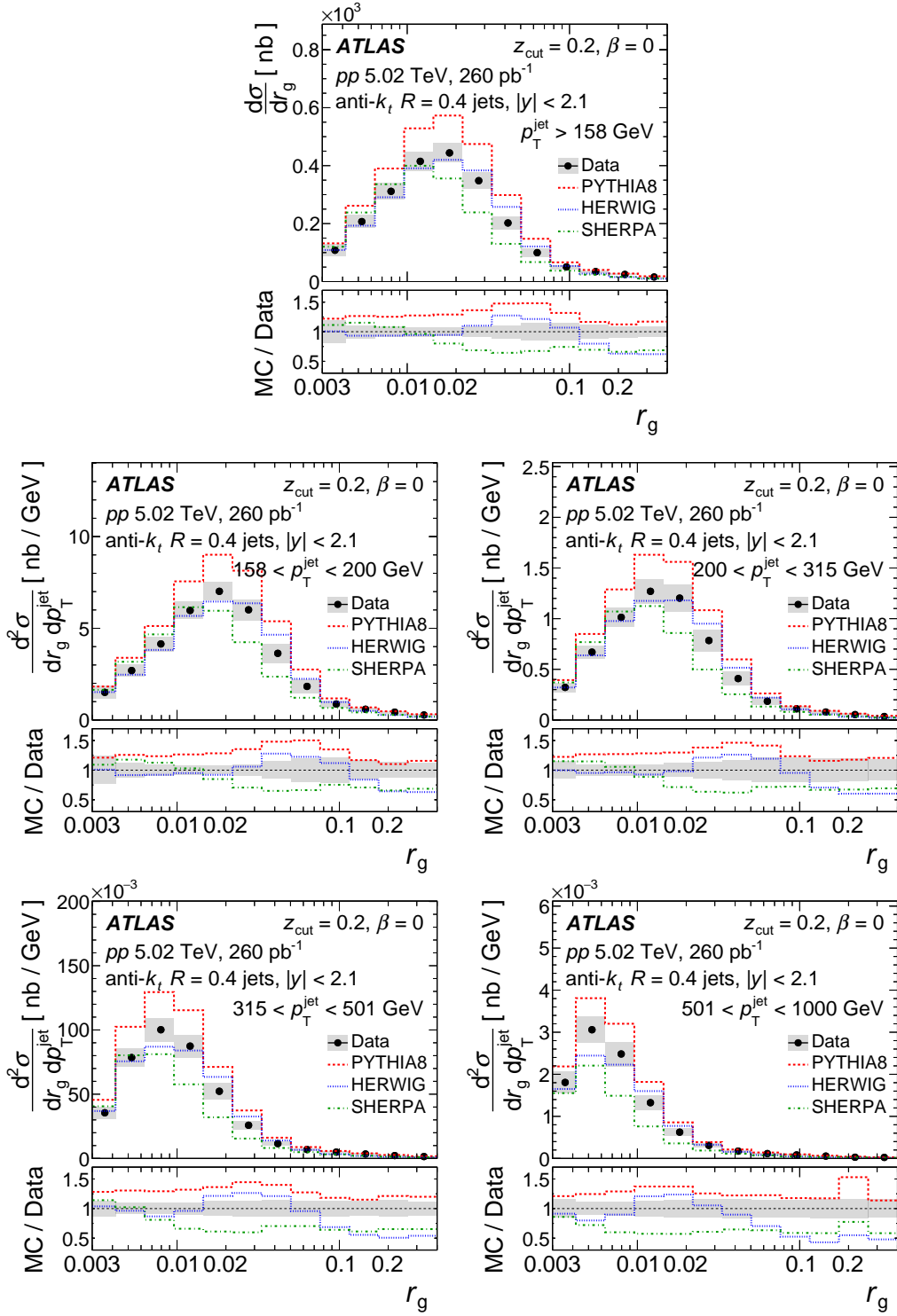


Figure 7: Differential cross-section of jets passing the soft-drop grooming condition in pp collisions at $\sqrt{s} = 5.02$ TeV as a function of r_g is shown for different p_T^{jet} intervals and also for $p_T^{\text{jet}} > 158$ GeV. The error bars represent statistical uncertainties, and are smaller than the marker size here, while the shaded bars represent systematic uncertainties. The 1.6% uncertainty in the pp luminosity is not shown. The last bin does not contain the overflow. The ratios of jet cross-section predictions from different MC generators to the unfolded data are shown in the lower panels. The shaded bars in the lower panels represent systematic uncertainties in cross-section ratios.

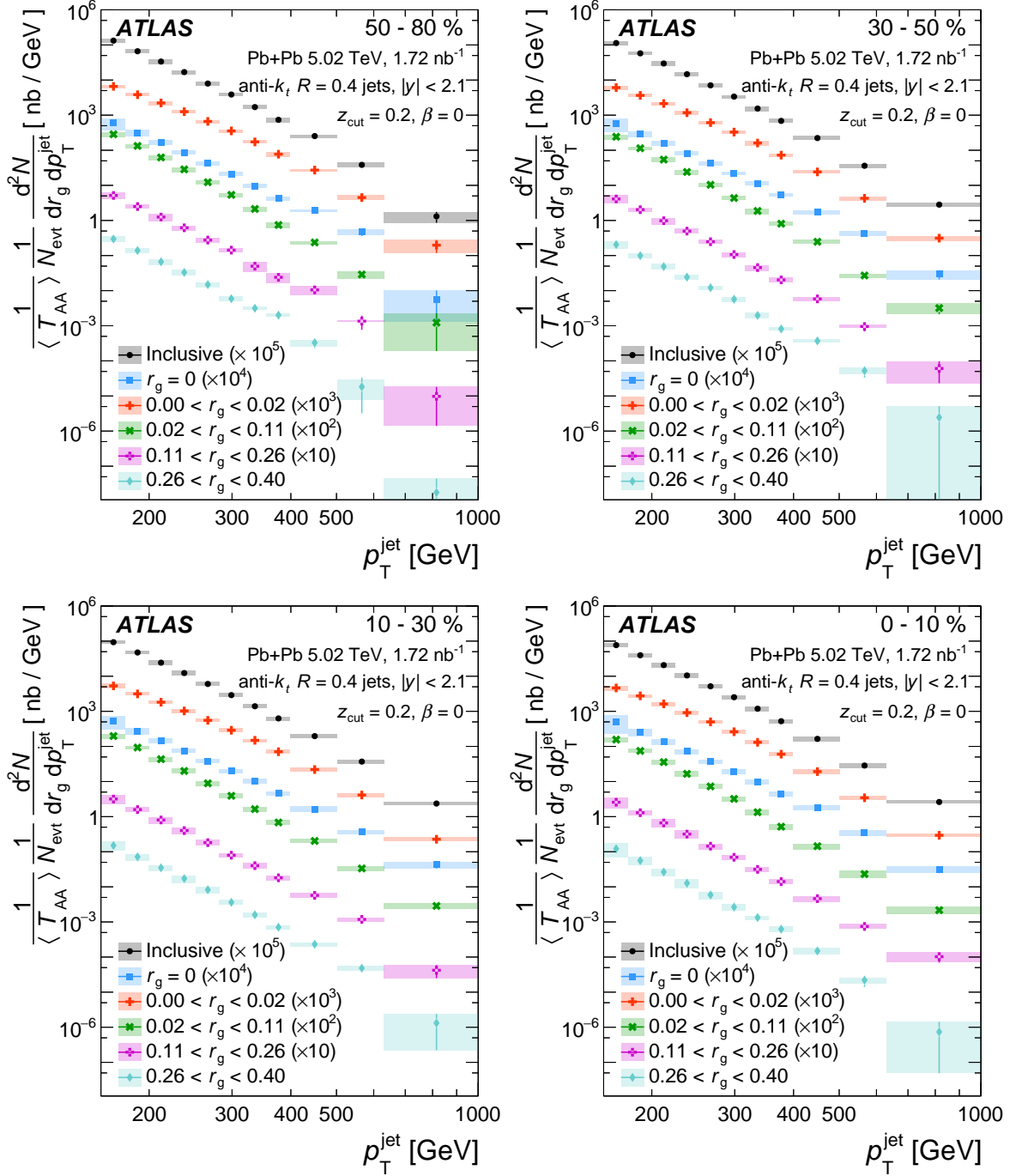


Figure 8: The per-event inclusive jet yields in Pb+Pb collisions at $\sqrt{s_{\text{NN}}} = 5.02$ TeV normalized by $\langle T_{AA} \rangle$ as a function of p_T^{jet} in four centrality intervals. Distributions for inclusive jets (no grooming) and for those jets that fail the soft-drop requirement (denoted by $r_g = 0$) are also shown. For visual clarity, the distributions are scaled by factors specified in the legend. The last bin does not contain the overflow. The statistical uncertainties are indicated by the error bars while the systematic uncertainties are indicated by the shaded bars. The normalization uncertainties of $\langle T_{AA} \rangle$ for each centrality interval are not shown, but are listed in Table 1.

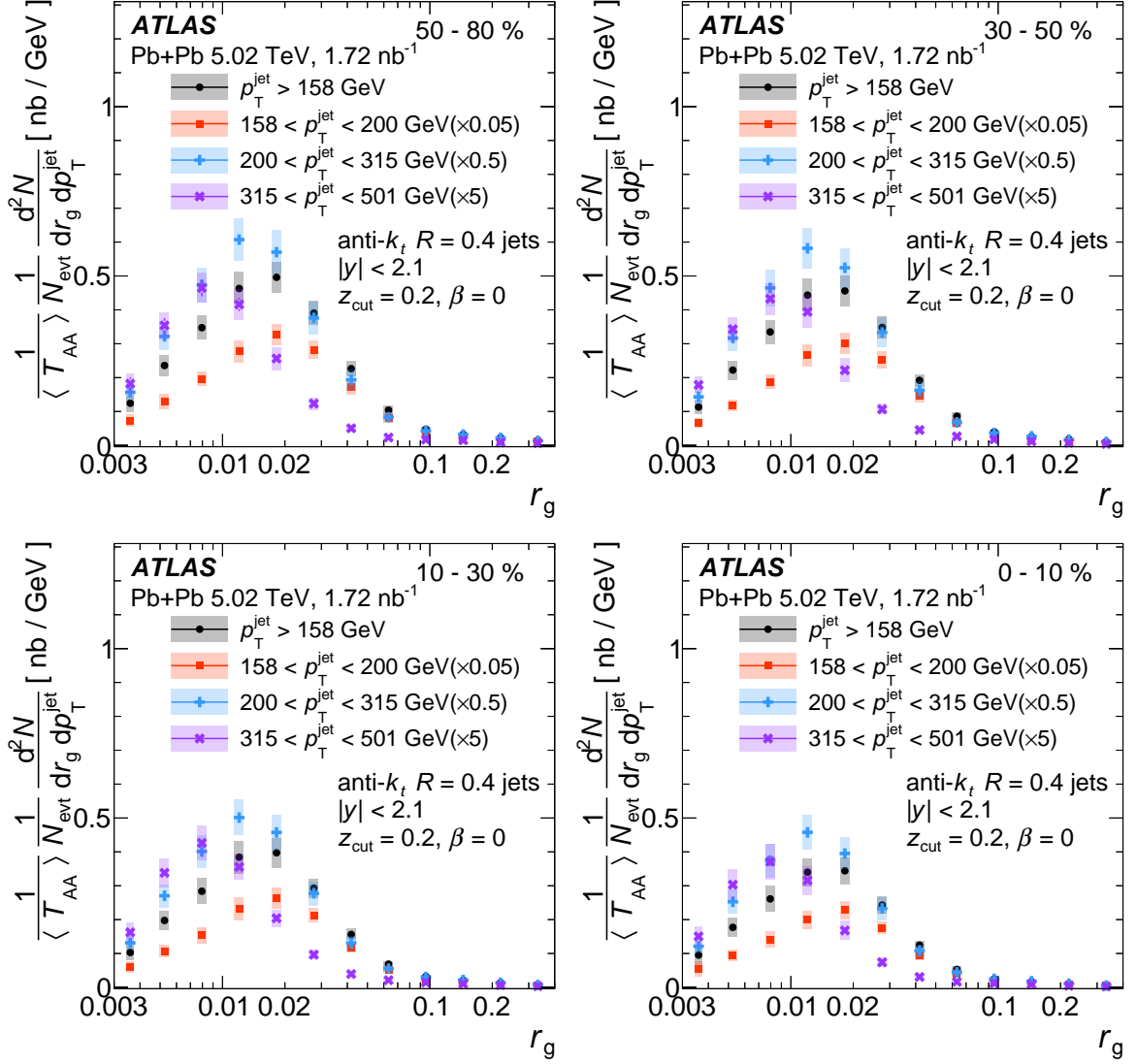


Figure 9: The per-event jet yields in Pb+Pb collisions at $\sqrt{s_{\text{NN}}} = 5.02$ TeV normalized by $\langle T_{AA} \rangle$ as a function of soft-drop r_g in four centrality intervals and three p_T^{jet} intervals as well for $p_T^{\text{jet}} > 158$ GeV. The last bin does not contain the overflow. The statistical uncertainties are indicated by the error bars while the systematic uncertainties are indicated by the shaded bars. The normalization uncertainties of $\langle T_{AA} \rangle$ for each centrality interval are not shown, but are listed in Table 1.

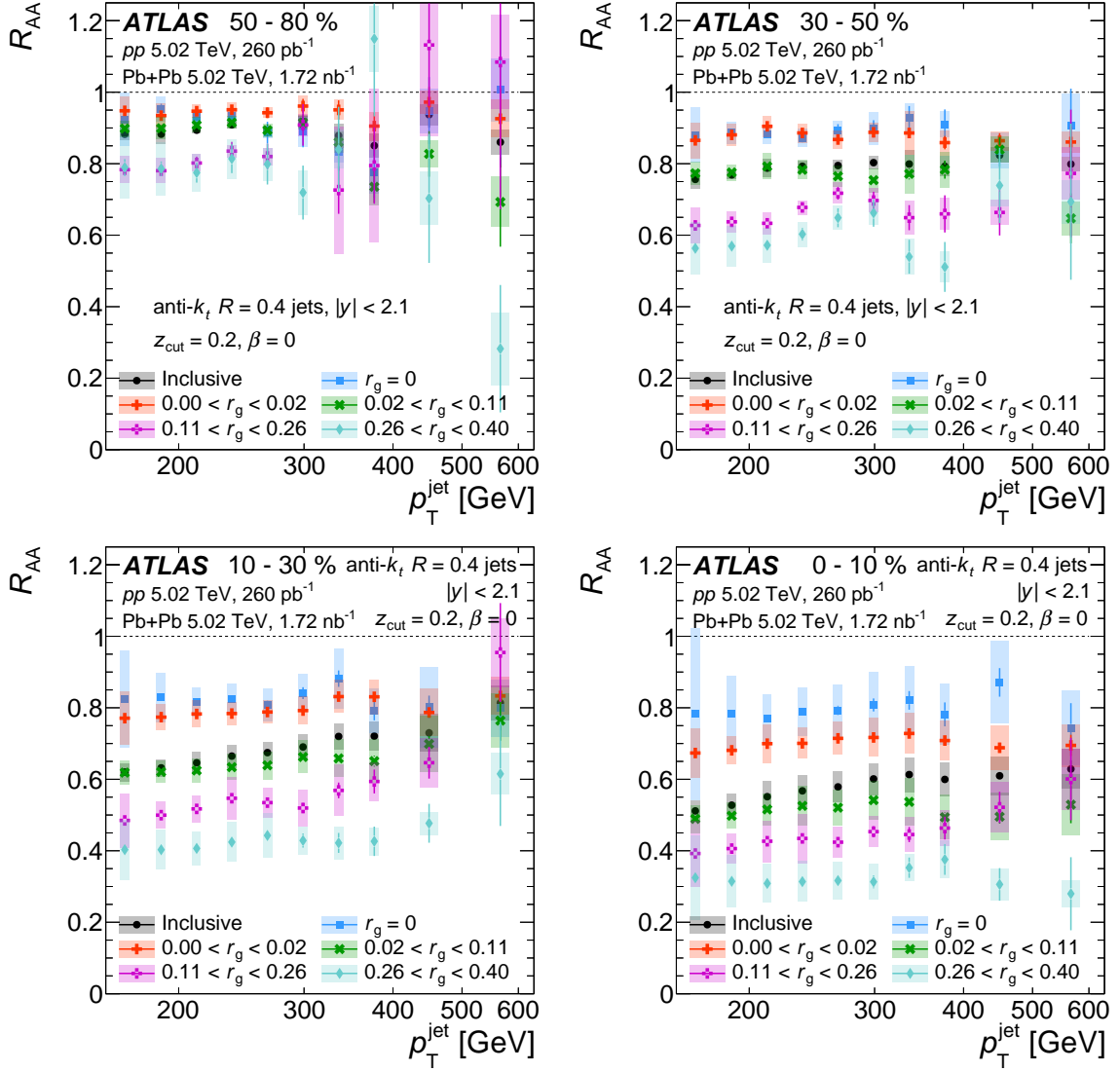


Figure 10: Nuclear modification factor, R_{AA} , as a function of p_T^{jet} for soft-drop groomed jets with $|y| < 2.1$ in four centrality intervals and four intervals of r_g . Groomed jet R_{AA} values are compared with R_{AA} values of jets without significant splitting identified by the soft-drop procedure ($r_g = 0$) and jets without grooming (inclusive). The error bars represent statistical uncertainties while the shaded bars represent bin-wise correlated systematic uncertainties. The uncertainties in the pp luminosity (1.6%) and $\langle T_{AA} \rangle$ are not included, but are listed in Table 1.

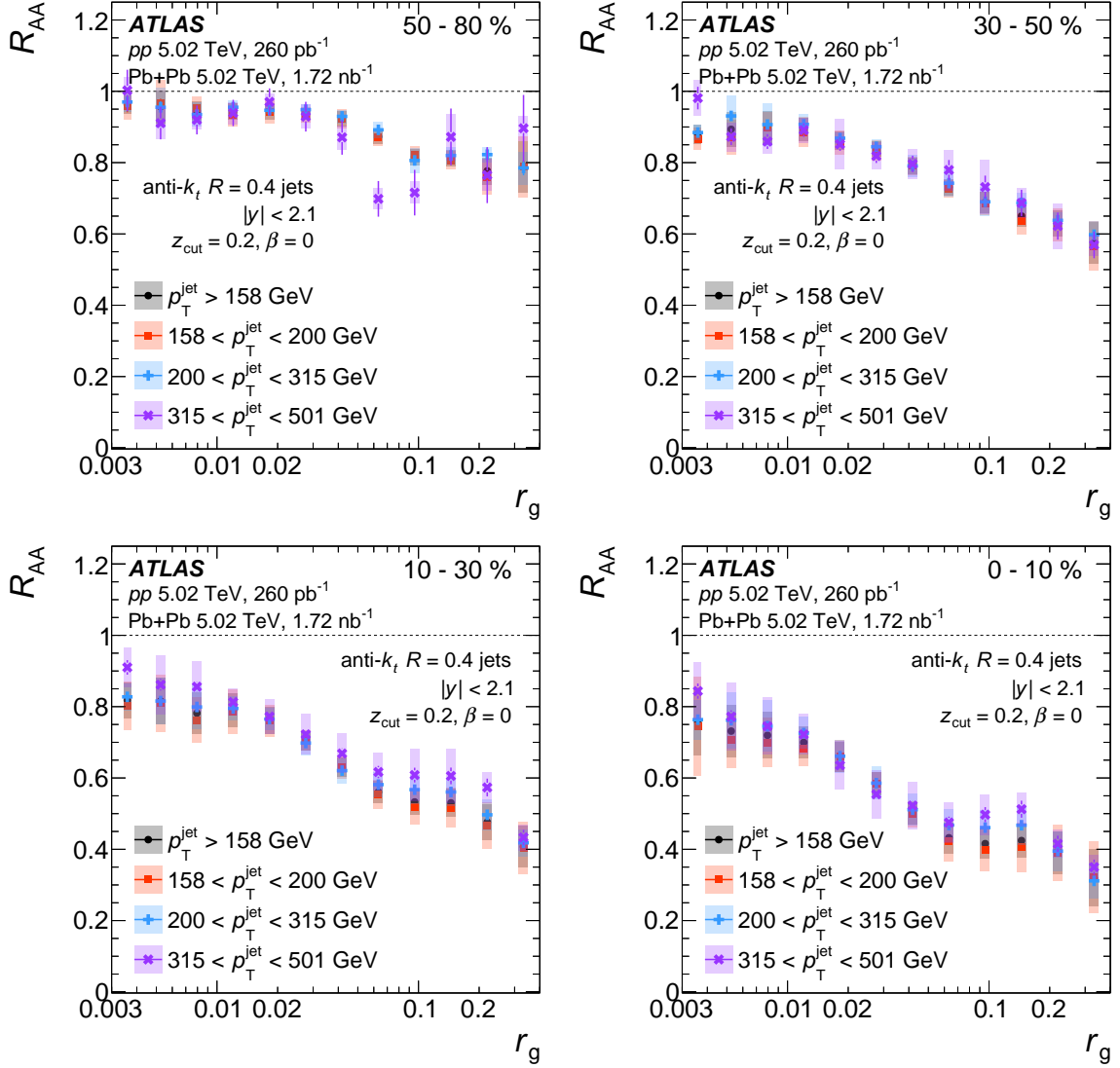


Figure 11: Nuclear modification factor, R_{AA} , as a function of r_g for soft-drop groomed jets with $|y| < 2.1$ in four centrality intervals and three intervals of p_T^{jet} , in comparison with the p_T -inclusive results. The error bars represent statistical uncertainties while the shaded bars represent bin-wise correlated systematic uncertainties. The uncertainties in the pp luminosity (1.6%) and $\langle T_{AA} \rangle$ are not included, but are listed in Table 1.

The jet suppression measurements are compared with predictions from various theoretical models and frameworks including those from the JETSCAPE MC framework [43, 91], Caucal et al. [41, 42, 92] and Ringer et al. [93]. JETSCAPE provides a multistage model of jet evolution by combining several jet-quenching formalisms applied in its range of validity in shower energy and virtuality. The JETSCAPE predictions combine jet energy-loss calculations from the MATTER [94] and LBT [95, 96] models at high and low virtualities of the parton shower in the QGP medium, respectively. The parameters used in generating the predictions, including the transport coefficient (\hat{q}) and the virtuality at which to switch parton energy loss from MATTER to LBT (Q_{sw}), can be found in Ref. [43]. JETSCAPE also includes a virtuality-dependent onset of coherence effects in order to model the inability of the medium to resolve narrow splittings of highly virtual partons at earlier timescales. The model from Caucal et al. presents a perturbative QCD (pQCD) picture of jet quenching dictated by the factorization of medium-induced parton branchings and vacuum-like emissions in a longitudinally expanding medium. An important aspect of this model is the onset of incoherent jet energy loss beyond a critical angle between the branches of the hardest jet splitting. It should be noted that the calculations from Caucal et al. are purely at the parton level and hadronization effects are not included. The analytic calculations for jet R_{AA} by Ringer et al. are based on medium-modified quark and gluon jet functions using a MC sampling approach. In conjunction with the quark and gluon differential jet energy loss, transverse momentum broadening is applied to all the subjects in this model, based on the transport coefficient parameter.

The jet R_{AA} results are compared with predictions from the above frameworks and models as a function of p_T^{jet} and r_g in Figures 12–14. Predictions from JETSCAPE (MATTER+LBT), shown in Figure 12, are able to capture the trend of r_g -dependent jet suppression in three centrality intervals of Pb+Pb collisions. However, JETSCAPE overestimates the R_{AA} values for jets in the low r_g (<0.01) region, especially at higher p_T^{jet} . The R_{AA} predictions from the pQCD picture modeled by Caucal et al., shown in Figure 13, qualitatively describe the r_g -dependent suppression trend observed in the most central collisions. Compared to the data in Figure 13, the parton-level pQCD model calculations predict a sharper drop in R_{AA} around the critical angle beyond which incoherent jet energy loss sets in. The quark vs. gluon differential quenching effects modeled by Ringer et al., labeled ‘med q/g’ in Figure 14, are able to describe the r_g -dependent jet suppression in three intervals of p_T^{jet} . Transverse momentum broadening effects are included in the model calculations by adding p_T kicks perpendicular to the direction of each subject by sampling from a simple Gaussian distribution, whose width is determined using the transport coefficient parameter [93]. The combined model calculations with quark and gluon differential jet energy loss and transverse momentum broadening effects are labeled as ‘med q/g + p_T broadening’ in Figure 14. Adding p_T -broadening effects to the model results in a significant suppression of jets at lower r_g values and a peak in R_{AA} at mid- r_g values, neither of which are observed in data.

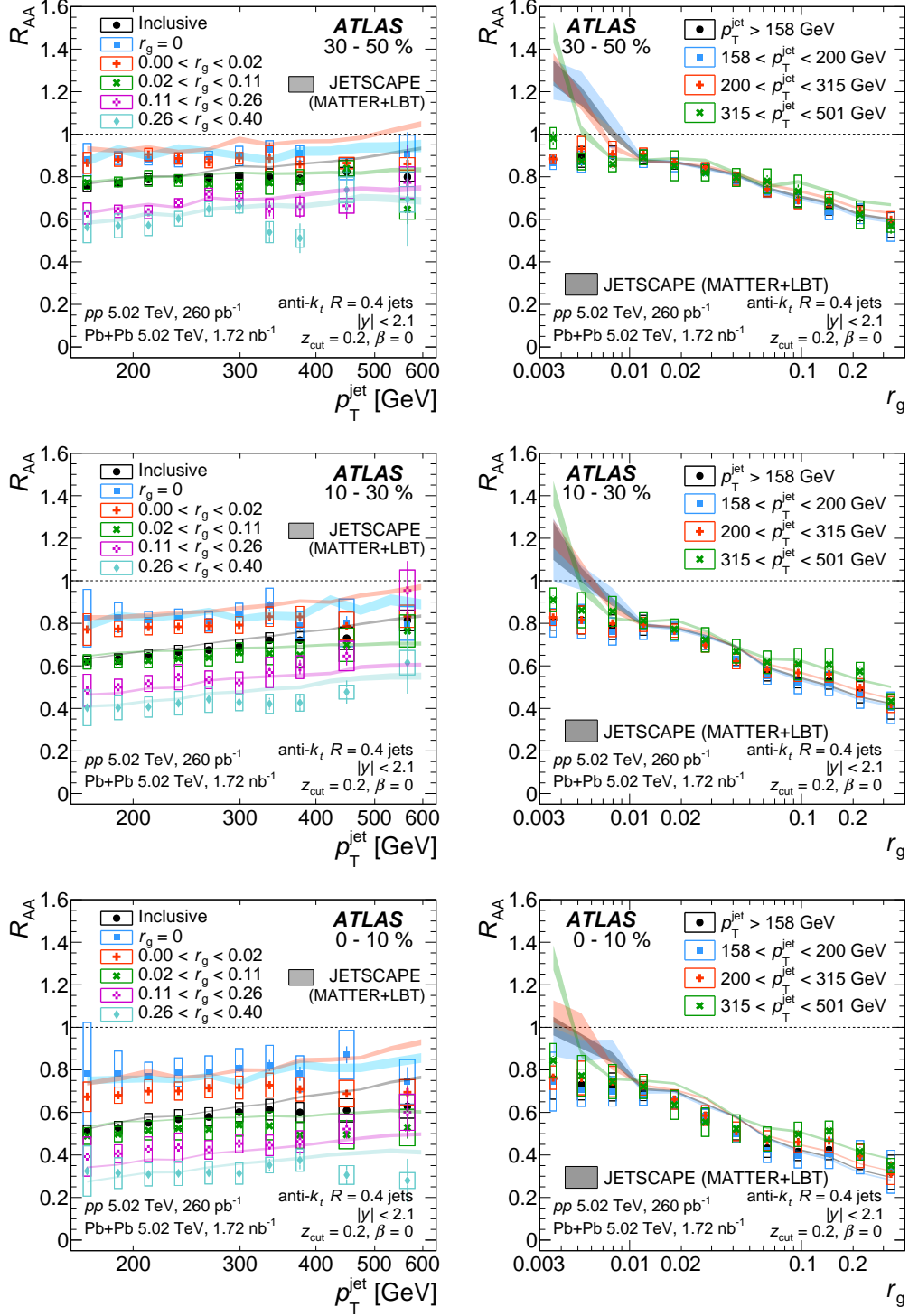


Figure 12: Comparison of R_{AA} as a function of (left) p_T^{jet} for inclusive jets and for four intervals of r_g , (right) r_g for inclusive jets and for three intervals of p_T^{jet} , and in three centrality intervals of Pb+Pb events with predictions from the JETSCAPE framework [43, 91]. The error bars and the open boxes around the data points represent the statistical and systematic uncertainties, respectively. The uncertainties in the pp luminosity (1.6%) and $\langle T_{AA} \rangle$ are not included, but are listed in Table 1. The widths of the bands representing the JETSCAPE predictions indicate their statistical uncertainties.

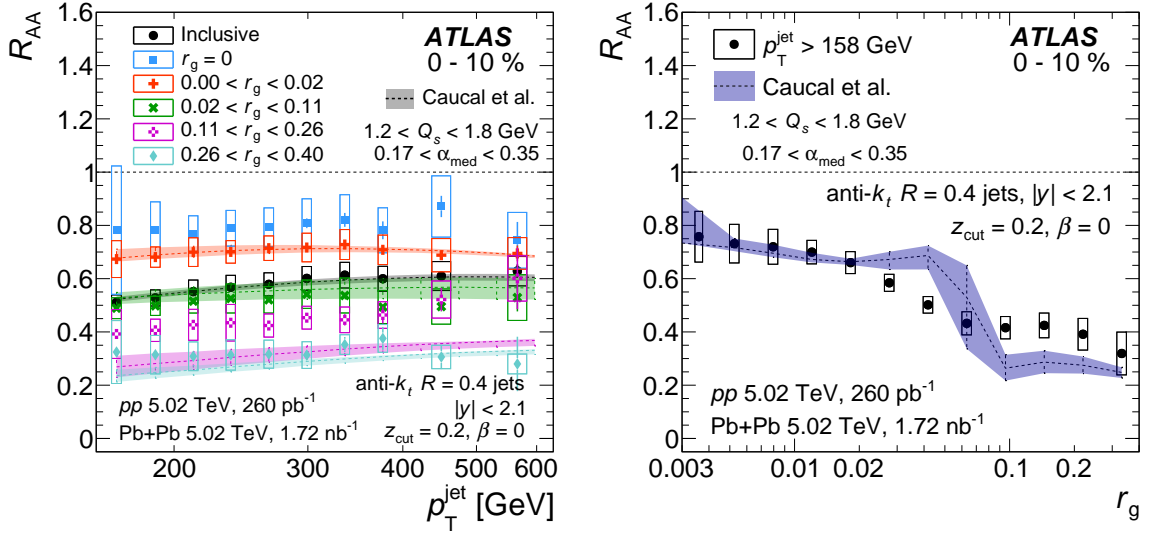


Figure 13: Comparison of R_{AA} as a function of (left) p_T^{jet} for inclusive jets and for four intervals of r_g and (right) as a function of r_g for inclusive jets in 0–10% centrality Pb+Pb events with theoretical predictions from the pQCD framework of Caucal et al., described in Refs. [41, 42, 92]. The error bars and the open boxes around the data points represent the statistical and systematic uncertainties, respectively. The uncertainties in the pp luminosity (1.6%) and $\langle T_{AA} \rangle$ are not included, but are listed in Table 1. The shaded areas around the theoretical predictions represent the uncertainties arising from the variation of the transport coefficient (\hat{q}) and shower cutoff parameters.

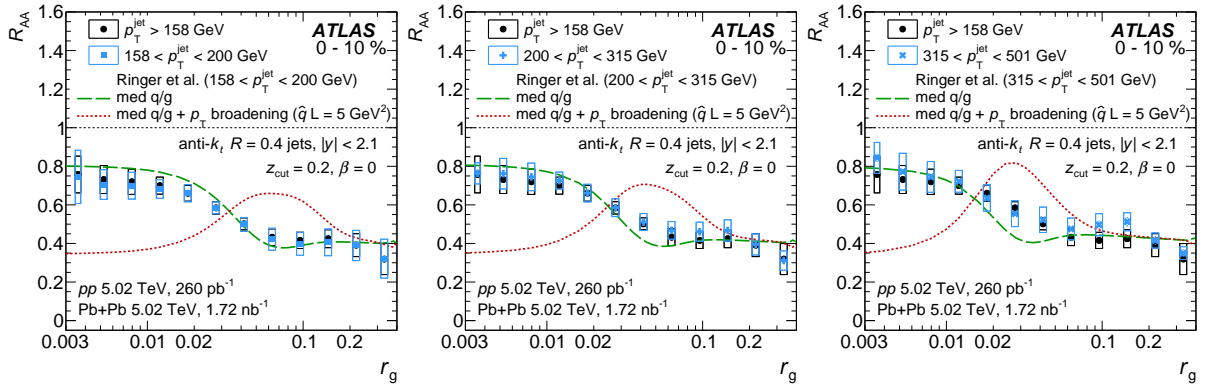


Figure 14: Comparison of R_{AA} as a function of r_g for three intervals of p_T^{jet} in 0–10% centrality Pb+Pb events with theoretical predictions from Ringer et al. [93]. The error bars and the open boxes around the data points represent the statistical and systematic uncertainties, respectively. The uncertainties in the pp luminosity (1.6%) and $\langle T_{AA} \rangle$ are not included, but are listed in Table 1. The green curve (med q/g) represents the quark and gluon differential energy loss setting. The red curve (med q/g + p_T broadening) adds transverse momentum broadening effects for all subjects in the medium.

7 Conclusion

Jet production in Pb+Pb and pp collisions, both at $\sqrt{s_{\text{NN}}} = 5.02$ TeV, is measured with the ATLAS detector at the LHC, using integrated luminosities of 1.72 nb^{-1} and 260 pb^{-1} , respectively. The jets are reconstructed using the anti- k_t algorithm with $R = 0.4$ and groomed using the soft-drop procedure with parameters $z_{\text{cut}} = 0.2$ and $\beta = 0$. The jet differential cross-sections and yields are presented as a function of $p_{\text{T}}^{\text{jet}}$ and r_{g} , the opening angle of the hardest splitting, and in intervals of collision centrality. Results unfolded to the particle level are presented for jets with $p_{\text{T}}^{\text{jet}} > 158$ GeV, $|y| < 2.1$, and $0 \leq r_{\text{g}} < 0.4$.

The r_{g} distributions obtained in pp collisions are observed to peak at lower values of r_{g} with increasing $p_{\text{T}}^{\text{jet}}$, indicating that higher-momentum jets are more collimated. The differential cross-sections as a function of $p_{\text{T}}^{\text{jet}}$ and r_{g} are compared with results from MC event generators (PYTHIA 8, HERWIG, and SHERPA), with the PYTHIA 8 predictions best describing the shape of the $p_{\text{T}}^{\text{jet}}$ and r_{g} spectra seen in pp collisions.

The jet energy loss and the resulting suppression in Pb+Pb collisions is quantified by the nuclear modification factor, R_{AA} . The R_{AA} values are observed to depend primarily on the jet r_{g} value and the event centrality. In the most central collisions, the R_{AA} value ranges between $R_{\text{AA}} \approx 0.75$ for the most collimated jets ($r_{\text{g}} < 0.02$) and $R_{\text{AA}} \approx 0.3$ for the widest jets ($0.26 < r_{\text{g}} < 0.4$). The R_{AA} values are observed to decrease monotonically with increasing r_{g} , and do not depend strongly on $p_{\text{T}}^{\text{jet}}$ for a selected r_{g} range. Although the energy loss is not measured directly and must be inferred from the R_{AA} values and slope of the differential cross-sections as a function of $p_{\text{T}}^{\text{jet}}$, the $p_{\text{T}}^{\text{jet}}$ -dependence is observed to be similar for different r_{g} ranges. These features together with the dependence of R_{AA} on r_{g} indicate that jets with larger opening angles lose more energy. Predictions from theoretical models of jet quenching are compared with the R_{AA} measurements presented here and are observed to describe the r_{g} -dependent jet suppression features with varying accuracy. The results presented here are qualitatively consistent with a picture of jet quenching dictated by coherence and provide the most direct evidence supporting this approach so far.

Acknowledgments

We thank CERN for the very successful operation of the LHC, as well as the support staff from our institutions without whom ATLAS could not be operated efficiently.

We acknowledge the support of ANPCyT, Argentina; YerPhI, Armenia; ARC, Australia; BMWFW and FWF, Austria; ANAS, Azerbaijan; CNPq and FAPESP, Brazil; NSERC, NRC and CFI, Canada; CERN; ANID, Chile; CAS, MOST and NSFC, China; Minciencias, Colombia; MEYS CR, Czech Republic; DNRf and DNSRC, Denmark; IN2P3-CNRS and CEA-DRF/IRFU, France; SRNSFG, Georgia; BMBF, HGF and MPG, Germany; GSRI, Greece; RGC and Hong Kong SAR, China; ISF and Benozziyo Center, Israel; INFN, Italy; MEXT and JSPS, Japan; CNRST, Morocco; NWO, Netherlands; RCN, Norway; MEiN, Poland; FCT, Portugal; MNE/IFA, Romania; MESTD, Serbia; MSSR, Slovakia; ARRS and MIZŠ, Slovenia; DSI/NRF, South Africa; MICINN, Spain; SRC and Wallenberg Foundation, Sweden; SERI, SNSF and Cantons of Bern and Geneva, Switzerland; MOST, Taiwan; TENMAK, Türkiye; STFC, United Kingdom; DOE and NSF, United States of America. In addition, individual groups and members have received support from BCKDF, CANARIE, Compute Canada and CRC, Canada; PRIMUS 21/SCI/017 and UNCE SCI/013, Czech Republic; COST, ERC, ERDF, Horizon 2020 and Marie Skłodowska-Curie Actions, European Union; Investissements d'Avenir Labex, Investissements d'Avenir Idex and ANR, France; DFG and AvH Foundation, Germany; Herakleitos, Thales and Aristeia programmes co-financed by EU-ESF and the

Greek NSRF, Greece; BSF-NSF and MINERVA, Israel; Norwegian Financial Mechanism 2014-2021, Norway; NCN and NAWA, Poland; La Caixa Banking Foundation, CERCA Programme Generalitat de Catalunya and PROMETEO and GenT Programmes Generalitat Valenciana, Spain; Göran Gustafssons Stiftelse, Sweden; The Royal Society and Leverhulme Trust, United Kingdom.

The crucial computing support from all WLCG partners is acknowledged gratefully, in particular from CERN, the ATLAS Tier-1 facilities at TRIUMF (Canada), NDGF (Denmark, Norway, Sweden), CC-IN2P3 (France), KIT/GridKA (Germany), INFN-CNAF (Italy), NL-T1 (Netherlands), PIC (Spain), ASGC (Taiwan), RAL (UK) and BNL (USA), the Tier-2 facilities worldwide and large non-WLCG resource providers. Major contributors of computing resources are listed in Ref. [97].

References

- [1] STAR Collaboration, *Experimental and theoretical challenges in the search for the quark gluon plasma: The STAR Collaboration's critical assessment of the evidence from RHIC collisions*, *Nucl. Phys. A* **757** (2005) 102, arXiv: [nucl-ex/0501009](#).
- [2] PHENIX Collaboration, *Formation of dense partonic matter in relativistic nucleus-nucleus collisions at RHIC: Experimental evaluation by the PHENIX collaboration*, *Nucl. Phys. A* **757** (2005) 184, arXiv: [nucl-ex/0410003](#).
- [3] M. Gyulassy and L. McLerran, *New forms of QCD matter discovered at RHIC*, *Nucl. Phys. A* **750** (2005) 30, arXiv: [nucl-th/0405013](#).
- [4] W. Busza, K. Rajagopal, and W. van der Schee, *Heavy Ion Collisions: The Big Picture, and the Big Questions*, *Ann. Rev. Nucl. Part. Sci.* **68** (2018) 339, arXiv: [1802.04801 \[hep-ph\]](#).
- [5] M. Gyulassy and M. Plümer, *Jet quenching in dense matter*, *Phys. Lett. B* **243** (1990) 432.
- [6] J. D. Bjorken, *Energy Loss of Energetic Partons in Quark - Gluon Plasma: Possible Extinction of High $p(t)$ Jets in Hadron - Hadron Collisions*, FERMILAB-PUB-82-059-THY (1982).
- [7] D. Krohn, J. Thaler, and L.-T. Wang, *Jet trimming*, *JHEP* **02** (2010) 084, arXiv: [0912.1342 \[hep-ph\]](#).
- [8] M. Dasgupta, A. Fregoso, S. Marzani, and G. P. Salam, *Towards an understanding of jet substructure*, *JHEP* **09** (2013) 029, arXiv: [1307.0007 \[hep-ph\]](#).
- [9] A. J. Larkoski, S. Marzani, G. Soyez, and J. Thaler, *Soft drop*, *JHEP* **05** (2014) 146, arXiv: [1402.2657 \[hep-ph\]](#).
- [10] ATLAS Collaboration, *Measurement of the Soft-Drop Jet Mass in pp Collisions at $\sqrt{s} = 13$ TeV with the ATLAS detector*, *Phys. Rev. Lett.* **121** (2018) 092001, arXiv: [1711.08341 \[hep-ex\]](#).
- [11] ATLAS Collaboration, *Measurement of soft-drop jet observables in pp collisions with the ATLAS detector at $\sqrt{s} = 13$ TeV*, *Phys. Rev. D* **101** (2020) 052007, arXiv: [1912.09837 \[hep-ex\]](#).
- [12] Y. Mehtar-Tani and K. Tywoniuk, *Groomed jets in heavy-ion collisions: sensitivity to medium-induced bremsstrahlung*, *JHEP* **04** (2017) 125, arXiv: [1610.08930 \[hep-ph\]](#).

- [13] Y.-T. Chien and I. Vitev, *Probing the Hardest Branching within Jets in Heavy-Ion Collisions*, *Phys. Rev. Lett.* **119** (2017) 112301, arXiv: [1608.07283 \[hep-ph\]](#).
- [14] H. A. Andrews et al., *Novel tools and observables for jet physics in heavy-ion collisions*, *J. Phys. G* **47** (2020) 065102, arXiv: [1808.03689 \[hep-ph\]](#).
- [15] CMS Collaboration, *Measurement of the Splitting Function in pp and PbPb collisions at $\sqrt{s_{NN}} = 5.02$ TeV*, *Phys. Rev. Lett.* **120** (2018) 142302, arXiv: [1708.09429 \[hep-ex\]](#).
- [16] CMS Collaboration, *Measurement of the groomed jet mass in PbPb and pp collisions at $\sqrt{s_{NN}} = 5.02$ TeV*, *JHEP* **10** (2018) 161, arXiv: [1805.05145 \[hep-ex\]](#).
- [17] ALICE Collaboration, *Exploration of jet substructure using iterative declustering in pp and Pb–Pb collisions at LHC energies*, *Phys. Lett. B* **802** (2020) 135227, arXiv: [1905.02512 \[nucl-ex\]](#).
- [18] ALICE Collaboration, *Measurement of the groomed jet radius and momentum splitting fraction in pp and Pb–Pb collisions at $\sqrt{s_{NN}} = 5.02$ TeV*, *Phys. Rev. Lett.* **128** (2022) 102001, arXiv: [2107.12984 \[nucl-ex\]](#).
- [19] STAR Collaboration, *Differential measurements of jet substructure and partonic energy loss in Au+Au collisions at $\sqrt{s_{NN}} = 200$ GeV*, *Phys. Rev. C* **105** (2022) 044906, arXiv: [2109.09793 \[nucl-ex\]](#).
- [20] P. Foka and M. A. Janik, *An overview of experimental results from ultra-relativistic heavy-ion collisions at the CERN LHC: Hard probes*, *Rev. Phys.* **1** (2016) 172, arXiv: [1702.07231 \[hep-ex\]](#).
- [21] L. Cunqueiro and A. M. Sickles, *Studying the QGP with Jets at the LHC and RHIC*, *Prog. Part. Nucl. Phys.* **124** (2022) 103940, arXiv: [2110.14490 \[nucl-ex\]](#).
- [22] ATLAS Collaboration, *Measurement of the jet radius and transverse momentum dependence of inclusive jet suppression in lead–lead collisions at $\sqrt{s_{NN}} = 2.76$ TeV with the ATLAS detector*, *Phys. Lett. B* **719** (2013) 220, arXiv: [1208.1967 \[hep-ex\]](#).
- [23] ATLAS Collaboration, *Measurements of the Nuclear Modification Factor for Jets in Pb+Pb Collisions at $\sqrt{s_{NN}} = 2.76$ TeV with the ATLAS Detector*, *Phys. Rev. Lett.* **114** (2015) 072302, arXiv: [1411.2357 \[hep-ex\]](#).
- [24] ATLAS Collaboration, *Measurement of the nuclear modification factor for inclusive jets in Pb+Pb collisions at $\sqrt{s_{NN}} = 5.02$ TeV with the ATLAS detector*, *Phys. Lett. B* **790** (2019) 108, arXiv: [1805.05635 \[hep-ex\]](#).
- [25] CMS Collaboration, *Measurement of inclusive jet cross-sections in pp and PbPb collisions at $\sqrt{s_{NN}} = 2.76$ TeV*, *Phys. Rev. C* **96** (2017) 015202, arXiv: [1609.05383 \[hep-ex\]](#).
- [26] CMS Collaboration, *First measurement of large area jet transverse momentum spectra in heavy-ion collisions*, *JHEP* **05** (2021) 284, arXiv: [2102.13080 \[hep-ex\]](#).
- [27] ATLAS Collaboration, *Observation of a Centrality-Dependent Dijet Asymmetry in Lead–Lead Collisions at $\sqrt{s_{NN}} = 2.76$ TeV with the ATLAS Detector at the LHC*, *Phys. Rev. Lett.* **105** (2010) 252303, arXiv: [1011.6182 \[hep-ex\]](#).

- [28] ATLAS Collaboration, *Measurement of photon-jet transverse momentum correlations in 5.02 TeV Pb+Pb and pp collisions with ATLAS*, *Phys. Lett. B* **789** (2019) 167, arXiv: [1809.07280 \[hep-ex\]](#).
- [29] CMS Collaboration, *In-medium modification of dijets in PbPb collisions at $\sqrt{s_{NN}} = 5.02$ TeV*, *JHEP* **05** (2021) 116, arXiv: [2101.04720 \[hep-ex\]](#).
- [30] CMS Collaboration, *Study of jet quenching with Z+jet correlations in PbPb and pp collisions at $\sqrt{s_{NN}} = 5.02$ TeV*, *Phys. Rev. Lett.* **119** (2017) 082301, arXiv: [1702.01060 \[hep-ex\]](#).
- [31] ATLAS Collaboration, *Measurement of jet fragmentation in Pb+Pb and pp collisions at $\sqrt{s_{NN}} = 5.02$ TeV with the ATLAS detector*, *Phys. Rev. C* **98** (2018) 024908, arXiv: [1805.05424 \[hep-ex\]](#).
- [32] ATLAS Collaboration, *Comparison of Fragmentation Functions for Jets Dominated by Light Quarks and Gluons from pp and Pb+Pb Collisions in ATLAS*, *Phys. Rev. Lett.* **123** (2019) 042001, arXiv: [1902.10007 \[hep-ex\]](#).
- [33] CMS Collaboration, *Measurement of jet fragmentation in PbPb and pp collisions at $\sqrt{s_{NN}} = 2.76$ TeV*, *Phys. Rev. C* **90** (2014) 024908, arXiv: [1406.0932 \[hep-ex\]](#).
- [34] CMS Collaboration, *Observation of Medium Induced Modifications of Jet Fragmentation in PbPb Collisions at $\sqrt{s_{NN}} = 5.02$ TeV Using Isolated Photon-Tagged Jets*, *Phys. Rev. Lett.* **121** (2018) 242301, arXiv: [1801.04895 \[hep-ex\]](#).
- [35] CMS Collaboration, *Jet properties in PbPb and pp collisions at $\sqrt{s_{NN}} = 5.02$ TeV*, *JHEP* **05** (2018) 006, arXiv: [1803.00042 \[hep-ex\]](#).
- [36] STAR Collaboration, *Measurement of groomed jet substructure observables in p+p collisions at $\sqrt{s} = 200$ GeV with STAR*, *Phys. Lett. B* **811** (2020) 135846, arXiv: [2003.02114 \[hep-ex\]](#).
- [37] Yu. L. Dokshitzer, V. A. Khoze, S. I. Troyan, and A. H. Mueller, *QCD coherence in high-energy reactions*, *Rev. Mod. Phys.* **60** (1988) 373.
- [38] R. Baier, Yu. L. Dokshitzer, A. H. Mueller, S. Peigné, and D. Schiff, *Radiative energy loss of high-energy quarks and gluons in a finite volume quark - gluon plasma*, *Nucl. Phys. B* **483** (1997) 291, arXiv: [hep-ph/9607355 \[hep-ph\]](#).
- [39] J. Casalderrey-Solana, Y. Mehtar-Tani, C. A. Salgado, and K. Tywoniuk, *New picture of jet quenching dictated by color coherence*, *Phys. Lett. B* **725** (2013) 357, arXiv: [1210.7765 \[hep-ph\]](#).
- [40] G. Milhano, U. A. Wiedemann, and K. C. Zapp, *Sensitivity of jet substructure to jet-induced medium response*, *Phys. Lett. B* **779** (2018) 409, arXiv: [1707.04142 \[hep-ph\]](#).
- [41] P. Caucal, E. Iancu, and G. Soyez, *Deciphering the z_g distribution in ultrarelativistic heavy ion collisions*, *JHEP* **10** (2019) 273, arXiv: [1907.04866 \[hep-ph\]](#).
- [42] P. Caucal, E. Iancu, and G. Soyez, *Jet radiation in a longitudinally expanding medium*, *JHEP* **04** (2021) 209, arXiv: [2012.01457 \[hep-ph\]](#).

- [43] A. Kumar et al., *Inclusive Jet and Hadron Suppression in a Multi-Stage Approach*, (2022), arXiv: [2204.01163 \[hep-ph\]](#).
- [44] M. Cacciari, G. P. Salam, and G. Soyez, *The anti- k_t jet clustering algorithm*, *JHEP* **04** (2008) 063, arXiv: [0802.1189 \[hep-ph\]](#).
- [45] ATLAS Collaboration, *The ATLAS Experiment at the CERN Large Hadron Collider*, *JINST* **3** (2008) S08003.
- [46] ATLAS Collaboration, *ATLAS Insertable B-Layer Technical Design Report*, ATLAS-TDR-19; CERN-LHCC-2010-013, 2010, URL: <https://cds.cern.ch/record/1291633>, Addendum: ATLAS-TDR-19-ADD-1; CERN-LHCC-2012-009, 2012, URL: <https://cds.cern.ch/record/1451888>.
- [47] B. Abbott et al., *Production and integration of the ATLAS Insertable B-Layer*, *JINST* **13** (2018) T05008, arXiv: [1803.00844 \[physics.ins-det\]](#).
- [48] ATLAS Collaboration, *Performance of the ATLAS trigger system in 2015*, *Eur. Phys. J. C* **77** (2017) 317, arXiv: [1611.09661 \[hep-ex\]](#).
- [49] ATLAS Collaboration, *The ATLAS Collaboration Software and Firmware*, ATL-SOFT-PUB-2021-001, 2021, URL: <https://cds.cern.ch/record/2767187>.
- [50] ATLAS Collaboration, *ATLAS data quality operations and performance for 2015–2018 data-taking*, *JINST* **15** (2020) P04003, arXiv: [1911.04632 \[physics.ins-det\]](#).
- [51] ATLAS Collaboration, *Measurement of azimuthal anisotropy of muons from charm and bottom hadrons in Pb+Pb collisions at $\sqrt{s_{NN}} = 5.02$ TeV with the ATLAS detector*, *Phys. Lett. B* **807** (2020) 135595, arXiv: [2003.03565 \[hep-ex\]](#).
- [52] M. L. Miller, K. Reygers, S. J. Sanders, and P. Steinberg, *Glauber Modeling in High-Energy Nuclear Collisions*, *Ann. Rev. Nucl. Part. Sci.* **57** (2007) 205, arXiv: [nucl-ex/0701025 \[nucl-ex\]](#).
- [53] C. Loizides, J. Nagle, and P. Steinberg, *Improved version of the PHOBOS Glauber Monte Carlo*, *SoftwareX* **1-2** (2015) 13, arXiv: [1408.2549 \[nucl-ex\]](#).
- [54] ATLAS Collaboration, *Measurement of W^\pm boson production in Pb+Pb collisions at $\sqrt{s_{NN}} = 5.02$ TeV with the ATLAS detector*, *Eur. Phys. J. C* **79** (2019) 935, arXiv: [1907.10414 \[hep-ex\]](#).
- [55] T. Sjöstrand et al., *An introduction to PYTHIA 8.2*, *Comput. Phys. Commun.* **191** (2015) 159, arXiv: [1410.3012 \[hep-ph\]](#).
- [56] ATLAS Collaboration, *ATLAS Pythia 8 tunes to 7 TeV data*, ATL-PHYS-PUB-2014-021, 2014, URL: <https://cds.cern.ch/record/1966419>.
- [57] R. D. Ball et al., *Parton distributions with LHC data*, *Nucl. Phys. B* **867** (2013) 244, arXiv: [1207.1303 \[hep-ph\]](#).
- [58] S. Agostinelli et al., *Geant4—a simulation toolkit*, *Nucl. Instrum. Meth. A* **506** (2003) 250, ISSN: 0168-9002.
- [59] ATLAS Collaboration, *The ATLAS Simulation Infrastructure*, *Eur. Phys. J. C* **70** (2010) 823, arXiv: [1005.4568 \[physics.ins-det\]](#).
- [60] ATLAS Collaboration, *Measurements of azimuthal anisotropies of jet production in Pb+Pb collisions at $\sqrt{s_{NN}} = 5.02$ TeV with the ATLAS detector*, *Phys. Rev. C* **105** (2022) 064903, arXiv: [2111.06606 \[nucl-ex\]](#).

- [61] M. Cacciari, G. P. Salam, and G. Soyez, *FastJet user manual*, *Eur. Phys. J. C* **72** (2012) 1896, arXiv: [1111.6097 \[hep-ph\]](#).
- [62] ATLAS Collaboration, *Jet energy measurement with the ATLAS detector in proton–proton collisions at $\sqrt{s} = 7$ TeV*, *Eur. Phys. J. C* **73** (2013) 2304, arXiv: [1112.6426 \[hep-ex\]](#).
- [63] ATLAS Collaboration, *Measurement of the azimuthal anisotropy of charged particles produced in $\sqrt{s_{NN}} = 5.02$ TeV Pb+Pb collisions with the ATLAS detector*, *Eur. Phys. J. C* **78** (2018) 997, arXiv: [1808.03951 \[hep-ex\]](#).
- [64] ATLAS Collaboration, *Observation of Long-Range Elliptical Azimuthal Anisotropies in $\sqrt{s} = 13$ and 2.76 TeV pp Collisions with the ATLAS Detector*, *Phys. Rev. Lett.* **116** (2016) 172301, arXiv: [1509.04776 \[hep-ex\]](#).
- [65] ATLAS Collaboration, *Jet energy scale and its uncertainty for jets reconstructed using the ATLAS heavy ion jet algorithm*, ATLAS-CONF-2015-016, 2015, URL: <https://cds.cern.ch/record/2008677>.
- [66] ATLAS Collaboration, *Topological cell clustering in the ATLAS calorimeters and its performance in LHC Run 1*, *Eur. Phys. J. C* **77** (2017) 490, arXiv: [1603.02934 \[hep-ex\]](#).
- [67] ATLAS Collaboration, *Improving jet substructure performance in ATLAS using Track-CaloClusters*, ATL-PHYS-PUB-2017-015, 2017, URL: <https://cds.cern.ch/record/2275636>.
- [68] ATLAS Collaboration, *A W/Z-boson tagger using Track-CaloCluster jets with ATLAS*, ATL-PHYS-PUB-2020-008, 2020, URL: <https://cds.cern.ch/record/2718218>.
- [69] ATLAS Collaboration, *Jet reconstruction and performance using particle flow with the ATLAS Detector*, *Eur. Phys. J. C* **77** (2017) 466, arXiv: [1703.10485 \[hep-ex\]](#).
- [70] ATLAS Collaboration, *Optimisation of large-radius jet reconstruction for the ATLAS detector in 13 TeV proton–proton collisions*, *Eur. Phys. J. C* **81** (2020) 334, arXiv: [2009.04986 \[hep-ex\]](#).
- [71] ATLAS Collaboration, *Performance of the ATLAS track reconstruction algorithms in dense environments in LHC Run 2*, *Eur. Phys. J. C* **77** (2017) 673, arXiv: [1704.07983 \[hep-ex\]](#).
- [72] ATLAS Collaboration, *Measurement of charged-particle spectra in Pb+Pb collisions at $\sqrt{s_{NN}} = 2.76$ TeV with the ATLAS detector at the LHC*, *JHEP* **09** (2015) 050, arXiv: [1504.04337 \[hep-ex\]](#).
- [73] M. Wobisch and T. Wengler, “Hadronization corrections to jet cross-sections in deep inelastic scattering,” *Workshop on Monte Carlo Generators for HERA Physics (Plenary Starting Meeting)*, 1998 270, arXiv: [hep-ph/9907280](#).
- [74] Yu. L. Dokshitzer, G. D. Leder, S. Moretti and B. R. Webber, *Better jet clustering algorithms*, *JHEP* **08** (1997) 001, arXiv: [hep-ph/9707323](#).
- [75] J. Mulligan and M. Ploskon, *Identifying groomed jet splittings in heavy-ion collisions*, *Phys. Rev. C* **102** (2020) 044913, arXiv: [2006.01812 \[hep-ph\]](#).

- [76] T. Auye, “Unfolding algorithms and tests using RooUnfold,” *Proceedings, 2011 Workshop on Statistical Issues Related to Discovery Claims in Search Experiments and Unfolding (PHYSTAT 2011)* (CERN, Geneva, Switzerland, Jan. 17–20, 2011) 313, arXiv: [1105.1160 \[physics.data-an\]](#).
- [77] G. D’Agostini, *A multidimensional unfolding method based on Bayes’ theorem*, *Nucl. Instrum. Meth. A* **362** (1995) 487, ISSN: 0168-9002.
- [78] ATLAS Collaboration, *Jet energy scale measurements and their systematic uncertainties in proton–proton collisions at $\sqrt{s} = 13$ TeV with the ATLAS detector*, *Phys. Rev. D* **96** (2017) 072002, arXiv: [1703.09665 \[hep-ex\]](#).
- [79] ATLAS Collaboration, *Jet energy resolution in proton–proton collisions at $\sqrt{s} = 7$ TeV recorded in 2010 with the ATLAS detector*, *Eur. Phys. J. C* **73** (2013) 2306, arXiv: [1210.6210 \[hep-ex\]](#).
- [80] ATLAS Collaboration, *Measurements of jet vetoes and azimuthal decorrelations in dijet events produced in pp collisions at $\sqrt{s} = 7$ TeV using the ATLAS detector*, *Eur. Phys. J. C* **74** (2014) 3117, arXiv: [1407.5756 \[hep-ex\]](#).
- [81] ATLAS Collaboration, *Study of the material of the ATLAS inner detector for Run 2 of the LHC*, *JINST* **12** (2017) P12009, arXiv: [1707.02826 \[hep-ex\]](#).
- [82] ATLAS Collaboration, *Measurement of track reconstruction inefficiencies in the core of jets via pixel dE/dx with the ATLAS experiment using $\sqrt{s} = 13$ TeV pp collision data*, ATL-PHYS-PUB-2016-007, 2016, URL: <https://cds.cern.ch/record/2140460>.
- [83] ATLAS Collaboration, *Evaluating statistical uncertainties and correlations using the bootstrap method*, ATL-PHYS-PUB-2021-011, 2021, URL: <https://cds.cern.ch/record/2759945>.
- [84] G. Avoni et al., *The new LUCID-2 detector for luminosity measurement and monitoring in ATLAS*, *JINST* **13** (2018) P07017.
- [85] ATLAS Collaboration, *Luminosity determination in pp collisions at $\sqrt{s} = 13$ TeV using the ATLAS detector at the LHC*, ATL-CONF-2019-021, 2019, URL: <https://cds.cern.ch/record/2677054>.
- [86] J. Bellm et al., *Herwig 7.1 Release Note*, (2017), arXiv: [1705.06919 \[hep-ph\]](#).
- [87] R. D. Ball et al., *Parton distributions for the LHC run II*, *JHEP* **04** (2015) 040, arXiv: [1410.8849 \[hep-ph\]](#).
- [88] E. Bothmann et al., *Event generation with Sherpa 2.2*, *SciPost Phys.* **7** (2019) 034, arXiv: [1905.09127 \[hep-ph\]](#).
- [89] S. Schumann and F. Krauss, *A parton shower algorithm based on Catani–Seymour dipole factorisation*, *JHEP* **03** (2008) 038, arXiv: [0709.1027 \[hep-ph\]](#).
- [90] S. Dulat et al., *New parton distribution functions from a global analysis of quantum chromodynamics*, *Phys. Rev. D* **93** (2016) 033006, arXiv: [1506.07443 \[hep-ph\]](#).
- [91] J. H. Putschke et al., *The JETSCAPE framework*, (2019), arXiv: [1903.07706 \[nucl-th\]](#).
- [92] P. Caucal, E. Iancu, A. H. Mueller, and G. Soyez, *Vacuumlike Jet Fragmentation in a Dense QCD Medium*, *Phys. Rev. Lett.* **120** (2018) 232001, arXiv: [1801.09703 \[hep-ph\]](#).

- [93] F. Ringer, B.-W. Xiao, and F. Yuan, *Can we observe jet P_T -broadening in heavy-ion collisions at the LHC?* [Phys. Lett. B **808** \(2020\) 135634](#), arXiv: [1907.12541 \[hep-ph\]](#).
- [94] A. Majumder, *Incorporating space-time within medium-modified jet event generators*, [Phys. Rev. C **88** \(2013\) 014909](#), arXiv: [1301.5323 \[nucl-th\]](#).
- [95] Y. He, T. Luo, X.-N. Wang, and Y. Zhu, *Linear Boltzmann transport for jet propagation in the quark-gluon plasma: Elastic processes and medium recoil*, [Phys. Rev. C **91** \(2015\) 054908](#), [Erratum: [Phys. Rev. C **97**, \(2018\) 019902](#)], arXiv: [1503.03313 \[nucl-th\]](#).
- [96] S. Cao, T. Luo, G.-Y. Qin, and X.-N. Wang, *Linearized Boltzmann transport model for jet propagation in the quark-gluon plasma: Heavy quark evolution*, [Phys. Rev. C **94** \(2016\) 014909](#), arXiv: [1605.06447 \[nucl-th\]](#).
- [97] ATLAS Collaboration, *ATLAS Computing Acknowledgements*, ATL-SOFT-PUB-2021-003, 2021, URL: <https://cds.cern.ch/record/2776662>.

The ATLAS Collaboration

G. Aad ¹⁰¹, B. Abbott ¹¹⁹, D.C. Abbott ¹⁰², K. Abeling ⁵⁵, S.H. Abidi ²⁹, A. Aboulhorma ^{35e}, H. Abramowicz ¹⁵⁰, H. Abreu ¹⁴⁹, Y. Abulaiti ¹¹⁶, A.C. Abusleme Hoffman ^{136a}, B.S. Acharya ^{68a,68b,p}, B. Achkar ⁵⁵, L. Adam ⁹⁹, C. Adam Bourdarios ⁴, L. Adamczyk ^{84a}, L. Adamek ¹⁵⁴, S.V. Addepalli ²⁶, J. Adelman ¹¹⁴, A. Adiguzel ^{21c}, S. Adorni ⁵⁶, T. Adye ¹³³, A.A. Affolder ¹³⁵, Y. Afik ³⁶, M.N. Agaras ¹³, J. Agarwala ^{72a,72b}, A. Aggarwal ⁹⁹, C. Agheorghiesei ^{27c}, J.A. Aguilar-Saavedra ^{129f}, A. Ahmad ³⁶, F. Ahmadov ^{38,z}, W.S. Ahmed ¹⁰³, S. Ahuja ⁹⁴, X. Ai ⁴⁸, G. Aielli ^{75a,75b}, I. Aizenberg ¹⁶⁸, M. Akbiyik ⁹⁹, T.P.A. Åkesson ⁹⁷, A.V. Akimov ³⁷, K. Al Khoury ⁴¹, G.L. Alberghi ^{23b}, J. Albert ¹⁶⁴, P. Albicocco ⁵³, M.J. Alconada Verzini ⁸⁹, S. Alderweireldt ⁵², M. Aleksa ³⁶, I.N. Aleksandrov ³⁸, C. Alexa ^{27b}, T. Alexopoulos ¹⁰, A. Alfonsi ¹¹³, F. Alfonsi ^{23b}, M. Alhroob ¹¹⁹, B. Ali ¹³¹, S. Ali ¹⁴⁷, M. Aliev ³⁷, G. Alimonti ^{70a}, C. Allaire ³⁶, B.M.M. Allbrooke ¹⁴⁵, P.P. Allport ²⁰, A. Aloisio ^{71a,71b}, F. Alonso ⁸⁹, C. Alpigiani ¹³⁷, E. Alunno Camelia ^{75a,75b}, M. Alvarez Estevez ⁹⁸, M.G. Alvigi ^{71a,71b}, Y. Amaral Coutinho ^{81b}, A. Ambler ¹⁰³, C. Amelung ³⁶, C.G. Ames ¹⁰⁸, D. Amidei ¹⁰⁵, S.P. Amor Dos Santos ^{129a}, S. Amoroso ⁴⁸, K.R. Amos ¹⁶², C.S. Amrouche ⁵⁶, V. Ananiev ¹²⁴, C. Anastopoulos ¹³⁸, N. Andari ¹³⁴, T. Andeen ¹¹, J.K. Anders ¹⁹, S.Y. Andrean ^{47a,47b}, A. Andreazza ^{70a,70b}, S. Angelidakis ⁹, A. Angerami ^{41,ac}, A.V. Anisenkov ³⁷, A. Annovi ^{73a}, C. Antel ⁵⁶, M.T. Anthony ¹³⁸, E. Antipov ¹²⁰, M. Antonelli ⁵³, D.J.A. Antrim ^{17a}, F. Anulli ^{74a}, M. Aoki ⁸², T. Aoki ¹⁵², J.A. Aparisi Pozo ¹⁶², M.A. Aparo ¹⁴⁵, L. Aperio Bella ⁴⁸, C. Appelt ¹⁸, N. Aranzabal ³⁶, V. Araujo Ferraz ^{81a}, C. Arcangeletti ⁵³, A.T.H. Arce ⁵¹, E. Arena ⁹¹, J-F. Arguin ¹⁰⁷, S. Argyropoulos ⁵⁴, J.-H. Arling ⁴⁸, A.J. Armbruster ³⁶, O. Arnaez ¹⁵⁴, H. Arnold ¹¹³, Z.P. Arrubarrena Tame ¹⁰⁸, G. Artoni ^{74a,74b}, H. Asada ¹¹⁰, K. Asai ¹¹⁷, S. Asai ¹⁵², N.A. Asbah ⁶¹, E.M. Asimakopoulou ¹⁶⁰, J. Assahsah ^{35d}, K. Assamagan ²⁹, R. Astalos ^{28a}, R.J. Atkin ^{33a}, M. Atkinson ¹⁶¹, N.B. Atlay ¹⁸, H. Atmani ^{62b}, P.A. Atmasiddha ¹⁰⁵, K. Augsten ¹³¹, S. Auricchio ^{71a,71b}, A.D. Auriol ²⁰, V.A. Austrup ¹⁷⁰, G. Avner ¹⁴⁹, G. Avolio ³⁶, K. Axiotis ⁵⁶, M.K. Ayoub ^{14c}, G. Azuelos ^{107,ag}, D. Babal ^{28a}, H. Bachacou ¹³⁴, K. Bachas ^{151,s}, A. Bachi ³⁴, F. Backman ^{47a,47b}, A. Badea ⁶¹, P. Bagnaia ^{74a,74b}, M. Bahmani ¹⁸, A.J. Bailey ¹⁶², V.R. Bailey ¹⁶¹, J.T. Baines ¹³³, C. Bakalis ¹⁰, O.K. Baker ¹⁷¹, P.J. Bakker ¹¹³, E. Bakos ¹⁵, D. Bakshi Gupta ⁸, S. Balaji ¹⁴⁶, R. Balasubramanian ¹¹³, E.M. Baldin ³⁷, P. Balek ¹³², E. Ballabene ^{70a,70b}, F. Balli ¹³⁴, L.M. Baltes ^{63a}, W.K. Balunas ³², J. Balz ⁹⁹, E. Banas ⁸⁵, M. Bandieramonte ¹²⁸, A. Bandyopadhyay ²⁴, S. Bansal ²⁴, L. Barak ¹⁵⁰, E.L. Barberio ¹⁰⁴, D. Barberis ^{57b,57a}, M. Barbero ¹⁰¹, G. Barbour ⁹⁵, K.N. Barends ^{33a}, T. Barillari ¹⁰⁹, M-S. Barisits ³⁶, J. Barkeloo ¹²², T. Barklow ¹⁴², R.M. Barnett ^{17a}, P. Baron ¹²¹, D.A. Baron Moreno ¹⁰⁰, A. Baroncelli ^{62a}, G. Barone ²⁹, A.J. Barr ¹²⁵, L. Barranco Navarro ^{47a,47b}, F. Barreiro ⁹⁸, J. Barreiro Guimarães da Costa ^{14a}, U. Barron ¹⁵⁰, M.G. Barros Teixeira ^{129a}, S. Barsov ³⁷, F. Bartels ^{63a}, R. Bartoldus ¹⁴², A.E. Barton ⁹⁰, P. Bartos ^{28a}, A. Basalae ⁴⁸, A. Basan ⁹⁹, M. Baselga ⁴⁹, I. Bashta ^{76a,76b}, A. Bassalat ^{66,b}, M.J. Basso ¹⁵⁴, C.R. Basson ¹⁰⁰, R.L. Bates ⁵⁹, S. Batlamous ^{35e}, J.R. Batley ³², B. Batool ¹⁴⁰, M. Battaglia ¹³⁵, M. Bauge ^{74a,74b}, P. Bauer ²⁴, A. Bayirli ^{21a}, J.B. Beacham ⁵¹, T. Beau ¹²⁶, P.H. Beauchemin ¹⁵⁷, F. Becherer ⁵⁴, P. Bechtel ²⁴, H.P. Beck ^{19,r}, K. Becker ¹⁶⁶, C. Becot ⁴⁸, A.J. Beddall ^{21d}, V.A. Bednyakov ³⁸, C.P. Bee ¹⁴⁴, L.J. Beemster ¹⁵, T.A. Beermann ³⁶, M. Begalli ^{81d}, M. Begel ²⁹, A. Behera ¹⁴⁴, J.K. Behr ⁴⁸, C. Beirao Da Cruz E Silva ³⁶, J.F. Beirer ^{55,36}, F. Beisiegel ²⁴, M. Belfkir ¹⁵⁸, G. Bella ¹⁵⁰, L. Bellagamba ^{23b}, A. Bellerive ³⁴, P. Bellos ²⁰, K. Beloborodov ³⁷, K. Belotskiy ³⁷, N.L. Belyaev ³⁷, D. Benckekroun ^{35a},

F. Bendebba ^{35a}, Y. Benhammou ¹⁵⁰, D.P. Benjamin ²⁹, M. Benoit ²⁹, J.R. Bensinger ²⁶, S. Bentvelsen ¹¹³, L. Beresford ³⁶, M. Beretta ⁵³, D. Berge ¹⁸, E. Bergeaas Kuutmann ¹⁶⁰, N. Berger ⁴, B. Bergmann ¹³¹, J. Beringer ^{17a}, S. Berlendis ⁷, G. Bernardi ⁵, C. Bernius ¹⁴², F.U. Bernlochner ²⁴, T. Berry ⁹⁴, P. Berta ¹³², A. Berthold ⁵⁰, I.A. Bertram ⁹⁰, S. Bethke ¹⁰⁹, A. Betti ^{74a,74b}, A.J. Bevan ⁹³, M. Bhamjee ^{33c}, S. Bhatta ¹⁴⁴, D.S. Bhattacharya ¹⁶⁵, P. Bhattarai ²⁶, V.S. Bhopatkar ⁶, R. Bi ¹²⁸, R. Bi ^{29,aj}, R.M. Bianchi ¹²⁸, O. Biebel ¹⁰⁸, R. Bielski ¹²², M. Biglietti ^{76a}, T.R.V. Billoud ¹³¹, M. Bindi ⁵⁵, A. Bingul ^{21b}, C. Bini ^{74a,74b}, S. Biondi ^{23b,23a}, A. Biondini ⁹¹, C.J. Birch-sykes ¹⁰⁰, G.A. Bird ^{20,133}, M. Birman ¹⁶⁸, T. Bisanz ³⁶, E. Bisceglie ^{43b,43a}, D. Biswas ^{169,1}, A. Bitadze ¹⁰⁰, K. Bjørke ¹²⁴, I. Bloch ⁴⁸, C. Blocker ²⁶, A. Blue ⁵⁹, U. Blumenschein ⁹³, J. Blumenthal ⁹⁹, G.J. Bobbink ¹¹³, V.S. Bobrovnikov ³⁷, M. Boehler ⁵⁴, D. Bogavac ³⁶, A.G. Bogdanchikov ³⁷, C. Bohm ^{47a}, V. Boisvert ⁹⁴, P. Bokan ⁴⁸, T. Bold ^{84a}, M. Bomben ⁵, M. Bona ⁹³, M. Boonekamp ¹³⁴, C.D. Booth ⁹⁴, A.G. Borbély ⁵⁹, H.M. Borecka-Bielska ¹⁰⁷, L.S. Borgna ⁹⁵, G. Borissov ⁹⁰, D. Bortoletto ¹²⁵, D. Boscherini ^{23b}, M. Bosman ¹³, J.D. Bossio Sola ³⁶, K. Bouaouda ^{35a}, J. Boudreau ¹²⁸, E.V. Bouhova-Thacker ⁹⁰, D. Boumediene ⁴⁰, R. Bouquet ⁵, A. Boveia ¹¹⁸, J. Boyd ³⁶, D. Boye ²⁹, I.R. Boyko ³⁸, J. Bracinik ²⁰, N. Brahimy ^{62d}, G. Brandt ¹⁷⁰, O. Brandt ³², F. Braren ⁴⁸, B. Brau ¹⁰², J.E. Brau ¹²², W.D. Breaden Madden ⁵⁹, K. Brendlinger ⁴⁸, R. Brenner ¹⁶⁸, L. Brenner ³⁶, R. Brenner ¹⁶⁰, S. Bressler ¹⁶⁸, B. Brickwedde ⁹⁹, D. Britton ⁵⁹, D. Britzger ¹⁰⁹, I. Brock ²⁴, G. Brooijmans ⁴¹, W.K. Brooks ^{136f}, E. Brost ²⁹, P.A. Bruckman de Renstrom ⁸⁵, B. Brüers ⁴⁸, D. Bruncko ^{28b,*}, A. Bruni ^{23b}, G. Bruni ^{23b}, M. Bruschi ^{23b}, N. Bruscinò ^{74a,74b}, L. Bryngemark ¹⁴², T. Buanes ¹⁶, Q. Buat ¹³⁷, P. Buchholz ¹⁴⁰, A.G. Buckley ⁵⁹, I.A. Budagov ^{38,*}, M.K. Bugge ¹²⁴, O. Bulekov ³⁷, B.A. Bullard ⁶¹, S. Burdin ⁹¹, C.D. Burgard ⁴⁸, A.M. Burger ⁴⁰, B. Burghgrave ⁸, J.T.P. Burr ³², C.D. Burton ¹¹, J.C. Burzynski ¹⁴¹, E.L. Busch ⁴¹, V. Büscher ⁹⁹, P.J. Bussey ⁵⁹, J.M. Butler ²⁵, C.M. Buttar ⁵⁹, J.M. Butterworth ⁹⁵, W. Buttinger ¹³³, C.J. Buxo Vazquez ¹⁰⁶, A.R. Buzykaev ³⁷, G. Cabras ^{23b}, S. Cabrera Urbán ¹⁶², D. Caforio ⁵⁸, H. Cai ¹²⁸, Y. Cai ^{14a,14d}, V.M.M. Cairo ³⁶, O. Cakir ^{3a}, N. Calace ³⁶, P. Calafiura ^{17a}, G. Calderini ¹²⁶, P. Calfayan ⁶⁷, G. Callea ⁵⁹, L.P. Caloba ^{81b}, D. Calvet ⁴⁰, S. Calvet ⁴⁰, T.P. Calvet ¹⁰¹, M. Calvetti ^{73a,73b}, R. Camacho Toro ¹²⁶, S. Camarda ³⁶, D. Camarero Munoz ⁹⁸, P. Camarri ^{75a,75b}, M.T. Camerlingo ^{76a,76b}, D. Cameron ¹²⁴, C. Camincher ¹⁶⁴, M. Campanelli ⁹⁵, A. Camplani ⁴², V. Canale ^{71a,71b}, A. Canesse ¹⁰³, M. Cano Bret ⁷⁹, J. Cantero ¹⁶², Y. Cao ¹⁶¹, F. Capocasa ²⁶, M. Capua ^{43b,43a}, A. Carbone ^{70a,70b}, R. Cardarelli ^{75a}, J.C.J. Cardenas ⁸, F. Cardillo ¹⁶², T. Carli ³⁶, G. Carlino ^{71a}, B.T. Carlson ^{128,t}, E.M. Carlson ^{164,155a}, L. Carminati ^{70a,70b}, M. Carnesale ^{74a,74b}, S. Caron ¹¹², E. Carquin ^{136f}, S. Carrá ^{70a,70b}, G. Carratta ^{23b,23a}, F. Carriò Argos ^{33g}, J.W.S. Carter ¹⁵⁴, T.M. Carter ⁵², M.P. Casado ^{13,i}, A.F. Casha ¹⁵⁴, E.G. Castiglia ¹⁷¹, F.L. Castillo ^{63a}, L. Castillo Garcia ¹³, V. Castillo Gimenez ¹⁶², N.F. Castro ^{129a,129e}, A. Catinaccio ³⁶, J.R. Catmore ¹²⁴, V. Cavaliere ²⁹, N. Cavalli ^{23b,23a}, V. Cavasinni ^{73a,73b}, E. Celebi ^{21a}, F. Celli ¹²⁵, M.S. Centonze ^{69a,69b}, K. Cerny ¹²¹, A.S. Cerqueira ^{81a}, A. Cerri ¹⁴⁵, L. Cerrito ^{75a,75b}, F. Cerutti ^{17a}, A. Cervelli ^{23b}, S.A. Cetin ^{21d}, Z. Chadi ^{35a}, D. Chakraborty ¹¹⁴, M. Chala ^{129f}, J. Chan ¹⁶⁹, W.S. Chan ¹¹³, W.Y. Chan ¹⁵², J.D. Chapman ³², B. Chargeishvili ^{148b}, D.G. Charlton ²⁰, T.P. Charman ⁹³, M. Chatterjee ¹⁹, S. Chekanov ⁶, S.V. Chekulaev ^{155a}, G.A. Chelkov ^{38,a}, A. Chen ¹⁰⁵, B. Chen ¹⁵⁰, B. Chen ¹⁶⁴, C. Chen ^{62a}, H. Chen ^{14c}, H. Chen ²⁹, J. Chen ^{62c}, J. Chen ²⁶, S. Chen ¹⁵², S.J. Chen ^{14c}, X. Chen ^{62c}, X. Chen ^{14b,af}, Y. Chen ^{62a}, C.L. Cheng ¹⁶⁹, H.C. Cheng ^{64a}, A. Cheplakov ³⁸, E. Cheremushkina ⁴⁸, E. Cherepanova ¹¹³, R. Cherkaoui El Moursli ^{35e}, E. Cheu ⁷, K. Cheung ⁶⁵, L. Chevalier ¹³⁴, V. Chiarella ⁵³, G. Chiarelli ^{73a}, N. Chiedde ¹⁰¹, G. Chiodini ^{69a}, A.S. Chisholm ²⁰, A. Chitan ^{27b}, Y.H. Chiu ¹⁶⁴, M.V. Chizhov ³⁸, K. Choi ¹¹,

A.R. Chomont [ID 74a,74b](#), Y. Chou [ID 102](#), E.Y.S. Chow [ID 113](#), T. Chowdhury [ID 33g](#), L.D. Christopher [ID 33g](#),
 K.L. Chu [ID 64a](#), M.C. Chu [ID 64a](#), X. Chu [ID 14a,14d](#), J. Chudoba [ID 130](#), J.J. Chwastowski [ID 85](#), D. Cieri [ID 109](#),
 K.M. Ciesla [ID 84a](#), V. Cindro [ID 92](#), A. Ciocio [ID 17a](#), F. Cirotto [ID 71a,71b](#), Z.H. Citron [ID 168,m](#), M. Citterio [ID 70a](#),
 D.A. Ciubotaru [ID 27b](#), B.M. Ciungu [ID 154](#), A. Clark [ID 56](#), P.J. Clark [ID 52](#), J.M. Clavijo Columbie [ID 48](#),
 S.E. Clawson [ID 100](#), C. Clement [ID 47a,47b](#), J. Clercx [ID 48](#), L. Clissa [ID 23b,23a](#), Y. Coadou [ID 101](#),
 M. Cobal [ID 68a,68c](#), A. Coccaro [ID 57b](#), R.F. Coelho Barrue [ID 129a](#), R. Coelho Lopes De Sa [ID 102](#),
 S. Coelli [ID 70a](#), H. Cohen [ID 150](#), A.E.C. Coimbra [ID 70a,70b](#), B. Cole [ID 41](#), J. Collot [ID 60](#),
 P. Conde Muiño [ID 129a,129g](#), M.P. Connell [ID 33c](#), S.H. Connell [ID 33c](#), I.A. Connelly [ID 59](#), E.I. Conroy [ID 125](#),
 F. Conventi [ID 71a,ah](#), H.G. Cooke [ID 20](#), A.M. Cooper-Sarkar [ID 125](#), F. Cormier [ID 163](#), L.D. Corpe [ID 36](#),
 M. Corradi [ID 74a,74b](#), E.E. Corrigan [ID 97](#), F. Corriveau [ID 103,y](#), A. Cortes-Gonzalez [ID 18](#), M.J. Costa [ID 162](#),
 F. Costanza [ID 4](#), D. Costanzo [ID 138](#), B.M. Cote [ID 118](#), G. Cowan [ID 94](#), J.W. Cowley [ID 32](#), K. Cranmer [ID 116](#),
 S. Crépe-Renaudin [ID 60](#), F. Crescioli [ID 126](#), M. Cristinziani [ID 140](#), M. Cristoforetti [ID 77a,77b,d](#), V. Croft [ID 157](#),
 G. Crosetti [ID 43b,43a](#), A. Cueto [ID 36](#), T. Cuhadar Donszelmann [ID 159](#), H. Cui [ID 14a,14d](#), Z. Cui [ID 7](#),
 A.R. Cukierman [ID 142](#), W.R. Cunningham [ID 59](#), F. Curcio [ID 43b,43a](#), P. Czodrowski [ID 36](#), M.M. Czurylo [ID 63b](#),
 M.J. Da Cunha Sargedas De Sousa [ID 62a](#), J.V. Da Fonseca Pinto [ID 81b](#), C. Da Via [ID 100](#), W. Dabrowski [ID 84a](#),
 T. Dado [ID 49](#), S. Dahbi [ID 33g](#), T. Dai [ID 105](#), C. Dallapiccola [ID 102](#), M. Dam [ID 42](#), G. D'amen [ID 29](#),
 V. D'Amico [ID 76a,76b](#), J. Damp [ID 99](#), J.R. Dandoy [ID 127](#), M.F. Daneri [ID 30](#), M. Danninger [ID 141](#), V. Dao [ID 36](#),
 G. Darbo [ID 57b](#), S. Darmora [ID 6](#), S.J. Das [ID 29,aj](#), A. Dattagupta [ID 122](#), S. D'Auria [ID 70a,70b](#), C. David [ID 155b](#),
 T. Davidek [ID 132](#), D.R. Davis [ID 51](#), B. Davis-Purcell [ID 34](#), I. Dawson [ID 93](#), K. De [ID 8](#), R. De Asmundis [ID 71a](#),
 M. De Beurs [ID 113](#), S. De Castro [ID 23b,23a](#), N. De Groot [ID 112](#), P. de Jong [ID 113](#), H. De la Torre [ID 106](#),
 A. De Maria [ID 14c](#), A. De Salvo [ID 74a](#), U. De Sanctis [ID 75a,75b](#), A. De Santo [ID 145](#),
 J.B. De Vivie De Regie [ID 60](#), D.V. Dedovich [ID 38](#), J. Degens [ID 113](#), A.M. Deiana [ID 44](#), F. Del Corso [ID 23b,23a](#),
 J. Del Peso [ID 98](#), F. Del Rio [ID 63a](#), F. Deliot [ID 134](#), C.M. Delitzsch [ID 49](#), M. Della Pietra [ID 71a,71b](#),
 D. Della Volpe [ID 56](#), A. Dell'Acqua [ID 36](#), L. Dell'Asta [ID 70a,70b](#), M. Delmastro [ID 4](#), P.A. Delsart [ID 60](#),
 S. Demers [ID 171](#), M. Demichev [ID 38](#), S.P. Denisov [ID 37](#), L. D'Eramo [ID 114](#), D. Derendarz [ID 85](#),
 F. Derue [ID 126](#), P. Dervan [ID 91](#), K. Desch [ID 24](#), K. Dette [ID 154](#), C. Deutsch [ID 24](#), P.O. Deviveiros [ID 36](#),
 F.A. Di Bello [ID 74a,74b](#), A. Di Ciaccio [ID 75a,75b](#), L. Di Ciaccio [ID 4](#), A. Di Domenico [ID 74a,74b](#),
 C. Di Donato [ID 71a,71b](#), A. Di Girolamo [ID 36](#), G. Di Gregorio [ID 73a,73b](#), A. Di Luca [ID 77a,77b](#),
 B. Di Micco [ID 76a,76b](#), R. Di Nardo [ID 76a,76b](#), C. Diaconu [ID 101](#), F.A. Dias [ID 113](#), T. Dias Do Vale [ID 141](#),
 M.A. Diaz [ID 136a,136b](#), F.G. Diaz Capriles [ID 24](#), M. Didenko [ID 162](#), E.B. Diehl [ID 105](#), L. Diehl [ID 54](#),
 S. Díez Cornell [ID 48](#), C. Diez Pardos [ID 140](#), C. Dimitriadi [ID 24,160](#), A. Dimitrievska [ID 17a](#), W. Ding [ID 14b](#),
 J. Dingfelder [ID 24](#), I-M. Dinu [ID 27b](#), S.J. Dittmeier [ID 63b](#), F. Dittus [ID 36](#), F. Djama [ID 101](#), T. Djobava [ID 148b](#),
 J.I. Djuvsland [ID 16](#), D. Dodsworth [ID 26](#), C. Doglioni [ID 100,97](#), J. Dolejsi [ID 132](#), Z. Dolezal [ID 132](#),
 M. Donadelli [ID 81c](#), B. Dong [ID 62c](#), J. Donini [ID 40](#), A. D'Onofrio [ID 14c](#), M. D'Onofrio [ID 91](#), J. Dopke [ID 133](#),
 A. Doria [ID 71a](#), M.T. Dova [ID 89](#), A.T. Doyle [ID 59](#), M.A. Draguet [ID 125](#), E. Drechsler [ID 141](#), E. Dreyer [ID 168](#),
 I. Drivas-koulouris [ID 10](#), A.S. Drobac [ID 157](#), D. Du [ID 62a](#), T.A. du Pree [ID 113](#), F. Dubinin [ID 37](#),
 M. Dubovsky [ID 28a](#), E. Duchovni [ID 168](#), G. Duckeck [ID 108](#), O.A. Ducu [ID 36](#), D. Duda [ID 109](#), A. Dudarev [ID 36](#),
 M. D'uffizi [ID 100](#), L. Duflot [ID 66](#), M. Dührssen [ID 36](#), C. Dülsen [ID 170](#), A.E. Dumitriu [ID 27b](#), M. Dunford [ID 63a](#),
 S. Dungs [ID 49](#), K. Dunne [ID 47a,47b](#), A. Duperrin [ID 101](#), H. Duran Yildiz [ID 3a](#), M. Düren [ID 58](#),
 A. Durglishvili [ID 148b](#), B.L. Dwyer [ID 114](#), G.I. Dyckes [ID 17a](#), M. Dyndal [ID 84a](#), S. Dysch [ID 100](#),
 B.S. Dziedzic [ID 85](#), Z.O. Earnshaw [ID 145](#), B. Eckerova [ID 28a](#), M.G. Eggleston [ID 51](#),
 E. Egidio Purcino De Souza [ID 81b](#), L.F. Ehrke [ID 56](#), G. Eigen [ID 16](#), K. Einsweiler [ID 17a](#), T. Ekelof [ID 160](#),
 P.A. Ekman [ID 97](#), Y. El Ghazali [ID 35b](#), H. El Jarrari [ID 35e,147](#), A. El Moussaouy [ID 35a](#), V. Ellajosyula [ID 160](#),
 M. Ellert [ID 160](#), F. Ellinghaus [ID 170](#), A.A. Elliot [ID 93](#), N. Ellis [ID 36](#), J. Elmsheuser [ID 29](#), M. Elsing [ID 36](#),
 D. Emelianov [ID 133](#), A. Emerman [ID 41](#), Y. Enari [ID 152](#), I. Ene [ID 17a](#), S. Epari [ID 13](#), J. Erdmann [ID 49](#),
 A. Ereditato [ID 19](#), P.A. Erland [ID 85](#), M. Errenst [ID 170](#), M. Escalier [ID 66](#), C. Escobar [ID 162](#), E. Etzion [ID 150](#),
 G. Evans [ID 129a](#), H. Evans [ID 67](#), M.O. Evans [ID 145](#), A. Ezhilov [ID 37](#), S. Ezzarqtouni [ID 35a](#), F. Fabbri [ID 59](#),

L. Fabbri [id](#)^{23b,23a}, G. Facini [id](#)⁹⁵, V. Fadeyev [id](#)¹³⁵, R.M. Fakhruddinov [id](#)³⁷, S. Falciano [id](#)^{74a},
 P.J. Falke [id](#)²⁴, S. Falke [id](#)³⁶, J. Faltova [id](#)¹³², Y. Fan [id](#)^{14a}, Y. Fang [id](#)^{14a,14d}, G. Fanourakis [id](#)⁴⁶,
 M. Fanti [id](#)^{70a,70b}, M. Faraj [id](#)^{68a,68b}, A. Farbin [id](#)⁸, A. Farilla [id](#)^{76a}, T. Faroque [id](#)¹⁰⁶, S.M. Farrington [id](#)⁵²,
 F. Fassi [id](#)^{35e}, D. Fassouliotis [id](#)⁹, M. Faucci Giannelli [id](#)^{75a,75b}, W.J. Fawcett [id](#)³², L. Fayard [id](#)⁶⁶,
 O.L. Fedin [id](#)^{37,a}, G. Fedotov [id](#)³⁷, M. Feickert [id](#)¹⁶¹, L. Feligioni [id](#)¹⁰¹, A. Fell [id](#)¹³⁸, D.E. Fellers [id](#)¹²²,
 C. Feng [id](#)^{62b}, M. Feng [id](#)^{14b}, Z. Feng [id](#)¹¹³, M.J. Fenton [id](#)¹⁵⁹, A.B. Fenyuk [id](#)³⁷, L. Ferencz [id](#)⁴⁸,
 S.W. Ferguson [id](#)⁴⁵, J. Ferrando [id](#)⁴⁸, A. Ferrari [id](#)¹⁶⁰, P. Ferrari [id](#)¹¹³, R. Ferrari [id](#)^{72a}, D. Ferrere [id](#)⁵⁶,
 C. Ferretti [id](#)¹⁰⁵, F. Fiedler [id](#)⁹⁹, A. Filipčič [id](#)⁹², E.K. Filmer [id](#)¹, F. Filthaut [id](#)¹¹²,
 M.C.N. Fiolhais [id](#)^{129a,129c,c}, L. Fiorini [id](#)¹⁶², F. Fischer [id](#)¹⁴⁰, W.C. Fisher [id](#)¹⁰⁶, T. Fitschen [id](#)^{20,66},
 I. Fleck [id](#)¹⁴⁰, P. Fleischmann [id](#)¹⁰⁵, T. Flick [id](#)¹⁷⁰, L. Flores [id](#)¹²⁷, M. Flores [id](#)^{33d,ad},
 L.R. Flores Castillo [id](#)^{64a}, F.M. Follega [id](#)^{77a,77b}, N. Fomin [id](#)¹⁶, J.H. Foo [id](#)¹⁵⁴, B.C. Forland [id](#)⁶⁷,
 A. Formica [id](#)¹³⁴, A.C. Forti [id](#)¹⁰⁰, E. Fortin [id](#)¹⁰¹, A.W. Fortman [id](#)⁶¹, M.G. Foti [id](#)^{17a}, L. Fountas [id](#)^{9,j},
 D. Fournier [id](#)⁶⁶, H. Fox [id](#)⁹⁰, P. Francavilla [id](#)^{73a,73b}, S. Francescato [id](#)⁶¹, M. Franchini [id](#)^{23b,23a},
 S. Franchino [id](#)^{63a}, D. Francis [id](#)³⁶, L. Franco [id](#)¹¹², L. Franconi [id](#)¹⁹, M. Franklin [id](#)⁶¹, G. Frattari [id](#)²⁶,
 A.C. Freegard [id](#)⁹³, P.M. Freeman [id](#)²⁰, W.S. Freund [id](#)^{81b}, N. Fritzsche [id](#)⁵⁰, A. Froch [id](#)⁵⁴,
 D. Froidevaux [id](#)³⁶, J.A. Frost [id](#)¹²⁵, Y. Fu [id](#)^{62a}, M. Fujimoto [id](#)¹¹⁷, E. Fullana Torregrosa [id](#)^{162,*},
 J. Fuster [id](#)¹⁶², A. Gabrielli [id](#)^{23b,23a}, A. Gabrielli [id](#)³⁶, P. Gadow [id](#)⁴⁸, G. Gagliardi [id](#)^{57b,57a},
 L.G. Gagnon [id](#)^{17a}, G.E. Gallardo [id](#)¹²⁵, E.J. Gallas [id](#)¹²⁵, B.J. Gallop [id](#)¹³³, R. Gamboa Goni [id](#)⁹³,
 K.K. Gan [id](#)¹¹⁸, S. Ganguly [id](#)¹⁵², J. Gao [id](#)^{62a}, Y. Gao [id](#)⁵², F.M. Garay Walls [id](#)^{136a,136b}, B. Garcia [id](#)^{29,aj},
 C. García [id](#)¹⁶², J.E. García Navarro [id](#)¹⁶², J.A. García Pascual [id](#)^{14a}, M. Garcia-Sciveres [id](#)^{17a},
 R.W. Gardner [id](#)³⁹, D. Garg [id](#)⁷⁹, R.B. Garg [id](#)^{142,q}, S. Gargiulo [id](#)⁵⁴, C.A. Garner [id](#)¹⁵⁴, V. Garonne [id](#)²⁹,
 S.J. Gasiorowski [id](#)¹³⁷, P. Gaspar [id](#)^{81b}, G. Gaudio [id](#)^{72a}, V. Gautam [id](#)¹³, P. Gauzzi [id](#)^{74a,74b},
 I.L. Gavrilenko [id](#)³⁷, A. Gavriyuk [id](#)³⁷, C. Gay [id](#)¹⁶³, G. Gaycken [id](#)⁴⁸, E.N. Gazis [id](#)¹⁰,
 A.A. Geanta [id](#)^{27b,27e}, C.M. Gee [id](#)¹³⁵, J. Geisen [id](#)⁹⁷, M. Geisen [id](#)⁹⁹, C. Gemme [id](#)^{57b}, M.H. Genest [id](#)⁶⁰,
 S. Gentile [id](#)^{74a,74b}, S. George [id](#)⁹⁴, W.F. George [id](#)²⁰, T. Geralis [id](#)⁴⁶, L.O. Gerlach [id](#)⁵⁵,
 P. Gessinger-Befurt [id](#)³⁶, M. Ghasemi Bostanabad [id](#)¹⁶⁴, M. Ghneimat [id](#)¹⁴⁰, A. Ghosal [id](#)¹⁴⁰,
 A. Ghosh [id](#)¹⁵⁹, A. Ghosh [id](#)⁷, B. Giacobbe [id](#)^{23b}, S. Giagu [id](#)^{74a,74b}, N. Giangiacomi [id](#)¹⁵⁴,
 P. Giannetti [id](#)^{73a}, A. Giannini [id](#)^{62a}, S.M. Gibson [id](#)⁹⁴, M. Gignac [id](#)¹³⁵, D.T. Gil [id](#)^{84b}, A.K. Gilbert [id](#)^{84a},
 B.J. Gilbert [id](#)⁴¹, D. Gillberg [id](#)³⁴, G. Gilles [id](#)¹¹³, N.E.K. Gillwald [id](#)⁴⁸, L. Ginabat [id](#)¹²⁶,
 D.M. Gingrich [id](#)^{2,ag}, M.P. Giordani [id](#)^{68a,68c}, P.F. Giraud [id](#)¹³⁴, G. Giugliarelli [id](#)^{68a,68c}, D. Giugni [id](#)^{70a},
 F. Giuli [id](#)³⁶, I. Gkialas [id](#)^{9,j}, L.K. Gladilin [id](#)³⁷, C. Glasman [id](#)⁹⁸, G.R. Gledhill [id](#)¹²², M. Glisic [id](#)¹²²,
 I. Gnesi [id](#)^{43b,f}, Y. Go [id](#)^{29,aj}, M. Goblirsch-Kolb [id](#)²⁶, D. Godin [id](#)¹⁰⁷, S. Goldfarb [id](#)¹⁰⁴, T. Golling [id](#)⁵⁶,
 M.G.D. Gololo [id](#)^{33g}, D. Golubkov [id](#)³⁷, J.P. Gombas [id](#)¹⁰⁶, A. Gomes [id](#)^{129a,129b}, G. Gomes Da Silva [id](#)¹⁴⁰,
 A.J. Gomez Delegido [id](#)¹⁶², R. Goncalves Gama [id](#)⁵⁵, R. Gonçalo [id](#)^{129a,129c}, G. Gonella [id](#)¹²²,
 L. Gonella [id](#)²⁰, A. Gongadze [id](#)³⁸, F. Gonnella [id](#)²⁰, J.L. Gonski [id](#)⁴¹, R.Y. González Andana [id](#)⁵²,
 S. González de la Hoz [id](#)¹⁶², S. Gonzalez Fernandez [id](#)¹³, R. Gonzalez Lopez [id](#)⁹¹,
 C. Gonzalez Renteria [id](#)^{17a}, R. Gonzalez Suarez [id](#)¹⁶⁰, S. Gonzalez-Sevilla [id](#)⁵⁶,
 G.R. Gonzalvo Rodriguez [id](#)¹⁶², L. Goossens [id](#)³⁶, N.A. Gorasia [id](#)²⁰, P.A. Gorbounov [id](#)³⁷, B. Gorini [id](#)³⁶,
 E. Gorini [id](#)^{69a,69b}, A. Gorišek [id](#)⁹², A.T. Goshaw [id](#)⁵¹, M.I. Gostkin [id](#)³⁸, C.A. Gottardo [id](#)³⁶,
 M. Goughri [id](#)^{35b}, V. Goumarre [id](#)⁴⁸, A.G. Goussiou [id](#)¹³⁷, N. Govender [id](#)^{33c}, C. Goy [id](#)⁴,
 I. Grabowska-Bold [id](#)^{84a}, K. Graham [id](#)³⁴, E. Gramstad [id](#)¹²⁴, S. Grancagnolo [id](#)¹⁸, M. Grandi [id](#)¹⁴⁵,
 V. Gratchev [id](#)^{37,*}, P.M. Gravila [id](#)^{27f}, F.G. Gravili [id](#)^{69a,69b}, H.M. Gray [id](#)^{17a}, M. Greco [id](#)^{69a,69b},
 C. Grefe [id](#)²⁴, I.M. Gregor [id](#)⁴⁸, P. Grenier [id](#)¹⁴², C. Grieco [id](#)¹³, A.A. Grillo [id](#)¹³⁵, K. Grimm [id](#)^{31,n},
 S. Grinstein [id](#)^{13,v}, J.-F. Grivaz [id](#)⁶⁶, E. Gross [id](#)¹⁶⁸, J. Grosse-Knetter [id](#)⁵⁵, C. Grud [id](#)¹⁰⁵, A. Grummer [id](#)¹¹¹,
 J.C. Grundy [id](#)¹²⁵, L. Guan [id](#)¹⁰⁵, W. Guan [id](#)¹⁶⁹, C. Gubbels [id](#)¹⁶³, J.G.R. Guerrero Rojas [id](#)¹⁶²,
 G. Guerrieri [id](#)^{68a,68b}, F. Guescini [id](#)¹⁰⁹, R. Gugel [id](#)⁹⁹, J.A.M. Guhit [id](#)¹⁰⁵, A. Guida [id](#)⁴⁸, T. Guillemin [id](#)⁴,
 E. Guilloton [id](#)^{166,133}, S. Guindon [id](#)³⁶, F. Guo [id](#)^{14a,14d}, J. Guo [id](#)^{62c}, L. Guo [id](#)⁶⁶, Y. Guo [id](#)¹⁰⁵,

R. Gupta ⁴⁸, S. Gurbuz ²⁴, S.S. Gurdasani ⁵⁴, G. Gustavino ³⁶, M. Guth ⁵⁶, P. Gutierrez ¹¹⁹, L.F. Gutierrez Zagazeta ¹²⁷, C. Gutschow ⁹⁵, C. Guyot ¹³⁴, C. Gwenlan ¹²⁵, C.B. Gwilliam ⁹¹, E.S. Haaland ¹²⁴, A. Haas ¹¹⁶, M. Habedank ⁴⁸, C. Haber ^{17a}, H.K. Hadavand ⁸, A. Hadeif ⁹⁹, S. Hadzic ¹⁰⁹, M. Haleem ¹⁶⁵, J. Haley ¹²⁰, J.J. Hall ¹³⁸, G.D. Hallowell ¹⁰¹, L. Halser ¹⁹, K. Hamano ¹⁶⁴, H. Hamdaoui ^{35e}, M. Hamer ²⁴, G.N. Hamity ⁵², J. Han ^{62b}, K. Han ^{62a}, L. Han ^{14c}, L. Han ^{62a}, S. Han ^{17a}, Y.F. Han ¹⁵⁴, K. Hanagaki ⁸², M. Hance ¹³⁵, D.A. Hangal ^{41,ac}, M.D. Hank ³⁹, R. Hankache ¹⁰⁰, J.B. Hansen ⁴², J.D. Hansen ⁴², P.H. Hansen ⁴², K. Hara ¹⁵⁶, D. Harada ⁵⁶, T. Harenberg ¹⁷⁰, S. Harkusha ³⁷, Y.T. Harris ¹²⁵, N.M. Harrison ¹¹⁸, P.F. Harrison ¹⁶⁶, N.M. Hartman ¹⁴², N.M. Hartmann ¹⁰⁸, Y. Hasegawa ¹³⁹, A. Hasib ⁵², S. Haug ¹⁹, R. Hauser ¹⁰⁶, M. Havranek ¹³¹, C.M. Hawkes ²⁰, R.J. Hawkins ³⁶, S. Hayashida ¹¹⁰, D. Hayden ¹⁰⁶, C. Hayes ¹⁰⁵, R.L. Hayes ¹⁶³, C.P. Hays ¹²⁵, J.M. Hays ⁹³, H.S. Hayward ⁹¹, F. He ^{62a}, Y. He ¹⁵³, Y. He ¹²⁶, M.P. Heath ⁵², V. Hedberg ⁹⁷, A.L. Heggelund ¹²⁴, N.D. Hehir ⁹³, C. Heidegger ⁵⁴, K.K. Heidegger ⁵⁴, W.D. Heidorn ⁸⁰, J. Heilman ³⁴, S. Heim ⁴⁸, T. Heim ^{17a}, J.G. Heinlein ¹²⁷, J.J. Heinrich ¹²², L. Heinrich ^{109,ac}, J. Hejbal ¹³⁰, L. Helary ⁴⁸, A. Held ¹⁶⁹, S. Hellesund ¹²⁴, C.M. Helling ¹⁶³, S. Hellman ^{47a,47b}, C. Hensens ³⁶, R.C.W. Henderson ⁹⁰, L. Henkelmann ³², A.M. Henriques Correia ³⁶, H. Herde ¹⁴², Y. Hernández Jiménez ¹⁴⁴, H. Herr ⁹⁹, M.G. Herrmann ¹⁰⁸, T. Herrmann ⁵⁰, G. Herten ⁵⁴, R. Hertenberger ¹⁰⁸, L. Hervas ³⁶, N.P. Hessey ^{155a}, H. Hibi ⁸³, E. Higón-Rodríguez ¹⁶², S.J. Hillier ²⁰, I. Hinchliffe ^{17a}, F. Hinterkeuser ²⁴, M. Hirose ¹²³, S. Hirose ¹⁵⁶, D. Hirschbuehl ¹⁷⁰, T.G. Hitchings ¹⁰⁰, B. Hiti ⁹², J. Hobbs ¹⁴⁴, R. Hobincu ^{27e}, N. Hod ¹⁶⁸, M.C. Hodgkinson ¹³⁸, B.H. Hodgkinson ³², A. Hoecker ³⁶, J. Hofer ⁴⁸, D. Hohn ⁵⁴, T. Holm ²⁴, M. Holzbock ¹⁰⁹, L.B.A.H. Hommels ³², B.P. Honan ¹⁰⁰, J. Hong ^{62c}, T.M. Hong ¹²⁸, Y. Hong ⁵⁵, J.C. Honig ⁵⁴, A. Hönle ¹⁰⁹, B.H. Hooberman ¹⁶¹, W.H. Hopkins ⁶, Y. Horii ¹¹⁰, S. Hou ¹⁴⁷, A.S. Howard ⁹², J. Howarth ⁵⁹, J. Hoya ⁸⁹, M. Hrabovsky ¹²¹, A. Hrynevich ³⁷, T. Hryn'ova ⁴, P.J. Hsu ⁶⁵, S.-C. Hsu ¹³⁷, Q. Hu ^{41,ac}, Y.F. Hu ^{14a,14d,ai}, D.P. Huang ⁹⁵, S. Huang ^{64b}, X. Huang ^{14c}, Y. Huang ^{62a}, Y. Huang ^{14a}, Z. Huang ¹⁰⁰, Z. Hubacek ¹³¹, M. Huebner ²⁴, F. Huegging ²⁴, T.B. Huffman ¹²⁵, M. Huhtinen ³⁶, S.K. Huiberts ¹⁶, R. Hulsken ¹⁰³, N. Huseynov ^{12,a}, J. Huston ¹⁰⁶, J. Huth ⁶¹, R. Hyneman ¹⁴², S. Hyrych ^{28a}, G. Iacobucci ⁵⁶, G. Iakovidis ²⁹, I. Ibragimov ¹⁴⁰, L. Iconomidou-Fayard ⁶⁶, P. Inengo ^{71a,71b}, R. Iguchi ¹⁵², T. Iizawa ⁵⁶, Y. Ikegami ⁸², A. Ilg ¹⁹, N. Ilic ¹⁵⁴, H. Imam ^{35a}, T. Ingebretsen Carlson ^{47a,47b}, G. Introzzi ^{72a,72b}, M. Iodice ^{76a}, V. Ippolito ^{74a,74b}, M. Ishino ¹⁵², W. Islam ¹⁶⁹, C. Issever ^{18,48}, S. Istin ^{21a,al}, H. Ito ¹⁶⁷, J.M. Iturbe Ponce ^{64a}, R. Iuppa ^{77a,77b}, A. Ivina ¹⁶⁸, J.M. Izen ⁴⁵, V. Izzo ^{71a}, P. Jacka ^{130,131}, P. Jackson ¹, R.M. Jacobs ⁴⁸, B.P. Jaeger ¹⁴¹, C.S. Jagfeld ¹⁰⁸, G. Jäkel ¹⁷⁰, K. Jakobs ⁵⁴, T. Jakoubek ¹⁶⁸, J. Jamieson ⁵⁹, K.W. Janas ^{84a}, G. Jarlskog ⁹⁷, A.E. Jaspán ⁹¹, T. Javůrek ³⁶, M. Javurkova ¹⁰², F. Jeanneau ¹³⁴, L. Jeanty ¹²², J. Jejelava ^{148a,aa}, P. Jenni ^{54,g}, C.E. Jessiman ³⁴, S. Jézéquel ⁴, J. Jia ¹⁴⁴, X. Jia ⁶¹, X. Jia ^{14a,14d}, Z. Jia ^{14c}, Y. Jiang ^{62a}, S. Jiggins ⁵², J. Jimenez Pena ¹⁰⁹, S. Jin ^{14c}, A. Jinaru ^{27b}, O. Jinnouchi ¹⁵³, H. Jivan ^{33g}, P. Johansson ¹³⁸, K.A. Johns ⁷, C.A. Johnson ⁶⁷, D.M. Jones ³², E. Jones ¹⁶⁶, P. Jones ³², R.W.L. Jones ⁹⁰, T.J. Jones ⁹¹, J. Jovicevic ¹⁵, X. Ju ^{17a}, J.J. Junggeburth ³⁶, A. Juste Rozas ^{13,v}, S. Kabana ^{136e}, A. Kaczmarska ⁸⁵, M. Kado ^{74a,74b}, H. Kagan ¹¹⁸, M. Kagan ¹⁴², A. Kahn ⁴¹, A. Kahn ¹²⁷, C. Kahra ⁹⁹, T. Kaji ¹⁶⁷, E. Kajomovitz ¹⁴⁹, N. Kakati ¹⁶⁸, C.W. Kalderon ²⁹, A. Kamenshchikov ¹⁵⁴, N.J. Kang ¹³⁵, Y. Kano ¹¹⁰, D. Kar ^{33g}, K. Karava ¹²⁵, M.J. Kareem ^{155b}, E. Karentzos ⁵⁴, I. Karkanias ¹⁵¹, S.N. Karpov ³⁸, Z.M. Karpova ³⁸, V. Kartvelishvili ⁹⁰, A.N. Karyukhin ³⁷, E. Kasimi ¹⁵¹, C. Kato ^{62d}, J. Katzy ⁴⁸, S. Kaur ³⁴, K. Kawade ¹³⁹, K. Kawagoe ⁸⁸, T. Kawaguchi ¹¹⁰, T. Kawamoto ¹³⁴, G. Kawamura ⁵⁵, E.F. Kay ¹⁶⁴, F.I. Kaya ¹⁵⁷, S. Kazakos ¹³, V.F. Kazanin ³⁷, Y. Ke ¹⁴⁴, J.M. Keaveney ^{33a}, R. Keeler ¹⁶⁴, G.V. Kehris ⁶¹, J.S. Keller ³⁴, A.S. Kelly ⁹⁵,

D. Kelsey ¹⁴⁵, J.J. Kempster ²⁰, J. Kendrick ²⁰, K.E. Kennedy ⁴¹, O. Kepka ¹³⁰,
 B.P. Kerridge ¹⁶⁶, S. Kersten ¹⁷⁰, B.P. Kerševan ⁹², L. Keszezhova ^{28a}, S. Ketabchi Haghghat ¹⁵⁴,
 M. Khandoga ¹²⁶, A. Khanov ¹²⁰, A.G. Kharlamov ³⁷, T. Kharlamova ³⁷, E.E. Khoda ¹³⁷,
 T.J. Khoo ¹⁸, G. Khoriali ¹⁶⁵, J. Khubua ^{148b}, Y.A.R. Khwaira ⁶⁶, M. Kiehn ³⁶,
 A. Kilgallon ¹²², D.W. Kim ^{47a,47b}, E. Kim ¹⁵³, Y.K. Kim ³⁹, N. Kimura ⁹⁵, A. Kirchhoff ⁵⁵,
 D. Kirchmeier ⁵⁰, C. Kirfel ²⁴, J. Kirk ¹³³, A.E. Kiryunin ¹⁰⁹, T. Kishimoto ¹⁵², D.P. Kisliuk ¹⁵⁴,
 C. Kitsaki ¹⁰, O. Kivernyk ²⁴, M. Klassen ^{63a}, C. Klein ³⁴, L. Klein ¹⁶⁵, M.H. Klein ¹⁰⁵,
 M. Klein ⁹¹, U. Klein ⁹¹, P. Klimek ³⁶, A. Klimentov ²⁹, F. Klimpel ¹⁰⁹, T. Klingl ²⁴,
 T. Klioutchnikova ³⁶, F.F. Klitzner ¹⁰⁸, P. Kluit ¹¹³, S. Kluth ¹⁰⁹, E. Kneringer ⁷⁸,
 T.M. Knight ¹⁵⁴, A. Knue ⁵⁴, D. Kobayashi ⁸⁸, R. Kobayashi ⁸⁶, M. Kocian ¹⁴², T. Kodama ¹⁵²,
 P. Kodyš ¹³², D.M. Koeck ¹⁴⁵, P.T. Koenig ²⁴, T. Koffas ³⁴, N.M. Köhler ³⁶, M. Kolb ¹³⁴,
 I. Koletsou ⁴, T. Komarek ¹²¹, K. Köneke ⁵⁴, A.X.Y. Kong ¹, T. Kono ¹¹⁷, N. Konstantinidis ⁹⁵,
 B. Konya ⁹⁷, R. Kopeliansky ⁶⁷, S. Koperny ^{84a}, K. Korcyl ⁸⁵, K. Kordas ¹⁵¹, G. Koren ¹⁵⁰,
 A. Korn ⁹⁵, S. Korn ⁵⁵, I. Korolkov ¹³, N. Korotkova ³⁷, B. Kortman ¹¹³, O. Kortner ¹⁰⁹,
 S. Kortner ¹⁰⁹, W.H. Kostecka ¹¹⁴, V.V. Kostyukhin ¹⁴⁰, A. Kotsokechagia ⁶⁶, A. Kotwal ⁵¹,
 A. Koulouris ³⁶, A. Kourkoumeli-Charalampidi ^{72a,72b}, C. Kourkoumelis ⁹, E. Kourlitis ⁶,
 O. Kovanda ¹⁴⁵, R. Kowalewski ¹⁶⁴, W. Kozanecki ¹³⁴, A.S. Kozhin ³⁷, V.A. Kramarenko ³⁷,
 G. Kramberger ⁹², P. Kramer ⁹⁹, M.W. Krasny ¹²⁶, A. Krasznahorkay ³⁶, J.A. Kremer ⁹⁹,
 T. Kresse ⁵⁰, J. Kretschmar ⁹¹, K. Kreul ¹⁸, P. Krieger ¹⁵⁴, F. Krieter ¹⁰⁸,
 S. Krishnamurthy ¹⁰², A. Krishnan ^{63b}, M. Krivos ¹³², K. Krizka ^{17a}, K. Kroeninger ⁴⁹,
 H. Kroha ¹⁰⁹, J. Kroll ¹³⁰, J. Kroll ¹²⁷, K.S. Krowpman ¹⁰⁶, U. Kruchonak ³⁸, H. Krüger ²⁴,
 N. Krumnack ⁸⁰, M.C. Kruse ⁵¹, J.A. Krzysiak ⁸⁵, A. Kubota ¹⁵³, O. Kuchinskaia ³⁷, S. Kuday ^{3a},
 D. Kuechler ⁴⁸, J.T. Kuechler ⁴⁸, S. Kuehn ³⁶, T. Kuhl ⁴⁸, V. Kukhtin ³⁸, Y. Kulchitsky ^{37,a},
 S. Kuleshov ^{136d,136b}, M. Kumar ^{33g}, N. Kumari ¹⁰¹, M. Kuna ⁶⁰, A. Kupco ¹³⁰, T. Kupfer ⁴⁹,
 A. Kupich ³⁷, O. Kuprash ⁵⁴, H. Kurashige ⁸³, L.L. Kurchaninov ^{155a}, Y.A. Kurochkin ³⁷,
 A. Kurova ³⁷, E.S. Kuwertz ³⁶, M. Kuze ¹⁵³, A.K. Kvam ¹⁰², J. Kvita ¹²¹, T. Kwan ¹⁰³,
 K.W. Kwok ^{64a}, N.G. Kyriacou ¹⁰⁵, L.A.O. Laatu ¹⁰¹, C. Lacasta ¹⁶², F. Lacava ^{74a,74b},
 H. Lacker ¹⁸, D. Lacour ¹²⁶, N.N. Lad ⁹⁵, E. Ladygin ³⁸, B. Laforge ¹²⁶, T. Lagouri ^{136e},
 S. Lai ⁵⁵, I.K. Lakomic ^{84a}, N. Lalloue ⁶⁰, J.E. Lambert ¹¹⁹, S. Lammers ⁶⁷, W. Lampl ⁷,
 C. Lampoudis ¹⁵¹, A.N. Lancaster ¹¹⁴, E. Lançon ²⁹, U. Landgraf ⁵⁴, M.P.J. Landon ⁹³,
 V.S. Lang ⁵⁴, R.J. Langenberg ¹⁰², A.J. Lankford ¹⁵⁹, F. Lanni ²⁹, K. Lantzsch ²⁴, A. Lanza ^{72a},
 A. Lapertosa ^{57b,57a}, J.F. Laporte ¹³⁴, T. Lari ^{70a}, F. Lasagni Manghi ^{23b}, M. Lassnig ³⁶,
 V. Latonova ¹³⁰, T.S. Lau ^{64a}, A. Laudrain ⁹⁹, A. Laurier ³⁴, S.D. Lawlor ⁹⁴, Z. Lawrence ¹⁰⁰,
 M. Lazzaroni ^{70a,70b}, B. Le ¹⁰⁰, B. Leban ⁹², A. Lebedev ⁸⁰, M. LeBlanc ³⁶, T. LeCompte ⁶,
 F. Ledroit-Guillon ⁶⁰, A.C.A. Lee ⁹⁵, G.R. Lee ¹⁶, L. Lee ⁶¹, S.C. Lee ¹⁴⁷, S. Lee ^{47a,47b},
 T.F. Lee ⁹¹, L.L. Leeuw ^{33c}, H.P. Lefebvre ⁹⁴, M. Lefebvre ¹⁶⁴, C. Leggett ^{17a}, K. Lehmann ¹⁴¹,
 G. Lehmann Miotto ³⁶, W.A. Leight ¹⁰², A. Leisos ^{151,u}, M.A.L. Leite ^{81c}, C.E. Leitgeb ⁴⁸,
 R. Leitner ¹³², K.J.C. Leney ⁴⁴, T. Lenz ²⁴, S. Leone ^{73a}, C. Leonidopoulos ⁵², A. Leopold ¹⁴³,
 C. Leroy ¹⁰⁷, R. Les ¹⁰⁶, C.G. Lester ³², M. Levchenko ³⁷, J. Levêque ⁴, D. Levin ¹⁰⁵,
 L.J. Levinson ¹⁶⁸, M.P. Lewicki ⁸⁵, D.J. Lewis ²⁰, B. Li ^{14b}, B. Li ^{62b}, C. Li ^{62a}, C-Q. Li ^{62c,62d},
 H. Li ^{62a}, H. Li ^{62b}, H. Li ^{14c}, H. Li ^{62b}, J. Li ^{62c}, K. Li ¹³⁷, L. Li ^{62c}, M. Li ^{14a,14d},
 Q.Y. Li ^{62a}, S. Li ^{62d,62c,e}, T. Li ^{62b}, X. Li ¹⁰³, Z. Li ^{62b}, Z. Li ¹²⁵, Z. Li ¹⁰³, Z. Li ⁹¹,
 Z. Liang ^{14a}, M. Liberatore ⁴⁸, B. Liberti ^{75a}, K. Lie ^{64c}, J. Lieber Marin ^{81b}, K. Lin ¹⁰⁶,
 R.A. Linck ⁶⁷, R.E. Lindley ⁷, J.H. Lindon ², A. Linss ⁴⁸, E. Lipeles ¹²⁷, A. Lipniacka ¹⁶,
 A. Lister ¹⁶³, J.D. Little ⁴, B. Liu ^{14a}, B.X. Liu ¹⁴¹, D. Liu ^{62d,62c}, J.B. Liu ^{62a}, J.K.K. Liu ³²,
 K. Liu ^{62d,62c}, M. Liu ^{62a}, M.Y. Liu ^{62a}, P. Liu ^{14a}, Q. Liu ^{62d,137,62c}, X. Liu ^{62a}, Y. Liu ⁴⁸,
 Y. Liu ^{14c,14d}, Y.L. Liu ¹⁰⁵, Y.W. Liu ^{62a}, M. Livan ^{72a,72b}, J. Llorente Merino ¹⁴¹, S.L. Lloyd ⁹³,

E.M. Lobodzinska ⁴⁸, P. Loch ⁷, S. Loffredo ^{75a,75b}, T. Lohse ¹⁸, K. Lohwasser ¹³⁸,
 M. Lokajicek ^{130,*}, J.D. Long ¹⁶¹, I. Longarini ^{74a,74b}, L. Longo ^{69a,69b}, R. Longo ¹⁶¹,
 I. Lopez Paz ³⁶, A. Lopez Solis ⁴⁸, J. Lorenz ¹⁰⁸, N. Lorenzo Martinez ⁴, A.M. Lory ¹⁰⁸,
 A. Lösle ⁵⁴, X. Lou ^{47a,47b}, X. Lou ^{14a,14d}, A. Lounis ⁶⁶, J. Love ⁶, P.A. Love ⁹⁰,
 J.J. Lozano Bahilo ¹⁶², G. Lu ^{14a,14d}, M. Lu ⁷⁹, S. Lu ¹²⁷, Y.J. Lu ⁶⁵, H.J. Lubatti ¹³⁷,
 C. Luci ^{74a,74b}, F.L. Lucio Alves ^{14c}, A. Lucotte ⁶⁰, F. Luehring ⁶⁷, I. Luise ¹⁴⁴,
 O. Lukianchuk ⁶⁶, O. Lundberg ¹⁴³, B. Lund-Jensen ¹⁴³, N.A. Luongo ¹²², M.S. Lutz ¹⁵⁰,
 D. Lynn ²⁹, H. Lyons⁹¹, R. Lysak ¹³⁰, E. Lytken ⁹⁷, F. Lyu ^{14a}, V. Lyubushkin ³⁸,
 T. Lyubushkina ³⁸, H. Ma ²⁹, L.L. Ma ^{62b}, Y. Ma ⁹⁵, D.M. Mac Donell ¹⁶⁴, G. Maccarrone ⁵³,
 J.C. MacDonald ¹³⁸, R. Madar ⁴⁰, W.F. Mader ⁵⁰, J. Maeda ⁸³, T. Maeno ²⁹, M. Maerker ⁵⁰,
 V. Magerl ⁵⁴, J. Magro ^{68a,68c}, H. Maguire ¹³⁸, D.J. Mahon ⁴¹, C. Maidantchik ^{81b},
 A. Maio ^{129a,129b,129d}, K. Maj ^{84a}, O. Majersky ^{28a}, S. Majewski ¹²², N. Makovec ⁶⁶,
 V. Maksimovic ¹⁵, B. Malaescu ¹²⁶, Pa. Malecki ⁸⁵, V.P. Maleev ³⁷, F. Malek ⁶⁰,
 D. Malito ^{43b,43a}, U. Mallik ⁷⁹, C. Malone ³², S. Maltezos¹⁰, S. Malyukov³⁸, J. Mamuzic ¹³,
 G. Mancini ⁵³, G. Manco ^{72a,72b}, J.P. Mandalia ⁹³, I. Mandić ⁹²,
 L. Manhaes de Andrade Filho ^{81a}, I.M. Maniatis ¹⁵¹, M. Manisha ¹³⁴, J. Manjarres Ramos ⁵⁰,
 D.C. Mankad ¹⁶⁸, K.H. Mankinen ⁹⁷, A. Mann ¹⁰⁸, A. Manousos ⁷⁸, B. Mansoulie ¹³⁴,
 S. Manzoni ³⁶, A. Marantis ^{151,u}, G. Marchiori ⁵, M. Marcisovsky ¹³⁰, L. Marcoccia ^{75a,75b},
 C. Marcon ^{70a,70b}, M. Marinescu ²⁰, M. Marjanovic ¹¹⁹, Z. Marshall ^{17a}, S. Marti-Garcia ¹⁶²,
 T.A. Martin ¹⁶⁶, V.J. Martin ⁵², B. Martin dit Latour ¹⁶, L. Martinelli ^{74a,74b}, M. Martinez ^{13,v},
 P. Martinez Agullo ¹⁶², V.I. Martinez Outschoorn ¹⁰², P. Martinez Suarez ¹³, S. Martin-Haugh ¹³³,
 V.S. Martoiu ^{27b}, A.C. Martyniuk ⁹⁵, A. Marzin ³⁶, S.R. Maschek ¹⁰⁹, L. Masetti ⁹⁹,
 T. Mashimo ¹⁵², J. Masik ¹⁰⁰, A.L. Maslennikov ³⁷, L. Massa ^{23b}, P. Massarotti ^{71a,71b},
 P. Mastrandrea ^{73a,73b}, A. Mastroberardino ^{43b,43a}, T. Masubuchi ¹⁵², T. Mathisen ¹⁶⁰,
 A. Matic ¹⁰⁸, N. Matsuzawa¹⁵², J. Maurer ^{27b}, B. Maček ⁹², D.A. Maximov ³⁷, R. Mazini ¹⁴⁷,
 I. Maznas ¹⁵¹, M. Mazza ¹⁰⁶, S.M. Mazza ¹³⁵, C. Mc Ginn ²⁹, J.P. Mc Gowan ¹⁰³,
 S.P. Mc Kee ¹⁰⁵, T.G. McCarthy ¹⁰⁹, W.P. McCormack ^{17a}, E.F. McDonald ¹⁰⁴,
 A.E. McDougall ¹¹³, J.A. Mcfayden ¹⁴⁵, G. Mchedlidze ^{148b}, R.P. Mckenzie ^{33g},
 T.C. McLachlan ⁴⁸, D.J. McLaughlin ⁹⁵, K.D. McLean ¹⁶⁴, S.J. McMahon ¹³³, P.C. McNamara ¹⁰⁴,
 R.A. McPherson ^{164,y}, J.E. Mdhluli ^{33g}, S. Meehan ³⁶, T. Megy ⁴⁰, S. Mehlhase ¹⁰⁸,
 A. Mehta ⁹¹, B. Meirose ⁴⁵, D. Melini ¹⁴⁹, B.R. Mellado Garcia ^{33g}, A.H. Melo ⁵⁵,
 F. Meloni ⁴⁸, E.D. Mendes Gouveia ^{129a}, A.M. Mendes Jacques Da Costa ²⁰, H.Y. Meng ¹⁵⁴,
 L. Meng ⁹⁰, S. Menke ¹⁰⁹, M. Mentink ³⁶, E. Meoni ^{43b,43a}, C. Merlassino ¹²⁵,
 L. Merola ^{71a,71b}, C. Meroni ^{70a,70b}, G. Merz¹⁰⁵, O. Meshkov ³⁷, J.K.R. Meshreki ¹⁴⁰,
 J. Metcalfe ⁶, A.S. Mete ⁶, C. Meyer ⁶⁷, J-P. Meyer ¹³⁴, M. Michetti ¹⁸, R.P. Middleton ¹³³,
 L. Mijović ⁵², G. Mikenberg ¹⁶⁸, M. Mikesikova ¹³⁰, M. Mikuž ⁹², H. Mildner ¹³⁸,
 A. Milic ¹⁵⁴, C.D. Milke ⁴⁴, D.W. Miller ³⁹, L.S. Miller ³⁴, A. Milov ¹⁶⁸, D.A. Milstead^{47a,47b},
 T. Min^{14c}, A.A. Minaenko ³⁷, I.A. Minashvili ^{148b}, L. Mince ⁵⁹, A.I. Mincer ¹¹⁶, B. Mindur ^{84a},
 M. Mineev ³⁸, Y. Minegishi¹⁵², Y. Mino ⁸⁶, L.M. Mir ¹³, M. Miralles Lopez ¹⁶²,
 M. Mironova ¹²⁵, T. Mitani ¹⁶⁷, A. Mitra ¹⁶⁶, V.A. Mitsou ¹⁶², O. Miu ¹⁵⁴, P.S. Miyagawa ⁹³,
 Y. Miyazaki⁸⁸, A. Mizukami ⁸², J.U. Mjörnmark ⁹⁷, T. Mkrtchyan ^{63a}, M. Mlynarikova ¹¹⁴,
 T. Moa ^{47a,47b}, S. Mobius ⁵⁵, K. Mochizuki ¹⁰⁷, P. Moder ⁴⁸, P. Mogg ¹⁰⁸,
 A.F. Mohammed ^{14a,14d}, S. Mohapatra ⁴¹, G. Mokgatitswane ^{33g}, B. Mondal ¹⁴⁰, S. Mondal ¹³¹,
 K. Möning ⁴⁸, E. Monnier ¹⁰¹, L. Monsonis Romero¹⁶², J. Montejo Berlingen ³⁶, M. Montella ¹¹⁸,
 F. Monticelli ⁸⁹, N. Morange ⁶⁶, A.L. Moreira De Carvalho ^{129a}, M. Moreno Llácer ¹⁶²,
 C. Moreno Martinez ¹³, P. Morettini ^{57b}, S. Morgenstern ¹⁶⁶, M. Morii ⁶¹, M. Morinaga ¹⁵²,
 V. Morisbak ¹²⁴, A.K. Morley ³⁶, F. Morodei ^{74a,74b}, L. Morvaj ³⁶, P. Moschovakos ³⁶,

B. Moser ³⁶, M. Mosidze^{148b}, T. Moskalets ⁵⁴, P. Moskvitina ¹¹², J. Moss ^{31,o}, E.J.W. Moyses ¹⁰²,
 S. Muanza ¹⁰¹, J. Mueller ¹²⁸, D. Muenstermann ⁹⁰, R. Müller ¹⁹, G.A. Mullier ⁹⁷, J.J. Mullin¹²⁷,
 D.P. Mungo ^{70a,70b}, J.L. Munoz Martinez ¹³, D. Munoz Perez ¹⁶², F.J. Munoz Sanchez ¹⁰⁰,
 M. Murin ¹⁰⁰, W.J. Murray ^{166,133}, A. Murrone ^{70a,70b}, J.M. Muse ¹¹⁹, M. Muškinja ^{17a},
 C. Mwewa ²⁹, A.G. Myagkov ^{37,a}, A.J. Myers ⁸, A.A. Myers¹²⁸, G. Myers ⁶⁷, M. Myska ¹³¹,
 B.P. Nachman ^{17a}, O. Nackenhorst ⁴⁹, A. Nag ⁵⁰, K. Nagai ¹²⁵, K. Nagano ⁸², J.L. Nagle ^{29,aj},
 E. Nagy ¹⁰¹, A.M. Nairz ³⁶, Y. Nakahama ⁸², K. Nakamura ⁸², H. Nanjo ¹²³, R. Narayan ⁴⁴,
 E.A. Narayanan ¹¹¹, I. Naryshkin ³⁷, M. Naseri ³⁴, C. Nass ²⁴, G. Navarro ^{22a},
 J. Navarro-Gonzalez ¹⁶², R. Nayak ¹⁵⁰, P.Y. Nechaeva ³⁷, F. Nechansky ⁴⁸, T.J. Neep ²⁰,
 A. Negri ^{72a,72b}, M. Negrini ^{23b}, C. Nellist ¹¹², C. Nelson ¹⁰³, K. Nelson ¹⁰⁵, S. Nemecek ¹³⁰,
 M. Nessi ^{36,h}, M.S. Neubauer ¹⁶¹, F. Neuhaus ⁹⁹, J. Neundorf ⁴⁸, R. Newhouse ¹⁶³,
 P.R. Newman ²⁰, C.W. Ng ¹²⁸, Y.S. Ng¹⁸, Y.W.Y. Ng ¹⁵⁹, B. Ngair ^{35e}, H.D.N. Nguyen ¹⁰⁷,
 R.B. Nickerson ¹²⁵, R. Nicolaidou ¹³⁴, J. Nielsen ¹³⁵, M. Niemeyer ⁵⁵, N. Nikiforou ³⁶,
 V. Nikolaenko ^{37,a}, I. Nikolic-Audit ¹²⁶, K. Nikolopoulos ²⁰, P. Nilsson ²⁹, H.R. Nindhito ⁵⁶,
 A. Nisati ^{74a}, N. Nishu ², R. Nisius ¹⁰⁹, J-E. Nitschke ⁵⁰, E.K. Nkadimeng ^{33g},
 S.J. Noacco Rosende ⁸⁹, T. Nobe ¹⁵², D.L. Noel ³², Y. Noguchi ⁸⁶, T. Nommensen ¹⁴⁶,
 M.A. Nomura²⁹, M.B. Norfolk ¹³⁸, R.R.B. Norisam ⁹⁵, B.J. Norman ³⁴, J. Novak ⁹², T. Novak ⁴⁸,
 O. Novgorodova ⁵⁰, L. Novotny ¹³¹, R. Novotny ¹¹¹, L. Nozka ¹²¹, K. Ntekas ¹⁵⁹, E. Nurse⁹⁵,
 F.G. Oakham ^{34,ag}, J. Ocariz ¹²⁶, A. Ochi ⁸³, I. Ochoa ^{129a}, S. Oerdek ¹⁶⁰, A. Ogrodnik ^{84a},
 A. Oh ¹⁰⁰, C.C. Ohm ¹⁴³, H. Oide ¹⁵³, R. Oishi ¹⁵², M.L. Ojeda ⁴⁸, Y. Okazaki ⁸⁶,
 M.W. O'Keefe⁹¹, Y. Okumura ¹⁵², A. Olariu^{27b}, L.F. Oleiro Seabra ^{129a}, S.A. Olivares Pino ^{136e},
 D. Oliveira Damazio ²⁹, D. Oliveira Goncalves ^{81a}, J.L. Oliver ¹⁵⁹, M.J.R. Olsson ¹⁵⁹,
 A. Olszewski ⁸⁵, J. Olszowska ^{85,*}, Ö.O. Öncel ⁵⁴, D.C. O'Neil ¹⁴¹, A.P. O'Neill ¹⁹,
 A. Onofre ^{129a,129e}, P.U.E. Onyisi ¹¹, M.J. Oreglia ³⁹, G.E. Orellana ⁸⁹, D. Orestano ^{76a,76b},
 N. Orlando ¹³, R.S. Orr ¹⁵⁴, V. O'Shea ⁵⁹, R. Ospanov ^{62a}, G. Otero y Garzon ³⁰, H. Otono ⁸⁸,
 P.S. Ott ^{63a}, G.J. Ottino ^{17a}, M. Ouchrif ^{35d}, J. Ouellette ^{29,aj}, F. Ould-Saada ¹²⁴, M. Owen ⁵⁹,
 R.E. Owen ¹³³, K.Y. Oyulmaz ^{21a}, V.E. Ozcan ^{21a}, N. Ozturk ⁸, S. Ozturk ^{21d}, J. Pacalt ¹²¹,
 H.A. Pacey ³², A. Pacheco Pages ¹³, C. Padilla Aranda ¹³, G. Padovano ^{74a,74b}, S. Pagan Griso ^{17a},
 G. Palacino ⁶⁷, A. Palazzo ^{69a,69b}, S. Palazzo ⁵², S. Palestini ³⁶, M. Palka ^{84b}, J. Pan ¹⁷¹,
 T. Pan ^{64a}, D.K. Panchal ¹¹, C.E. Pandini ¹¹³, J.G. Panduro Vazquez ⁹⁴, H. Pang ^{14b}, P. Pani ⁴⁸,
 G. Panizzo ^{68a,68c}, L. Paolozzi ⁵⁶, C. Papadatos ¹⁰⁷, S. Parajuli ⁴⁴, A. Paramonov ⁶,
 C. Paraskevopoulos ¹⁰, D. Paredes Hernandez ^{64b}, T.H. Park ¹⁵⁴, M.A. Parker ³², F. Parodi ^{57b,57a},
 E.W. Parrish ¹¹⁴, V.A. Parrish ⁵², J.A. Parsons ⁴¹, U. Parzefall ⁵⁴, B. Pascual Dias ¹⁰⁷,
 L. Pascual Dominguez ¹⁵⁰, V.R. Pascuzzi ^{17a}, F. Pasquali ¹¹³, E. Pasqualucci ^{74a}, S. Passaggio ^{57b},
 F. Pastore ⁹⁴, P. Pasuwan ^{47a,47b}, J.R. Pater ¹⁰⁰, J. Patton⁹¹, T. Pauly ³⁶, J. Pearkes ¹⁴²,
 M. Pedersen ¹²⁴, R. Pedro ^{129a}, S.V. Peleganchuk ³⁷, O. Penc ³⁶, C. Peng ^{64b}, H. Peng ^{62a},
 K.E. Pensi ¹⁰⁸, M. Penzin ³⁷, B.S. Peralva ^{81d}, A.P. Pereira Peixoto ⁶⁰, L. Pereira Sanchez ^{47a,47b},
 D.V. Perepelitsa ^{29,aj}, E. Perez Codina ^{155a}, M. Perganti ¹⁰, L. Perini ^{70a,70b,*}, H. Pernegger ³⁶,
 A. Perrevoort ¹¹², O. Perrin ⁴⁰, K. Peters ⁴⁸, R.F.Y. Peters ¹⁰⁰, B.A. Petersen ³⁶,
 T.C. Petersen ⁴², E. Petit ¹⁰¹, V. Petousis ¹³¹, C. Petridou ¹⁵¹, A. Petrukhin ¹⁴⁰, M. Pettee ^{17a},
 N.E. Pettersson ³⁶, A. Petukhov ³⁷, K. Petukhova ¹³², A. Peyaud ¹³⁴, R. Pezoa ^{136f},
 L. Pezzotti ³⁶, G. Pezzullo ¹⁷¹, T. Pham ¹⁰⁴, P.W. Phillips ¹³³, M.W. Phipps ¹⁶¹,
 G. Piacquadio ¹⁴⁴, E. Pianori ^{17a}, F. Piazza ^{70a,70b}, R. Piegaia ³⁰, D. Pietreanu ^{27b},
 A.D. Pilkington ¹⁰⁰, M. Pinamonti ^{68a,68c}, J.L. Pinfold ², B.C. Pinheiro Pereira ^{129a},
 C. Pitman Donaldson⁹⁵, D.A. Pizzi ³⁴, L. Pizzimento ^{75a,75b}, A. Pizzini ¹¹³, M.-A. Pleier ²⁹,
 V. Plesanovs⁵⁴, V. Pleskot ¹³², E. Plotnikova³⁸, G. Poddar ⁴, R. Poettgen ⁹⁷, L. Poggioli ¹²⁶,
 I. Pogrebnyak ¹⁰⁶, D. Pohl ²⁴, I. Pokharel ⁵⁵, S. Polacek ¹³², G. Polesello ^{72a}, A. Poley ^{141,155a},

R. Polifka ¹³¹, A. Polini ^{23b}, C.S. Pollard ¹²⁵, Z.B. Pollock ¹¹⁸, V. Polychronakos ²⁹,
 D. Ponomarenko ³⁷, L. Pontecorvo ³⁶, S. Popa ^{27a}, G.A. Popeneciu ^{27d},
 D.M. Portillo Quintero ^{155a}, S. Pospisil ¹³¹, P. Postolache ^{27c}, K. Potamianos ¹²⁵, I.N. Potrap ³⁸,
 C.J. Potter ³², H. Potti ¹, T. Poulsen ⁴⁸, J. Poveda ¹⁶², G. Pownall ⁴⁸, M.E. Pozo Astigarraga ³⁶,
 A. Prades Ibanez ¹⁶², M.M. Prapa ⁴⁶, J. Pretel ⁵⁴, D. Price ¹⁰⁰, M. Primavera ^{69a},
 M.A. Principe Martin ⁹⁸, M.L. Proffitt ¹³⁷, N. Proklova ³⁷, K. Prokofiev ^{64c}, G. Proto ^{75a,75b},
 S. Protopopescu ²⁹, J. Proudfoot ⁶, M. Przybycien ^{84a}, J.E. Puddefoot ¹³⁸, D. Pudzha ³⁷,
 P. Puzo ⁶⁶, D. Pyatiizbyantseva ³⁷, J. Qian ¹⁰⁵, Y. Qin ¹⁰⁰, T. Qiu ⁹³, A. Quadt ⁵⁵,
 M. Queitsch-Maitland ¹⁰⁰, G. Rabanal Bolanos ⁶¹, D. Rafanoharana ⁵⁴, F. Ragusa ^{70a,70b},
 J.L. Rainbolt ³⁹, J.A. Raine ⁵⁶, S. Rajagopalan ²⁹, E. Ramakoti ³⁷, K. Ran ^{48,14d}, V. Raskina ¹²⁶,
 D.F. Rassloff ^{63a}, S. Rave ⁹⁹, B. Ravina ⁵⁹, I. Ravinovich ¹⁶⁸, M. Raymond ³⁶, A.L. Read ¹²⁴,
 N.P. Readioff ¹³⁸, D.M. Rebuzzi ^{72a,72b}, G. Redlinger ²⁹, K. Reeves ⁴⁵, J.A. Reidelsturz ¹⁷⁰,
 D. Reikher ¹⁵⁰, A. Reiss ⁹⁹, A. Rej ¹⁴⁰, C. Rembser ³⁶, A. Renardi ⁴⁸, M. Renda ^{27b},
 M.B. Rendel ¹⁰⁹, A.G. Rennie ⁵⁹, S. Resconi ^{70a}, M. Ressegotti ^{57b,57a}, E.D. Resseguie ^{17a},
 S. Rettie ⁹⁵, B. Reynolds ¹¹⁸, E. Reynolds ^{17a}, M. Rezaei Estabragh ¹⁷⁰, O.L. Rezanova ³⁷,
 P. Reznicek ¹³², E. Ricci ^{77a,77b}, R. Richter ¹⁰⁹, S. Richter ^{47a,47b}, E. Richter-Was ^{84b},
 M. Ridel ¹²⁶, P. Rieck ¹¹⁶, P. Riedler ³⁶, M. Rijssenbeek ¹⁴⁴, A. Rimoldi ^{72a,72b}, M. Rimoldi ⁴⁸,
 L. Rinaldi ^{23b,23a}, T.T. Rinn ²⁹, M.P. Rinnagel ¹⁰⁸, G. Ripellino ¹⁴³, I. Riu ¹³, P. Rivadeneira ⁴⁸,
 J.C. Rivera Vergara ¹⁶⁴, F. Rizatdinova ¹²⁰, E. Rizvi ⁹³, C. Rizzi ⁵⁶, B.A. Roberts ¹⁶⁶,
 B.R. Roberts ^{17a}, S.H. Robertson ^{103,y}, M. Robin ⁴⁸, D. Robinson ³², C.M. Robles Gajardo ^{136f},
 M. Robles Manzano ⁹⁹, A. Robson ⁵⁹, A. Rocchi ^{75a,75b}, C. Roda ^{73a,73b}, S. Rodriguez Bosca ^{63a},
 Y. Rodriguez Garcia ^{22a}, A. Rodriguez Rodriguez ⁵⁴, A.M. Rodríguez Vera ^{155b}, S. Roe ³⁶,
 J.T. Roemer ¹⁵⁹, A.R. Roepe-Gier ¹¹⁹, J. Roggel ¹⁷⁰, O. Røhne ¹²⁴, R.A. Rojas ¹⁶⁴,
 B. Roland ⁵⁴, C.P.A. Roland ⁶⁷, J. Roloff ²⁹, A. Romaniouk ³⁷, E. Romano ^{72a,72b},
 M. Romano ^{23b}, A.C. Romero Hernandez ¹⁶¹, N. Rompotis ⁹¹, L. Roos ¹²⁶, S. Rosati ^{74a},
 B.J. Rosser ³⁹, E. Rossi ⁴, E. Rossi ^{71a,71b}, L.P. Rossi ^{57b}, L. Rossini ⁴⁸, R. Rosten ¹¹⁸,
 M. Rotaru ^{27b}, B. Rottler ⁵⁴, D. Rousseau ⁵⁶, D. Rousso ³², G. Rovelli ^{72a,72b}, A. Roy ¹⁶¹,
 A. Rozanov ¹⁰¹, Y. Rozen ¹⁴⁹, X. Ruan ^{33g}, A. Rubio Jimenez ¹⁶², A.J. Ruby ⁹¹,
 V.H. Ruelas Rivera ¹⁸, T.A. Ruggeri ¹, F. Rühr ⁵⁴, A. Ruiz-Martinez ¹⁶², A. Rummler ³⁶,
 Z. Rurikova ⁵⁴, N.A. Rusakovich ³⁸, H.L. Russell ¹⁶⁴, J.P. Rutherford ⁷, E.M. Rüttinger ¹³⁸,
 K. Rybacki ⁹⁰, M. Rybar ¹³², E.B. Rye ¹²⁴, A. Ryzhov ³⁷, J.A. Sabater Iglesias ⁵⁶, P. Sabatini ¹⁶²,
 L. Sabetta ^{74a,74b}, H.F-W. Sadrozinski ¹³⁵, F. Safai Tehrani ^{74a}, B. Safarzadeh Samani ¹⁴⁵,
 M. Safdari ¹⁴², S. Saha ¹⁰³, M. Sahinsoy ¹⁰⁹, M. Saimpert ¹³⁴, M. Saito ¹⁵², T. Saito ¹⁵²,
 D. Salamani ³⁶, G. Salamanna ^{76a,76b}, A. Salnikov ¹⁴², J. Salt ¹⁶², A. Salvador Salas ¹³,
 D. Salvatore ^{43b,43a}, F. Salvatore ¹⁴⁵, A. Salzburger ³⁶, D. Sammel ⁵⁴, D. Sampsonidis ¹⁵¹,
 D. Sampsonidou ^{62d,62c}, J. Sánchez ¹⁶², A. Sanchez Pineda ⁴, V. Sanchez Sebastian ¹⁶²,
 H. Sandaker ¹²⁴, C.O. Sander ⁴⁸, J.A. Sandesara ¹⁰², M. Sandhoff ¹⁷⁰, C. Sandoval ^{22b},
 D.P.C. Sankey ¹³³, A. Sansoni ⁵³, L. Santi ^{74a,74b}, C. Santoni ⁴⁰, H. Santos ^{129a,129b},
 S.N. Santpur ^{17a}, A. Santra ¹⁶⁸, K.A. Saoucha ¹³⁸, J.G. Saraiva ^{129a,129d}, J. Sardain ⁷,
 O. Sasaki ⁸², K. Sato ¹⁵⁶, C. Sauer ^{63b}, F. Sauerburger ⁵⁴, E. Sauvan ⁴, P. Savard ^{154,ag},
 R. Sawada ¹⁵², C. Sawyer ¹³³, L. Sawyer ⁹⁶, I. Sayago Galvan ¹⁶², C. Sbarra ^{23b}, A. Sbrizzi ^{23b,23a},
 T. Scanlon ⁹⁵, J. Schaarschmidt ¹³⁷, P. Schacht ¹⁰⁹, D. Schaefer ³⁹, U. Schäfer ⁹⁹,
 A.C. Schaffer ⁶⁶, D. Schaile ¹⁰⁸, R.D. Schamberger ¹⁴⁴, E. Schanet ¹⁰⁸, C. Scharf ¹⁸,
 V.A. Schegelsky ³⁷, D. Scheirich ¹³², F. Schenck ¹⁸, M. Schernau ¹⁵⁹, C. Scheulen ⁵⁵,
 C. Schiavi ^{57b,57a}, Z.M. Schillaci ²⁶, E.J. Schioppa ^{69a,69b}, M. Schioppa ^{43b,43a}, B. Schlag ⁹⁹,
 K.E. Schleicher ⁵⁴, S. Schlenker ³⁶, K. Schmieden ⁹⁹, C. Schmitt ⁹⁹, S. Schmitt ⁴⁸,
 L. Schoeffel ¹³⁴, A. Schoening ^{63b}, P.G. Scholer ⁵⁴, E. Schopf ¹²⁵, M. Schott ⁹⁹,

J. Schovancova ³⁶, S. Schramm ⁵⁶, F. Schroeder ¹⁷⁰, H-C. Schultz-Coulon ^{63a}, M. Schumacher ⁵⁴,
 B.A. Schumm ¹³⁵, Ph. Schune ¹³⁴, A. Schwartzman ¹⁴², T.A. Schwarz ¹⁰⁵, Ph. Schwemling ¹³⁴,
 R. Schwienhorst ¹⁰⁶, A. Sciandra ¹³⁵, G. Sciolla ²⁶, F. Scuri ^{73a}, F. Scutti ¹⁰⁴, C.D. Sebastiani ⁹¹,
 K. Sedlaczek ⁴⁹, P. Seema ¹⁸, S.C. Seidel ¹¹¹, A. Seiden ¹³⁵, B.D. Seidlitz ⁴¹, T. Seiss ³⁹,
 C. Seitz ⁴⁸, J.M. Seixas ^{81b}, G. Sekhniaidze ^{71a}, S.J. Sekula ⁴⁴, L. Selem ⁴,
 N. Semprini-Cesari ^{23b,23a}, S. Sen ⁵¹, D. Sengupta ⁵⁶, V. Senthilkumar ¹⁶², L. Serin ⁶⁶,
 L. Serkin ^{68a,68b}, M. Sessa ^{76a,76b}, H. Severini ¹¹⁹, S. Sevova ¹⁴², F. Sforza ^{57b,57a}, A. Sfyrla ⁵⁶,
 E. Shabalina ⁵⁵, R. Shaheen ¹⁴³, J.D. Shahinian ¹²⁷, N.W. Shaikh ^{47a,47b}, D. Shaked Renous ¹⁶⁸,
 L.Y. Shan ^{14a}, M. Shapiro ^{17a}, A. Sharma ³⁶, A.S. Sharma ¹⁶³, P. Sharma ⁷⁹, S. Sharma ⁴⁸,
 P.B. Shatalov ³⁷, K. Shaw ¹⁴⁵, S.M. Shaw ¹⁰⁰, Q. Shen ^{62c}, P. Sherwood ⁹⁵, L. Shi ⁹⁵,
 C.O. Shimmin ¹⁷¹, Y. Shimogama ¹⁶⁷, J.D. Shinner ⁹⁴, I.P.J. Shipsey ¹²⁵, S. Shirabe ⁶⁰,
 M. Shiyakova ^{38,x}, J. Shlomi ¹⁶⁸, M.J. Shochet ³⁹, J. Shojaii ¹⁰⁴, D.R. Shope ¹⁴³,
 S. Shrestha ^{118,ak}, E.M. Shrif ^{33g}, M.J. Shroff ¹⁶⁴, P. Sicho ¹³⁰, A.M. Sickles ¹⁶¹,
 E. Sideras Haddad ^{33g}, O. Sidiropoulou ³⁶, A. Sidoti ^{23b}, F. Siegert ⁵⁰, Dj. Sijacki ¹⁵,
 R. Sikora ^{84a}, F. Sili ⁸⁹, J.M. Silva ²⁰, M.V. Silva Oliveira ³⁶, S.B. Silverstein ^{47a}, S. Simion ⁶⁶,
 R. Simoniello ³⁶, E.L. Simpson ⁵⁹, N.D. Simpson ⁹⁷, S. Simsek ^{21d}, S. Sindhu ⁵⁵, P. Sinervo ¹⁵⁴,
 V. Sinetckii ³⁷, S. Singh ¹⁴¹, S. Singh ¹⁵⁴, S. Sinha ⁴⁸, S. Sinha ^{33g}, M. Sioli ^{23b,23a},
 I. Siral ¹²², S.Yu. Sivoklokov ^{37,*}, J. Sjölin ^{47a,47b}, A. Skaf ⁵⁵, E. Skorda ⁹⁷, P. Skubic ¹¹⁹,
 M. Slawinska ⁸⁵, V. Smakhtin ¹⁶⁸, B.H. Smart ¹³³, J. Smiesko ¹³², S.Yu. Smirnov ³⁷,
 Y. Smirnov ³⁷, L.N. Smirnova ^{37,a}, O. Smirnova ⁹⁷, A.C. Smith ⁴¹, E.A. Smith ³⁹,
 H.A. Smith ¹²⁵, J.L. Smith ⁹¹, R. Smith ¹⁴², M. Smizanska ⁹⁰, K. Smolek ¹³¹, A. Smykiewicz ⁸⁵,
 A.A. Snesarev ³⁷, H.L. Snoek ¹¹³, S. Snyder ²⁹, R. Sobie ^{164,y}, A. Soffer ¹⁵⁰,
 C.A. Solans Sanchez ³⁶, E.Yu. Soldatov ³⁷, U. Soldevila ¹⁶², A.A. Solodkov ³⁷, S. Solomon ⁵⁴,
 A. Soloshenko ³⁸, K. Solovieva ⁵⁴, O.V. Solovyanov ³⁷, V. Solovyev ³⁷, P. Sommer ³⁶,
 A. Sonay ¹³, W.Y. Song ^{155b}, A. Sopczak ¹³¹, A.L. Sopio ⁹⁵, F. Sopkova ^{28b}, V. Sothilingam ^{63a},
 S. Sottocornola ^{72a,72b}, R. Soualah ^{115b}, Z. Soumami ^{35e}, D. South ⁴⁸, S. Spagnolo ^{69a,69b},
 M. Spalla ¹⁰⁹, F. Spanò ⁹⁴, D. Sperlich ⁵⁴, G. Spigo ³⁶, M. Spina ¹⁴⁵, S. Spinali ⁹⁰,
 D.P. Spiteri ⁵⁹, M. Spousta ¹³², E.J. Staats ³⁴, A. Stabile ^{70a,70b}, R. Stamen ^{63a},
 M. Stamenkovic ¹¹³, A. Stampekis ²⁰, M. Standke ²⁴, E. Stanecka ⁸⁵, B. Stanislaus ^{17a},
 M.M. Stanitzki ⁴⁸, M. Stankaityte ¹²⁵, B. Stapf ⁴⁸, E.A. Starchenko ³⁷, G.H. Stark ¹³⁵,
 J. Stark ^{101,ab}, D.M. Starko ^{155b}, P. Staroba ¹³⁰, P. Starovoitov ^{63a}, S. Stärz ¹⁰³, R. Staszewski ⁸⁵,
 G. Stavropoulos ⁴⁶, J. Steentoft ¹⁶⁰, P. Steinberg ²⁹, A.L. Steinhebel ¹²², B. Stelzer ^{141,155a},
 H.J. Stelzer ¹²⁸, O. Stelzer-Chilton ^{155a}, H. Stenzel ⁵⁸, T.J. Stevenson ¹⁴⁵, G.A. Stewart ³⁶,
 M.C. Stockton ³⁶, G. Stoicea ^{27b}, M. Stolarski ^{129a}, S. Stonjek ¹⁰⁹, A. Straessner ⁵⁰,
 J. Strandberg ¹⁴³, S. Strandberg ^{47a,47b}, M. Strauss ¹¹⁹, T. Strebler ¹⁰¹, P. Strizenec ^{28b},
 R. Ströhmer ¹⁶⁵, D.M. Strom ¹²², L.R. Strom ⁴⁸, R. Stroynowski ⁴⁴, A. Strubig ^{47a,47b},
 S.A. Stucci ²⁹, B. Stugu ¹⁶, J. Stupak ¹¹⁹, N.A. Styles ⁴⁸, D. Su ¹⁴², S. Su ^{62a},
 W. Su ^{62d,137,62c}, X. Su ^{62a,66}, K. Sugizaki ¹⁵², V.V. Sulin ³⁷, M.J. Sullivan ⁹¹,
 D.M.S. Sultan ^{77a,77b}, L. Sultanaliev ³⁷, S. Sultansoy ^{3b}, T. Sumida ⁸⁶, S. Sun ¹⁰⁵, S. Sun ¹⁶⁹,
 O. Sunneborn Gudnadottir ¹⁶⁰, M.R. Sutton ¹⁴⁵, M. Svatos ¹³⁰, M. Swiatlowski ^{155a},
 T. Swirski ¹⁶⁵, I. Sykora ^{28a}, M. Sykora ¹³², T. Sykora ¹³², D. Ta ⁹⁹, K. Tackmann ^{48,w},
 A. Taffard ¹⁵⁹, R. Tafirout ^{155a}, J.S. Tafoya Vargas ⁶⁶, R.H.M. Taibah ¹²⁶, R. Takashima ⁸⁷,
 K. Takeda ⁸³, E.P. Takeva ⁵², Y. Takubo ⁸², M. Talby ¹⁰¹, A.A. Talyshev ³⁷, K.C. Tam ^{64b},
 N.M. Tamir ¹⁵⁰, A. Tanaka ¹⁵², J. Tanaka ¹⁵², R. Tanaka ⁶⁶, M. Tanasini ^{57b,57a}, J. Tang ^{62c},
 Z. Tao ¹⁶³, S. Tapia Araya ⁸⁰, S. Tapprogge ⁹⁹, A. Tarek Abouelfadl Mohamed ¹⁰⁶, S. Tarem ¹⁴⁹,
 K. Tariq ^{62b}, G. Tarna ^{27b}, G.F. Tartarelli ^{70a}, P. Tas ¹³², M. Tasevsky ¹³⁰, E. Tassi ^{43b,43a},
 A.C. Tate ¹⁶¹, G. Tateno ¹⁵², Y. Tayalati ^{35e}, G.N. Taylor ¹⁰⁴, W. Taylor ^{155b}, H. Teagle ⁹¹,

A.S. Tee ¹⁶⁹, R. Teixeira De Lima ¹⁴², P. Teixeira-Dias ⁹⁴, J.J. Teoh ¹⁵⁴, K. Terashi ¹⁵²,
 J. Terron ⁹⁸, S. Terzo ¹³, M. Testa ⁵³, R.J. Teuscher ^{154,y}, A. Thaler ⁷⁸, O. Theiner ⁵⁶,
 N. Themistokleous ⁵², T. Thevenaux-Pelzer ¹⁸, O. Thielmann ¹⁷⁰, D.W. Thomas ⁹⁴, J.P. Thomas ²⁰,
 E.A. Thompson ⁴⁸, P.D. Thompson ²⁰, E. Thomson ¹²⁷, E.J. Thorpe ⁹³, Y. Tian ⁵⁵,
 V. Tikhomirov ^{37,a}, Yu.A. Tikhonov ³⁷, S. Timoshenko ³⁷, E.X.L. Ting ¹, P. Tipton ¹⁷¹,
 S. Tisserant ¹⁰¹, S.H. Tlou ^{33g}, A. Tnourji ⁴⁰, K. Todome ^{23b,23a}, S. Todorova-Nova ¹³², S. Todt ⁵⁰,
 M. Togawa ⁸², J. Tojo ⁸⁸, S. Tokár ^{28a}, K. Tokushuku ⁸², R. Tombs ³², M. Tomoto ^{82,110},
 L. Tompkins ^{142,q}, K.W. Topolnicki ^{84b}, P. Tornambe ¹⁰², E. Torrence ¹²², H. Torres ⁵⁰,
 E. Torró Pastor ¹⁶², M. Toscani ³⁰, C. Tosciri ³⁹, D.R. Tovey ¹³⁸, A. Traeet ¹⁶, I.S. Trandafir ^{27b},
 T. Trefzger ¹⁶⁵, A. Tricoli ²⁹, I.M. Trigger ^{155a}, S. Trincaz-Duvoid ¹²⁶, D.A. Trischuk ¹⁶³,
 B. Trocmé ⁶⁰, A. Trofymov ⁶⁶, C. Troncon ^{70a}, L. Truong ^{33c}, M. Trzebinski ⁸⁵, A. Trzupsek ⁸⁵,
 F. Tsai ¹⁴⁴, M. Tsai ¹⁰⁵, A. Tsiamis ¹⁵¹, P.V. Tsiarehka ³⁷, S. Tsigaridas ^{155a}, A. Tsigiriotis ^{151,u},
 V. Tsiskaridze ¹⁴⁴, E.G. Tskhadadze ^{148a}, M. Tsopoulou ¹⁵¹, Y. Tsujikawa ⁸⁶, I.I. Tsukerman ³⁷,
 V. Tsulaia ^{17a}, S. Tsuno ⁸², O. Tsur ¹⁴⁹, D. Tsybychev ¹⁴⁴, Y. Tu ^{64b}, A. Tudorache ^{27b},
 V. Tudorache ^{27b}, A.N. Tuna ³⁶, S. Turchikhin ³⁸, I. Turk Cakir ^{3a}, R. Turra ^{70a}, T. Turtuvshin ³⁸,
 P.M. Tuts ⁴¹, S. Tzamarias ¹⁵¹, P. Tzani ¹⁰, E. Tzovara ⁹⁹, K. Uchida ¹⁵², F. Ukegawa ¹⁵⁶,
 P.A. Ulloa Poblete ^{136c}, G. Unal ³⁶, M. Unal ¹¹, A. Undrus ²⁹, G. Unel ¹⁵⁹, K. Uno ¹⁵²,
 J. Urban ^{28b}, P. Urquijo ¹⁰⁴, G. Usai ⁸, R. Ushioda ¹⁵³, M. Usman ¹⁰⁷, Z. Uysal ^{21b},
 V. Vacek ¹³¹, B. Vachon ¹⁰³, K.O.H. Vadla ¹²⁴, T. Vafeiadis ³⁶, C. Valderanis ¹⁰⁸,
 E. Valdes Santurio ^{47a,47b}, M. Valente ^{155a}, S. Valentinetti ^{23b,23a}, A. Valero ¹⁶², A. Vallier ^{101,ab},
 J.A. Valls Ferrer ¹⁶², T.R. Van Daalen ¹³⁷, P. Van Gemmeren ⁶, M. Van Rijnbach ^{124,36},
 S. Van Stroud ⁹⁵, I. Van Vulpen ¹¹³, M. Vanadia ^{75a,75b}, W. Vandelli ³⁶, M. Vandenbroucke ¹³⁴,
 E.R. Vandewall ¹²⁰, D. Vannicola ¹⁵⁰, L. Vannoli ^{57b,57a}, R. Vari ^{74a}, E.W. Varnes ⁷,
 C. Varni ^{17a}, T. Varol ¹⁴⁷, D. Varouchas ⁶⁶, L. Varriale ¹⁶², K.E. Varvell ¹⁴⁶, M.E. Vasile ^{27b},
 L. Vaslin ⁴⁰, G.A. Vasquez ¹⁶⁴, F. Vazeille ⁴⁰, T. Vazquez Schroeder ³⁶, J. Veatch ³¹,
 V. Vecchio ¹⁰⁰, M.J. Veen ¹¹³, I. Veliscek ¹²⁵, L.M. Veloce ¹⁵⁴, F. Veloso ^{129a,129c},
 S. Veneziano ^{74a}, A. Ventura ^{69a,69b}, A. Verbytskyi ¹⁰⁹, M. Verducci ^{73a,73b}, C. Vergis ²⁴,
 M. Verissimo De Araujo ^{81b}, W. Verkerke ¹¹³, J.C. Vermeulen ¹¹³, C. Vernieri ¹⁴²,
 P.J. Verschuuren ⁹⁴, M. Vessella ¹⁰², M.L. Vesterbacka ¹¹⁶, M.C. Vetterli ^{141,ag},
 A. Vgenopoulos ¹⁵¹, N. Viaux Maira ^{136f}, T. Vickey ¹³⁸, O.E. Vickey Boeriu ¹³⁸,
 G.H.A. Viehhauser ¹²⁵, L. Vigani ^{63b}, M. Villa ^{23b,23a}, M. Villaplana Perez ¹⁶², E.M. Villhauer ⁵²,
 E. Vilucchi ⁵³, M.G. Vincter ³⁴, G.S. Virdee ²⁰, A. Vishwakarma ⁵², C. Vittori ^{23b,23a},
 I. Vivarelli ¹⁴⁵, V. Vladimirov ¹⁶⁶, E. Voevodina ¹⁰⁹, F. Vogel ¹⁰⁸, P. Vokac ¹³¹, J. Von Ahnen ⁴⁸,
 E. Von Toerne ²⁴, B. Vormwald ³⁶, V. Vorobel ¹³², K. Vorobev ³⁷, M. Vos ¹⁶²,
 J.H. Vosseveld ⁹¹, M. Vozak ¹¹³, L. Vozdecky ⁹³, N. Vranjes ¹⁵, M. Vranjes Milosavljevic ¹⁵,
 M. Vreeswijk ¹¹³, R. Vuillermet ³⁶, O. Vujanovic ⁹⁹, I. Vukotic ³⁹, S. Wada ¹⁵⁶, C. Wagner ¹⁰²,
 W. Wagner ¹⁷⁰, S. Wahdan ¹⁷⁰, H. Wahlberg ⁸⁹, R. Wakasa ¹⁵⁶, M. Wakida ¹¹⁰,
 V.M. Walbrecht ¹⁰⁹, J. Walder ¹³³, R. Walker ¹⁰⁸, W. Walkowiak ¹⁴⁰, A.M. Wang ⁶¹,
 A.Z. Wang ¹⁶⁹, C. Wang ^{62a}, C. Wang ^{62c}, H. Wang ^{17a}, J. Wang ^{64a}, P. Wang ⁴⁴,
 R.-J. Wang ⁹⁹, R. Wang ⁶¹, R. Wang ⁶, S.M. Wang ¹⁴⁷, S. Wang ^{62b}, T. Wang ^{62a},
 W.T. Wang ⁷⁹, W.X. Wang ^{62a}, X. Wang ^{14c}, X. Wang ¹⁶¹, X. Wang ^{62c}, Y. Wang ^{62d},
 Y. Wang ^{14c}, Z. Wang ¹⁰⁵, Z. Wang ^{62d,51,62c}, Z. Wang ¹⁰⁵, A. Warburton ¹⁰³, R.J. Ward ²⁰,
 N. Warrack ⁵⁹, A.T. Watson ²⁰, M.F. Watson ²⁰, G. Watts ¹³⁷, B.M. Waugh ⁹⁵, A.F. Webb ¹¹,
 C. Weber ²⁹, M.S. Weber ¹⁹, S.A. Weber ³⁴, S.M. Weber ^{63a}, C. Wei ^{62a}, Y. Wei ¹²⁵,
 A.R. Weidberg ¹²⁵, J. Weingarten ⁴⁹, M. Weirich ⁹⁹, C. Weiser ⁵⁴, C.J. Wells ⁴⁸, T. Wenaus ²⁹,
 B. Wendland ⁴⁹, T. Wengler ³⁶, N.S. Wenke ¹⁰⁹, N. Vermes ²⁴, M. Wessels ^{63a}, K. Whalen ¹²²,
 A.M. Wharton ⁹⁰, A.S. White ⁶¹, A. White ⁸, M.J. White ¹, D. Whiteson ¹⁵⁹,

L. Wickremasinghe ¹²³, W. Wiedenmann ¹⁶⁹, C. Wiel ⁵⁰, M. Wielers ¹³³, N. Wieseotte ⁹⁹, C. Wiglesworth ⁴², L.A.M. Wiik-Fuchs ⁵⁴, D.J. Wilbern ¹¹⁹, H.G. Wilkens ³⁶, D.M. Williams ⁴¹, H.H. Williams ¹²⁷, S. Williams ³², S. Willocq ¹⁰², P.J. Windischhofer ¹²⁵, F. Winklmeier ¹²², B.T. Winter ⁵⁴, M. Wittgen ¹⁴², M. Wobisch ⁹⁶, A. Wolf ⁹⁹, R. Wölker ¹²⁵, J. Wollrath ¹⁵⁹, M.W. Wolter ⁸⁵, H. Wolters ^{129a,129c}, V.W.S. Wong ¹⁶³, A.F. Wongel ⁴⁸, S.D. Worm ⁴⁸, B.K. Wosiek ⁸⁵, K.W. Woźniak ⁸⁵, K. Wraight ⁵⁹, J. Wu ^{14a,14d}, M. Wu ^{64a}, S.L. Wu ¹⁶⁹, X. Wu ⁵⁶, Y. Wu ^{62a}, Z. Wu ^{134,62a}, J. Wuerzinger ¹²⁵, T.R. Wyatt ¹⁰⁰, B.M. Wynne ⁵², S. Xella ⁴², L. Xia ^{14c}, M. Xia ^{14b}, J. Xiang ^{64c}, X. Xiao ¹⁰⁵, M. Xie ^{62a}, X. Xie ^{62a}, J. Xiong ^{17a}, I. Xiotidis ¹⁴⁵, D. Xu ^{14a}, H. Xu ^{62a}, H. Xu ^{62a}, L. Xu ^{62a}, R. Xu ¹²⁷, T. Xu ¹⁰⁵, W. Xu ¹⁰⁵, Y. Xu ^{14b}, Z. Xu ^{62b}, Z. Xu ¹⁴², B. Yabsley ¹⁴⁶, S. Yacoob ^{33a}, N. Yamaguchi ⁸⁸, Y. Yamaguchi ¹⁵³, H. Yamauchi ¹⁵⁶, T. Yamazaki ^{17a}, Y. Yamazaki ⁸³, J. Yan ^{62c}, S. Yan ¹²⁵, Z. Yan ²⁵, H.J. Yang ^{62c,62d}, H.T. Yang ^{17a}, S. Yang ^{62a}, T. Yang ^{64c}, X. Yang ^{62a}, X. Yang ^{14a}, Y. Yang ⁴⁴, Z. Yang ^{62a,105}, W-M. Yao ^{17a}, Y.C. Yap ⁴⁸, H. Ye ^{14c}, J. Ye ⁴⁴, S. Ye ²⁹, X. Ye ^{62a}, Y. Yeh ⁹⁵, I. Yeletsikh ³⁸, M.R. Yexley ⁹⁰, P. Yin ⁴¹, K. Yorita ¹⁶⁷, C.J.S. Young ⁵⁴, C. Young ¹⁴², M. Yuan ¹⁰⁵, R. Yuan ^{62b,k}, L. Yue ⁹⁵, X. Yue ^{63a}, M. Zaazoua ^{35e}, B. Zabinski ⁸⁵, E. Zaid ⁵², T. Zakareishvili ^{148b}, N. Zakharchuk ³⁴, S. Zambito ⁵⁶, J.A. Zamora Saa ^{136d}, J. Zang ¹⁵², D. Zanzi ⁵⁴, O. Zaplatilek ¹³¹, S.V. Zeibner ⁴⁹, C. Zeitnitz ¹⁷⁰, J.C. Zeng ¹⁶¹, D.T. Zenger Jr ²⁶, O. Zenin ³⁷, T. Ženiš ^{28a}, S. Zenz ⁹³, S. Zerradi ^{35a}, D. Zerwas ⁶⁶, B. Zhang ^{14c}, D.F. Zhang ¹³⁸, G. Zhang ^{14b}, J. Zhang ⁶, K. Zhang ^{14a,14d}, L. Zhang ^{14c}, P. Zhang ^{14a,14d}, R. Zhang ¹⁶⁹, S. Zhang ¹⁰⁵, T. Zhang ¹⁵², X. Zhang ^{62c}, X. Zhang ^{62b}, Z. Zhang ^{17a}, Z. Zhang ⁶⁶, H. Zhao ¹³⁷, P. Zhao ⁵¹, T. Zhao ^{62b}, Y. Zhao ¹³⁵, Z. Zhao ^{62a}, A. Zhemchugov ³⁸, Z. Zheng ¹⁴², D. Zhong ¹⁶¹, B. Zhou ¹⁰⁵, C. Zhou ¹⁶⁹, H. Zhou ⁷, N. Zhou ^{62c}, Y. Zhou ⁷, C.G. Zhu ^{62b}, C. Zhu ^{14a,14d}, H.L. Zhu ^{62a}, H. Zhu ^{14a}, J. Zhu ¹⁰⁵, Y. Zhu ^{62c}, Y. Zhu ^{62a}, X. Zhuang ^{14a}, K. Zhukov ³⁷, V. Zhulanov ³⁷, N.I. Zimine ³⁸, J. Zinsser ^{63b}, M. Ziolkowski ¹⁴⁰, L. Živković ¹⁵, A. Zoccoli ^{23b,23a}, K. Zoch ⁵⁶, T.G. Zorbas ¹³⁸, O. Zormpa ⁴⁶, W. Zou ⁴¹, L. Zwalinski ³⁶.

¹Department of Physics, University of Adelaide, Adelaide; Australia.

²Department of Physics, University of Alberta, Edmonton AB; Canada.

³(^a)Department of Physics, Ankara University, Ankara; (^b)Division of Physics, TOBB University of Economics and Technology, Ankara; Türkiye.

⁴LAPP, Université Savoie Mont Blanc, CNRS/IN2P3, Annecy; France.

⁵APC, Université Paris Cité, CNRS/IN2P3, Paris; France.

⁶High Energy Physics Division, Argonne National Laboratory, Argonne IL; United States of America.

⁷Department of Physics, University of Arizona, Tucson AZ; United States of America.

⁸Department of Physics, University of Texas at Arlington, Arlington TX; United States of America.

⁹Physics Department, National and Kapodistrian University of Athens, Athens; Greece.

¹⁰Physics Department, National Technical University of Athens, Zografou; Greece.

¹¹Department of Physics, University of Texas at Austin, Austin TX; United States of America.

¹²Institute of Physics, Azerbaijan Academy of Sciences, Baku; Azerbaijan.

¹³Institut de Física d'Altes Energies (IFAE), Barcelona Institute of Science and Technology, Barcelona; Spain.

¹⁴(^a)Institute of High Energy Physics, Chinese Academy of Sciences, Beijing; (^b)Physics Department, Tsinghua University, Beijing; (^c)Department of Physics, Nanjing University, Nanjing; (^d)University of Chinese Academy of Science (UCAS), Beijing; China.

¹⁵Institute of Physics, University of Belgrade, Belgrade; Serbia.

¹⁶Department for Physics and Technology, University of Bergen, Bergen; Norway.

- ^{17(a)}Physics Division, Lawrence Berkeley National Laboratory, Berkeley CA;^(b)University of California, Berkeley CA; United States of America.
- ¹⁸Institut für Physik, Humboldt Universität zu Berlin, Berlin; Germany.
- ¹⁹Albert Einstein Center for Fundamental Physics and Laboratory for High Energy Physics, University of Bern, Bern; Switzerland.
- ²⁰School of Physics and Astronomy, University of Birmingham, Birmingham; United Kingdom.
- ^{21(a)}Department of Physics, Bogazici University, Istanbul;^(b)Department of Physics Engineering, Gaziantep University, Gaziantep;^(c)Department of Physics, Istanbul University, Istanbul;^(d)Istinye University, Sariyer, Istanbul; Türkiye.
- ^{22(a)}Facultad de Ciencias y Centro de Investigaciones, Universidad Antonio Nariño, Bogotá;^(b)Departamento de Física, Universidad Nacional de Colombia, Bogotá; Colombia.
- ^{23(a)}Dipartimento di Fisica e Astronomia A. Righi, Università di Bologna, Bologna;^(b)INFN Sezione di Bologna; Italy.
- ²⁴Physikalisches Institut, Universität Bonn, Bonn; Germany.
- ²⁵Department of Physics, Boston University, Boston MA; United States of America.
- ²⁶Department of Physics, Brandeis University, Waltham MA; United States of America.
- ^{27(a)}Transilvania University of Brasov, Brasov;^(b)Horia Hulubei National Institute of Physics and Nuclear Engineering, Bucharest;^(c)Department of Physics, Alexandru Ioan Cuza University of Iasi, Iasi;^(d)National Institute for Research and Development of Isotopic and Molecular Technologies, Physics Department, Cluj-Napoca;^(e)University Politehnica Bucharest, Bucharest;^(f)West University in Timisoara, Timisoara;^(g)Faculty of Physics, University of Bucharest, Bucharest; Romania.
- ^{28(a)}Faculty of Mathematics, Physics and Informatics, Comenius University, Bratislava;^(b)Department of Subnuclear Physics, Institute of Experimental Physics of the Slovak Academy of Sciences, Kosice; Slovak Republic.
- ²⁹Physics Department, Brookhaven National Laboratory, Upton NY; United States of America.
- ³⁰Universidad de Buenos Aires, Facultad de Ciencias Exactas y Naturales, Departamento de Física, y CONICET, Instituto de Física de Buenos Aires (IFIBA), Buenos Aires; Argentina.
- ³¹California State University, CA; United States of America.
- ³²Cavendish Laboratory, University of Cambridge, Cambridge; United Kingdom.
- ^{33(a)}Department of Physics, University of Cape Town, Cape Town;^(b)iThemba Labs, Western Cape;^(c)Department of Mechanical Engineering Science, University of Johannesburg, Johannesburg;^(d)National Institute of Physics, University of the Philippines Diliman (Philippines);^(e)University of South Africa, Department of Physics, Pretoria;^(f)University of Zululand, KwaDlangezwa;^(g)School of Physics, University of the Witwatersrand, Johannesburg; South Africa.
- ³⁴Department of Physics, Carleton University, Ottawa ON; Canada.
- ^{35(a)}Faculté des Sciences Ain Chock, Réseau Universitaire de Physique des Hautes Energies - Université Hassan II, Casablanca;^(b)Faculté des Sciences, Université Ibn-Tofail, Kénitra;^(c)Faculté des Sciences Semlalia, Université Cadi Ayyad, LPHEA-Marrakech;^(d)LPMR, Faculté des Sciences, Université Mohamed Premier, Oujda;^(e)Faculté des sciences, Université Mohammed V, Rabat;^(f)Institute of Applied Physics, Mohammed VI Polytechnic University, Ben Guerir; Morocco.
- ³⁶CERN, Geneva; Switzerland.
- ³⁷Affiliated with an institute covered by a cooperation agreement with CERN.
- ³⁸Affiliated with an international laboratory covered by a cooperation agreement with CERN.
- ³⁹Enrico Fermi Institute, University of Chicago, Chicago IL; United States of America.
- ⁴⁰LPC, Université Clermont Auvergne, CNRS/IN2P3, Clermont-Ferrand; France.
- ⁴¹Nevis Laboratory, Columbia University, Irvington NY; United States of America.
- ⁴²Niels Bohr Institute, University of Copenhagen, Copenhagen; Denmark.

- ^{43(a)}Dipartimento di Fisica, Università della Calabria, Rende; ^(b)INFN Gruppo Collegato di Cosenza, Laboratori Nazionali di Frascati; Italy.
- ⁴⁴Physics Department, Southern Methodist University, Dallas TX; United States of America.
- ⁴⁵Physics Department, University of Texas at Dallas, Richardson TX; United States of America.
- ⁴⁶National Centre for Scientific Research "Demokritos", Agia Paraskevi; Greece.
- ^{47(a)}Department of Physics, Stockholm University; ^(b)Oskar Klein Centre, Stockholm; Sweden.
- ⁴⁸Deutsches Elektronen-Synchrotron DESY, Hamburg and Zeuthen; Germany.
- ⁴⁹Fakultät Physik, Technische Universität Dortmund, Dortmund; Germany.
- ⁵⁰Institut für Kern- und Teilchenphysik, Technische Universität Dresden, Dresden; Germany.
- ⁵¹Department of Physics, Duke University, Durham NC; United States of America.
- ⁵²SUPA - School of Physics and Astronomy, University of Edinburgh, Edinburgh; United Kingdom.
- ⁵³INFN e Laboratori Nazionali di Frascati, Frascati; Italy.
- ⁵⁴Physikalisches Institut, Albert-Ludwigs-Universität Freiburg, Freiburg; Germany.
- ⁵⁵II. Physikalisches Institut, Georg-August-Universität Göttingen, Göttingen; Germany.
- ⁵⁶Département de Physique Nucléaire et Corpusculaire, Université de Genève, Genève; Switzerland.
- ^{57(a)}Dipartimento di Fisica, Università di Genova, Genova; ^(b)INFN Sezione di Genova; Italy.
- ⁵⁸II. Physikalisches Institut, Justus-Liebig-Universität Giessen, Giessen; Germany.
- ⁵⁹SUPA - School of Physics and Astronomy, University of Glasgow, Glasgow; United Kingdom.
- ⁶⁰LPSC, Université Grenoble Alpes, CNRS/IN2P3, Grenoble INP, Grenoble; France.
- ⁶¹Laboratory for Particle Physics and Cosmology, Harvard University, Cambridge MA; United States of America.
- ^{62(a)}Department of Modern Physics and State Key Laboratory of Particle Detection and Electronics, University of Science and Technology of China, Hefei; ^(b)Institute of Frontier and Interdisciplinary Science and Key Laboratory of Particle Physics and Particle Irradiation (MOE), Shandong University, Qingdao; ^(c)School of Physics and Astronomy, Shanghai Jiao Tong University, Key Laboratory for Particle Astrophysics and Cosmology (MOE), SKLPPC, Shanghai; ^(d)Tsung-Dao Lee Institute, Shanghai; China.
- ^{63(a)}Kirchhoff-Institut für Physik, Ruprecht-Karls-Universität Heidelberg, Heidelberg; ^(b)Physikalisches Institut, Ruprecht-Karls-Universität Heidelberg, Heidelberg; Germany.
- ^{64(a)}Department of Physics, Chinese University of Hong Kong, Shatin, N.T., Hong Kong; ^(b)Department of Physics, University of Hong Kong, Hong Kong; ^(c)Department of Physics and Institute for Advanced Study, Hong Kong University of Science and Technology, Clear Water Bay, Kowloon, Hong Kong; China.
- ⁶⁵Department of Physics, National Tsing Hua University, Hsinchu; Taiwan.
- ⁶⁶IJCLab, Université Paris-Saclay, CNRS/IN2P3, 91405, Orsay; France.
- ⁶⁷Department of Physics, Indiana University, Bloomington IN; United States of America.
- ^{68(a)}INFN Gruppo Collegato di Udine, Sezione di Trieste, Udine; ^(b)ICTP, Trieste; ^(c)Dipartimento Politecnico di Ingegneria e Architettura, Università di Udine, Udine; Italy.
- ^{69(a)}INFN Sezione di Lecce; ^(b)Dipartimento di Matematica e Fisica, Università del Salento, Lecce; Italy.
- ^{70(a)}INFN Sezione di Milano; ^(b)Dipartimento di Fisica, Università di Milano, Milano; Italy.
- ^{71(a)}INFN Sezione di Napoli; ^(b)Dipartimento di Fisica, Università di Napoli, Napoli; Italy.
- ^{72(a)}INFN Sezione di Pavia; ^(b)Dipartimento di Fisica, Università di Pavia, Pavia; Italy.
- ^{73(a)}INFN Sezione di Pisa; ^(b)Dipartimento di Fisica E. Fermi, Università di Pisa, Pisa; Italy.
- ^{74(a)}INFN Sezione di Roma; ^(b)Dipartimento di Fisica, Sapienza Università di Roma, Roma; Italy.
- ^{75(a)}INFN Sezione di Roma Tor Vergata; ^(b)Dipartimento di Fisica, Università di Roma Tor Vergata, Roma; Italy.
- ^{76(a)}INFN Sezione di Roma Tre; ^(b)Dipartimento di Matematica e Fisica, Università Roma Tre, Roma; Italy.
- ^{77(a)}INFN-TIFPA; ^(b)Università degli Studi di Trento, Trento; Italy.

- ⁷⁸Universität Innsbruck, Department of Astro and Particle Physics, Innsbruck; Austria.
- ⁷⁹University of Iowa, Iowa City IA; United States of America.
- ⁸⁰Department of Physics and Astronomy, Iowa State University, Ames IA; United States of America.
- ⁸¹(^a) Departamento de Engenharia Elétrica, Universidade Federal de Juiz de Fora (UFJF), Juiz de Fora; (^b) Universidade Federal do Rio De Janeiro COPPE/EE/IF, Rio de Janeiro; (^c) Instituto de Física, Universidade de São Paulo, São Paulo; (^d) Rio de Janeiro State University, Rio de Janeiro; Brazil.
- ⁸²KEK, High Energy Accelerator Research Organization, Tsukuba; Japan.
- ⁸³Graduate School of Science, Kobe University, Kobe; Japan.
- ⁸⁴(^a) AGH University of Krakow, Faculty of Physics and Applied Computer Science, Krakow; (^b) Marian Smoluchowski Institute of Physics, Jagiellonian University, Krakow; Poland.
- ⁸⁵Institute of Nuclear Physics Polish Academy of Sciences, Krakow; Poland.
- ⁸⁶Faculty of Science, Kyoto University, Kyoto; Japan.
- ⁸⁷Kyoto University of Education, Kyoto; Japan.
- ⁸⁸Research Center for Advanced Particle Physics and Department of Physics, Kyushu University, Fukuoka ; Japan.
- ⁸⁹Instituto de Física La Plata, Universidad Nacional de La Plata and CONICET, La Plata; Argentina.
- ⁹⁰Physics Department, Lancaster University, Lancaster; United Kingdom.
- ⁹¹Oliver Lodge Laboratory, University of Liverpool, Liverpool; United Kingdom.
- ⁹²Department of Experimental Particle Physics, Jožef Stefan Institute and Department of Physics, University of Ljubljana, Ljubljana; Slovenia.
- ⁹³School of Physics and Astronomy, Queen Mary University of London, London; United Kingdom.
- ⁹⁴Department of Physics, Royal Holloway University of London, Egham; United Kingdom.
- ⁹⁵Department of Physics and Astronomy, University College London, London; United Kingdom.
- ⁹⁶Louisiana Tech University, Ruston LA; United States of America.
- ⁹⁷Fysiska institutionen, Lunds universitet, Lund; Sweden.
- ⁹⁸Departamento de Física Teórica C-15 and CIAFF, Universidad Autónoma de Madrid, Madrid; Spain.
- ⁹⁹Institut für Physik, Universität Mainz, Mainz; Germany.
- ¹⁰⁰School of Physics and Astronomy, University of Manchester, Manchester; United Kingdom.
- ¹⁰¹CPPM, Aix-Marseille Université, CNRS/IN2P3, Marseille; France.
- ¹⁰²Department of Physics, University of Massachusetts, Amherst MA; United States of America.
- ¹⁰³Department of Physics, McGill University, Montreal QC; Canada.
- ¹⁰⁴School of Physics, University of Melbourne, Victoria; Australia.
- ¹⁰⁵Department of Physics, University of Michigan, Ann Arbor MI; United States of America.
- ¹⁰⁶Department of Physics and Astronomy, Michigan State University, East Lansing MI; United States of America.
- ¹⁰⁷Group of Particle Physics, University of Montreal, Montreal QC; Canada.
- ¹⁰⁸Fakultät für Physik, Ludwig-Maximilians-Universität München, München; Germany.
- ¹⁰⁹Max-Planck-Institut für Physik (Werner-Heisenberg-Institut), München; Germany.
- ¹¹⁰Graduate School of Science and Kobayashi-Maskawa Institute, Nagoya University, Nagoya; Japan.
- ¹¹¹Department of Physics and Astronomy, University of New Mexico, Albuquerque NM; United States of America.
- ¹¹²Institute for Mathematics, Astrophysics and Particle Physics, Radboud University/Nikhef, Nijmegen; Netherlands.
- ¹¹³Nikhef National Institute for Subatomic Physics and University of Amsterdam, Amsterdam; Netherlands.
- ¹¹⁴Department of Physics, Northern Illinois University, DeKalb IL; United States of America.
- ¹¹⁵(^a) New York University Abu Dhabi, Abu Dhabi; (^b) University of Sharjah, Sharjah; United Arab

Emirates.

¹¹⁶Department of Physics, New York University, New York NY; United States of America.

¹¹⁷Ochanomizu University, Otsuka, Bunkyo-ku, Tokyo; Japan.

¹¹⁸Ohio State University, Columbus OH; United States of America.

¹¹⁹Homer L. Dodge Department of Physics and Astronomy, University of Oklahoma, Norman OK; United States of America.

¹²⁰Department of Physics, Oklahoma State University, Stillwater OK; United States of America.

¹²¹Palacký University, Joint Laboratory of Optics, Olomouc; Czech Republic.

¹²²Institute for Fundamental Science, University of Oregon, Eugene, OR; United States of America.

¹²³Graduate School of Science, Osaka University, Osaka; Japan.

¹²⁴Department of Physics, University of Oslo, Oslo; Norway.

¹²⁵Department of Physics, Oxford University, Oxford; United Kingdom.

¹²⁶LPNHE, Sorbonne Université, Université Paris Cité, CNRS/IN2P3, Paris; France.

¹²⁷Department of Physics, University of Pennsylvania, Philadelphia PA; United States of America.

¹²⁸Department of Physics and Astronomy, University of Pittsburgh, Pittsburgh PA; United States of America.

¹²⁹(^a)Laboratório de Instrumentação e Física Experimental de Partículas - LIP, Lisboa; (^b)Departamento de Física, Faculdade de Ciências, Universidade de Lisboa, Lisboa; (^c)Departamento de Física, Universidade de Coimbra, Coimbra; (^d)Centro de Física Nuclear da Universidade de Lisboa, Lisboa; (^e)Departamento de Física, Universidade do Minho, Braga; (^f)Departamento de Física Teórica y del Cosmos, Universidad de Granada, Granada (Spain); (^g)Departamento de Física, Instituto Superior Técnico, Universidade de Lisboa, Lisboa; Portugal.

¹³⁰Institute of Physics of the Czech Academy of Sciences, Prague; Czech Republic.

¹³¹Czech Technical University in Prague, Prague; Czech Republic.

¹³²Charles University, Faculty of Mathematics and Physics, Prague; Czech Republic.

¹³³Particle Physics Department, Rutherford Appleton Laboratory, Didcot; United Kingdom.

¹³⁴IRFU, CEA, Université Paris-Saclay, Gif-sur-Yvette; France.

¹³⁵Santa Cruz Institute for Particle Physics, University of California Santa Cruz, Santa Cruz CA; United States of America.

¹³⁶(^a)Departamento de Física, Pontificia Universidad Católica de Chile, Santiago; (^b)Millennium Institute for Subatomic physics at high energy frontier (SAPHIR), Santiago; (^c)Instituto de Investigación Multidisciplinario en Ciencia y Tecnología, y Departamento de Física, Universidad de La Serena; (^d)Universidad Andres Bello, Department of Physics, Santiago; (^e)Instituto de Alta Investigación, Universidad de Tarapacá, Arica; (^f)Departamento de Física, Universidad Técnica Federico Santa María, Valparaíso; Chile.

¹³⁷Department of Physics, University of Washington, Seattle WA; United States of America.

¹³⁸Department of Physics and Astronomy, University of Sheffield, Sheffield; United Kingdom.

¹³⁹Department of Physics, Shinshu University, Nagano; Japan.

¹⁴⁰Department Physik, Universität Siegen, Siegen; Germany.

¹⁴¹Department of Physics, Simon Fraser University, Burnaby BC; Canada.

¹⁴²SLAC National Accelerator Laboratory, Stanford CA; United States of America.

¹⁴³Department of Physics, Royal Institute of Technology, Stockholm; Sweden.

¹⁴⁴Departments of Physics and Astronomy, Stony Brook University, Stony Brook NY; United States of America.

¹⁴⁵Department of Physics and Astronomy, University of Sussex, Brighton; United Kingdom.

¹⁴⁶School of Physics, University of Sydney, Sydney; Australia.

¹⁴⁷Institute of Physics, Academia Sinica, Taipei; Taiwan.

- ¹⁴⁸(^a)E. Andronikashvili Institute of Physics, Iv. Javakhishvili Tbilisi State University, Tbilisi;^(b)High Energy Physics Institute, Tbilisi State University, Tbilisi;^(c)University of Georgia, Tbilisi; Georgia.
- ¹⁴⁹Department of Physics, Technion, Israel Institute of Technology, Haifa; Israel.
- ¹⁵⁰Raymond and Beverly Sackler School of Physics and Astronomy, Tel Aviv University, Tel Aviv; Israel.
- ¹⁵¹Department of Physics, Aristotle University of Thessaloniki, Thessaloniki; Greece.
- ¹⁵²International Center for Elementary Particle Physics and Department of Physics, University of Tokyo, Tokyo; Japan.
- ¹⁵³Department of Physics, Tokyo Institute of Technology, Tokyo; Japan.
- ¹⁵⁴Department of Physics, University of Toronto, Toronto ON; Canada.
- ¹⁵⁵(^a)TRIUMF, Vancouver BC;^(b)Department of Physics and Astronomy, York University, Toronto ON; Canada.
- ¹⁵⁶Division of Physics and Tomonaga Center for the History of the Universe, Faculty of Pure and Applied Sciences, University of Tsukuba, Tsukuba; Japan.
- ¹⁵⁷Department of Physics and Astronomy, Tufts University, Medford MA; United States of America.
- ¹⁵⁸United Arab Emirates University, Al Ain; United Arab Emirates.
- ¹⁵⁹Department of Physics and Astronomy, University of California Irvine, Irvine CA; United States of America.
- ¹⁶⁰Department of Physics and Astronomy, University of Uppsala, Uppsala; Sweden.
- ¹⁶¹Department of Physics, University of Illinois, Urbana IL; United States of America.
- ¹⁶²Instituto de Física Corpuscular (IFIC), Centro Mixto Universidad de Valencia - CSIC, Valencia; Spain.
- ¹⁶³Department of Physics, University of British Columbia, Vancouver BC; Canada.
- ¹⁶⁴Department of Physics and Astronomy, University of Victoria, Victoria BC; Canada.
- ¹⁶⁵Fakultät für Physik und Astronomie, Julius-Maximilians-Universität Würzburg, Würzburg; Germany.
- ¹⁶⁶Department of Physics, University of Warwick, Coventry; United Kingdom.
- ¹⁶⁷Waseda University, Tokyo; Japan.
- ¹⁶⁸Department of Particle Physics and Astrophysics, Weizmann Institute of Science, Rehovot; Israel.
- ¹⁶⁹Department of Physics, University of Wisconsin, Madison WI; United States of America.
- ¹⁷⁰Fakultät für Mathematik und Naturwissenschaften, Fachgruppe Physik, Bergische Universität Wuppertal, Wuppertal; Germany.
- ¹⁷¹Department of Physics, Yale University, New Haven CT; United States of America.
- ^a Also Affiliated with an institute covered by a cooperation agreement with CERN.
- ^b Also at An-Najah National University, Nablus; Palestine.
- ^c Also at Borough of Manhattan Community College, City University of New York, New York NY; United States of America.
- ^d Also at Bruno Kessler Foundation, Trento; Italy.
- ^e Also at Center for High Energy Physics, Peking University; China.
- ^f Also at Centro Studi e Ricerche Enrico Fermi; Italy.
- ^g Also at CERN, Geneva; Switzerland.
- ^h Also at Département de Physique Nucléaire et Corpusculaire, Université de Genève, Genève; Switzerland.
- ⁱ Also at Departament de Física de la Universitat Autònoma de Barcelona, Barcelona; Spain.
- ^j Also at Department of Financial and Management Engineering, University of the Aegean, Chios; Greece.
- ^k Also at Department of Physics and Astronomy, Michigan State University, East Lansing MI; United States of America.
- ^l Also at Department of Physics and Astronomy, University of Louisville, Louisville, KY; United States of America.
- ^m Also at Department of Physics, Ben Gurion University of the Negev, Beer Sheva; Israel.

- ⁿ Also at Department of Physics, California State University, East Bay; United States of America.
- ^o Also at Department of Physics, California State University, Sacramento; United States of America.
- ^p Also at Department of Physics, King's College London, London; United Kingdom.
- ^q Also at Department of Physics, Stanford University, Stanford CA; United States of America.
- ^r Also at Department of Physics, University of Fribourg, Fribourg; Switzerland.
- ^s Also at Department of Physics, University of Thessaly; Greece.
- ^t Also at Department of Physics, Westmont College, Santa Barbara; United States of America.
- ^u Also at Hellenic Open University, Patras; Greece.
- ^v Also at Institutio Catalana de Recerca i Estudis Avancats, ICREA, Barcelona; Spain.
- ^w Also at Institut für Experimentalphysik, Universität Hamburg, Hamburg; Germany.
- ^x Also at Institute for Nuclear Research and Nuclear Energy (INRNE) of the Bulgarian Academy of Sciences, Sofia; Bulgaria.
- ^y Also at Institute of Particle Physics (IPP); Canada.
- ^z Also at Institute of Physics, Azerbaijan Academy of Sciences, Baku; Azerbaijan.
- ^{aa} Also at Institute of Theoretical Physics, Ilia State University, Tbilisi; Georgia.
- ^{ab} Also at L2IT, Université de Toulouse, CNRS/IN2P3, UPS, Toulouse; France.
- ^{ac} Also at Lawrence Livermore National Laboratory, Livermore; United States of America.
- ^{ad} Also at National Institute of Physics, University of the Philippines Diliman (Philippines); Philippines.
- ^{ae} Also at Technical University of Munich, Munich; Germany.
- ^{af} Also at The Collaborative Innovation Center of Quantum Matter (CICQM), Beijing; China.
- ^{ag} Also at TRIUMF, Vancouver BC; Canada.
- ^{ah} Also at Università di Napoli Parthenope, Napoli; Italy.
- ^{ai} Also at University of Chinese Academy of Sciences (UCAS), Beijing; China.
- ^{aj} Also at University of Colorado Boulder, Department of Physics, Colorado; United States of America.
- ^{ak} Also at Washington College, Maryland; United States of America.
- ^{al} Also at Yeditepe University, Physics Department, Istanbul; Türkiye.
- * Deceased